

ECOSYSTEM, CELLULAR AND SUB-CELLULAR DYNAMICS OF THE MARINE,

DIATOM PLASTID

by

Joseph John Grzymiski

A Dissertation submitted to the

Graduate School-New Brunswick

Rutgers, The State University of New Jersey

in partial fulfillment of the requirements

for the degree of

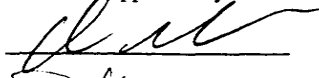
Doctor of Philosophy

Graduate Program in Oceanography

written under the direction of

Dr. Oscar M. Schofield

and approved by



Paul Sunda



New Brunswick, New Jersey

January, 2002

UMI Number: 3046736

Copyright 2002 by
Grzymski, Joseph John

All rights reserved.

UMI[®]

UMI Microform 3046736

Copyright 2002 by ProQuest Information and Learning Company.
All rights reserved. This microform edition is protected against
unauthorized copying under Title 17, United States Code.

ProQuest Information and Learning Company
300 North Zeeb Road
P.O. Box 1346
Ann Arbor, MI 48106-1346

Reproduced with permission of the copyright owner. Further reproduction prohibited without permission.

©2002

Joseph John Grzymski

ALL RIGHTS RESERVED

ABSTRACT OF THE DISSERTATION

Ecosystem, cellular and sub-cellular dynamics of the marine, photosynthetic plastid

By JOSEPH JOHN GRZYMSKI

Dissertation Director:

Oscar M. Schofield

The function of marine diatom plastids was examined at three levels of metabolic complexity: ecosystem, cellular and sub-cellular. Trophic transfer efficiencies of two size classes of phytoplankton: diatoms and the less suitable autotrophic food source, cryptophytes were examined. Decreased diatom abundances caused by increasing Antarctic temperatures are negatively affecting krill abundance and result in a doubling in the carbon biomass that is either remineralized in the surface water or exported to deeper water. At the cellular level, carbon fixation and photosystem II (PSII) efficiency were examined in low light adapted cultures of the marine diatom *Thalassiosira pseudonana* (3H) under monochromatic wavelengths of ultraviolet radiation. Maximum damage to the quantum yield for stable charge separations was found in the UVB (280-320nm) wavelengths without background PAR light while the damage under PAR was 30% less. Various fluorescent transients were measured and the results indicate localized damage most likely on the acceptor side of the photosystem II reaction center. However, dark adapted measurements of fluorescence transients with and without DCMU do not result

in similar functions. A strong correlation was found between the weightings of the induction curves without DCMU and carbon fixation. This was due to a loss of electron transport from the reaction center to plastoquinone. At the sub-cellular level, plastid structure and function was examined in the benthic foraminifera *Nonionella stella*. I characterize and identify the chloroplasts sequestered in the foraminifer inhabiting sediments collected off California from a water depth of about 600 m. Two unique sequences of diatoms were found in all samples examined: a diatom 16S rDNA sequence resembling *Skeletonema costatum* was the most prevalent and a diatom sequence resembling *Odontella sinensis* was also abundant. Three hypotheses on the possible function of sequestered chloroplasts in the deep sea are presented. My results suggest that the potential for photo or chemoautotrophy is low and instead the chloroplasts are used to meet the nitrogen requirements of the host. The organism and its metabolic adaptations are presented as a modern analog of protistan evolution and the evolution of nitrogen metabolism.

Preface

I would like to thank my advisor and friend Oscar Schofield. I am grateful and very proud to be his first graduate student. The smartest thing I did upon returning from Norway in 1995 was seek Oscar's help on an ASLO abstract- thus beginning our adventure at Rutgers. We have shared successes, calamities, and incredibly good times. In typical Oscar fashion our relationship has been "epic" and I thank him for it.

Acknowledgements

Many people helped and supported me during my years at Rutgers University. I thank them all. The graduate students, faculty and staff of IMCS have been very supportive. I would especially like to thank my committee: Oscar, Paul Falkowski, John Reinfelder and John Raven. They have gone out of their way to support me and challenge me. Every graduate student should experience having an office across from Paul's- it is a challenging but incredibly rewarding experience. Thank you, Paul. Clarice Yentsch, Egil Sakshaug, Geir Johnsen, Joan Bernhard and Mark Moline have been great mentors and collaborators. Jay Cullen was a great officemate and is an even better friend.

Most importantly, I would like to thank my family and friends who have supported me unconditionally throughout my life. Mom, Mark, Brian and Elizabeth no words can express my love and my thanks.

**In a time of heroes,
this is dedicated to mine:
my mother and late father
Doris and Joseph Grzymski**

Table of Contents

ABSTRACT OF THE DISSERTATION	ii
Preface	iv
Acknowledgements	v
Table of Contents	vii
Lists of tables	ix
List of illustrations	x
1 Introduction	1
1.1 General Introduction	1
1.2 Summary of dissertation chapters	4
1.3 References	7
1.4 Tables	9
2 Trophic transfer efficiency decreases in HNLC-like and Antarctic peninsula environments	10
2.1 Abstract	10
2.2 Introduction	11
2.2.1 Greenhouse gases and climate	13
2.2.2 High nutrient low chlorophyll regions (HNLC)	14
2.2.3 Antarctic peninsular region	16
2.3 Atmosphere-Ocean interaction model	18
2.3.1 Inorganic carbon fluxes	18
2.3.2 Nutrient regulation of phytoplankton carbon fixation	20
2.4 Trophic transfer model	24
2.5 Model results and discussion	25
2.5.1 HNLC	25
2.5.2 Antarctic peninsular ecosystem	28
2.6 Conclusions	32
2.7 References	34
2.8 Tables	37
2.9 Figures	38
2.10 Atmosphere-ocean interaction model	49
3 Monochromatic ultraviolet light induced damage to photosystem II efficiency and carbon fixation in the marine diatom <i>Thalassiosira pseudonana</i> (3H)	52
3.1 Abstract	52
3.2 Introduction	53
3.3 Materials and methods	56
3.3.1 Culture conditions	56
3.3.2 Ultraviolet light incubations	56
3.3.3 Fluorescence parameters of <i>Thalassiosira pseudonana</i>	57
3.3.4 Measurements of UV effects without PAR light	57
3.3.5 Analytical measurements in the presence of PAR light	59
3.3.6 Calculation of ϵ_H ($J\ m^{-2})^{-1}$	61
3.4 Results	61
3.4.1 Acclimation state of <i>T. pseudonana</i>	61
3.4.2 Signature of photosystem II damage without PAR	62
3.4.3 Signature of photosystem II damage with PAR	63
3.4.4 UVR induced changes in photosynthetic function. Carbon Fixation	63
3.4.5 Connectivity between reaction centers	64
3.4.6 Photosystem II light utilization	64
3.5 Discussion	65
3.6 References	70
3.7 Tables	74
3.8 Figures	78

4	<i>Nonionella stella</i> , a modern analog to the protist undergoing secondary endosymbiosis 250 Mya:	
	plastid structure and function.....	84
4.1	Abstract.....	84
4.2	Introduction.....	85
4.3	Materials and methods	88
4.3.1	Sample collection	88
4.3.2	Electron microscopy	89
4.3.3	Molecular identification of chloroplasts	89
4.3.4	Chloroplast proteins	90
4.3.5	Pigment characterization.....	90
4.3.6	Photochemical yields	91
4.3.7	Enzyme assays	92
4.3.8	Redox chemistry of the NADP ⁺ /NADPH couple.....	92
4.3.9	Immunolocalization of nitrate reductase	94
4.4	Results.....	95
4.4.1	Chloroplast identification.....	95
4.4.2	Chloroplast proteins	96
4.4.3	Pigment characterization.....	97
4.4.4	Photochemical yields and enzyme activity assays	98
4.4.5	Abiotic NADPH reduction.....	99
4.4.6	Immunolocalization of nitrate reductase	100
4.5	Discussion	101
4.5.1	Ultrastructure and sequence identity	101
4.5.2	Bio-optical properties of sequestered plastids.....	102
4.5.3	Enzyme activity and longevity of proteins.....	103
4.5.4	Chloroplast function: the light hypothesis	105
4.5.5	Chloroplast function: the sulfur hypothesis	106
4.5.6	Chloroplast function: the nitrogen hypothesis	107
4.6	References.....	109
4.7	Tables.....	112
4.8	Figures	113
5	Curriculum Vita	126

Lists of tables

Table 1.1 Gibbs free energy changes for the oxidation of a mole of glucose ($C_6H_{12}O_6$) given various electron acceptors. Data take from Froelich et al. (1979).	9
Table 2.1 Variables for the open ocean iron/nitrate model	37
Table 3.1 Symbols and abbreviations. Units are given in brackets unless dimensionless	74
Table 3.2 Growth characteristics of <i>T. pseudonana</i> . (20° C, 12:12 L:D, 80 $\mu\text{mol photons m}^{-2} \text{s}^{-1}$)	
Production units are $\mu\text{g C } \mu\text{g Chl a}^{-1} \text{hr}^{-1}$	75
Table 3.3 Calculated fluorescence parameters \pm the standard deviation from 30 minute treatments with PAR and UVR ($n>4$). Bold numbers indicate a significant difference from PAR ($p<0.05$)	76
Table 3.4 Parameters for type II linear regressions from the data in figure 3.6b comparing the weightings of the fluorescence parameters to the damage to carbon fixation. Linear regressions were solved using a cubic equation and the standard deviations of the error in both the x and y directions. Values of the slope and Y-intercept are shown \pm the 95% confidence interval	77
Table 4.1 Measured and calculated parameters of electron transport rates and enzyme activities in <i>N. stella</i> .	
	112

List of illustrations

Figure 2.1 Schematic of the relationship between CO ₂ in the four sections of the model: atmosphere, surface ocean, deep ocean and sediment.....	38
Figure 2.2 Schematic of the nitrate flow in the three sections of the model: surface ocean, deep ocean and sediment.....	39
Figure 2.3 Schematic of the iron flow in the three sections of the model: surface ocean, deep ocean and sediment Note that iron can also enter the system from aeolian sources but not exit the surface ocean to the atmosphere.....	40
Figure 2.4 Schematic of the Antarctic food web model where primary production is divided into two relative size classes of phytoplankton, diatoms and other phytoplankton and cryptophytes.....	41
Figure 2.5 Model output of atmospheric pCO ₂ (ppm) and air-sea exchange under the initial conditions (Case A, table 2.1). The model runs for 3000 years after which the atmosphere and surface ocean are in equilibrium.....	42
Figure 2.6 Model output of surface Fe inventory (mol) versus particulate N (mol N m ⁻² yr ⁻¹) under the initial conditions (table 2.1).....	43
Figure 2.7 Model output of atmospheric pCO ₂ (ppm) and air-sea exchange under Case E (table 2.1). The model runs for 3000 years after which the atmosphere and surface ocean are in equilibrium. Note the different scales compared to figure 2.5.....	44
Figure 2.8 Model output of surface Fe inventory (mol) versus particulate N (mol N m ⁻² yr ⁻¹) under Case E (table 2.1). Note the different scales compared to figure 2.6.....	45
Figure 2.9 Model output of atmospheric pCO ₂ (ppm) and air-sea exchange under the model conditions specified in table 2.1. The model runs for 3000 years after which the atmosphere and surface ocean are in equilibrium.....	46
Figure 2.10 Schematic of the iron flow in the three sections of the model: surface ocean, deep ocean and sediment Note that iron can also enter the system from aeolian sources but not exit the surface ocean to the atmosphere.....	47
Figure 2.11 Results from the model used to calculate the partitioning of energy throughout the Antarctic food web. A). The calculated flow of carbon through either krill (shaded) or salps (open) based on the percentage of cryptophyte primary production. The percent of cryptophyte primary production ranged from 19% in 1991-92 to 53% in 1993-94. B). the partitioning of carbon into higher trophic levels (light shade), respiration (stippled), sedimentation or microbial loop (open) and autotrophic losses (dark shade) was calculated based on changing krill to salp ratios. Krill to salp ratios ranging from 0.0641 to 33.3 (Loeb et al 1997) were used and corresponded to 19 and 53% cryptophytes, respectively.....	48
Figure 3.1 A. Action spectra of damage to the maximum quantum yield as calculated from induction curves without DCMU ϕ_{IIeo} (Kaut) (circles) after a thirty minute incubation under monochromatic UVR only (error bars are the 95% confidence limits, n>4) Calculations of ϕ_{IIeo} explained in the methods. B. As in A, but as calculated from the maximum quantum yield as calculated from induction curves with DCMU ϕ_{IIeo} (DCMU) (squares).....	78
Figure 3.2 A. Induction curves with and without DCMU before (grey) and after (black) a 30 minute treatment with 300 nm UVR. Curves were normalized to F_0 because the majority of the decrease in F_v/F_m was due to changes in F_m . B. As in A, but after a 30 minute treatment with both 300nm UVR and 60 μ mol photons m ⁻² s ⁻¹ PAR. The measurements and light intensities of the induction curves are explained in the methods.....	79
Figure 3.3 Action spectra of damage to ϕ_{IIeo} (Kaut) (circles) and ϕ_{IIeo} (DCMU) (squares) after a thirty minute incubation under monochromatic UVR and 60 μ mol photons m ⁻² s ⁻¹ PAR (error bars are the 95% confidence limits, n>4).....	80
Figure 3.4 Action spectrum of damage to carbon fixation after a thirty minute incubation under monochromatic UVR and 60 μ mol photons m ⁻² s ⁻¹ PAR (error bars are the 95% confidence limits, n>4).....	81
Figure 3.5 A. Measurement of the parameter J_{con} as calculated from induction curves with DCMU after a thirty-minute incubation under monochromatic UVR only (error bars are the 95% confidence limits).....	

B. As in A, but after a 30 minute incubation under monochromatic UVR and 60 $\mu\text{mol photons m}^{-2} \text{s}^{-1}$ PAR.	82
Figure 3.6 A. Circles indicate measurements for the efficiency of photon trapping by PSII after a 30 minute incubation under monochromatic UVR and 60 $\mu\text{mol photons m}^{-2} \text{s}^{-1}$ PAR (ϕ_{exc}) (error bars are the 95% confidence limits, n>4). Squares indicate measurements for the apparent quantum yield of PSII (ϕ_{II}) after a 30 minute incubation under monochromatic UVR and 60 $\mu\text{mol photons m}^{-2} \text{s}^{-1}$ PAR (error bars as indicated above). Values of ϕ_{II} and ϕ_{exc} under PAR alone were 0.68 (0.005) and 0.63 (0.01) respectively. B. The relationship between the weights ϵ as calculated from fluorescence parameters, $\phi_{\text{II}}^{\circ}(\text{closed circle})$, $\phi_{\text{II}}^{\circ}(\text{closed square})$, ϕ_{II} (open square), and ϕ_{exc} (open circle) versus the weights ϵ as calculated from measurements of carbon fixation. The corresponding type II linear regressions of the slopes and R^2 values are presented in Table 4.4 for clarity.	83
Figure 4.1 Electron micrographs of three <i>N. stella</i> plastids. Note the similarity of the plastids: the outer lamella and the single pyrenoid with the transverse lamella.	113
Figure 4.2 Restriction fragment length polymorphism of 16S clonal library from <i>N. stella</i> . The two dominant patterns denoted N.sChl1 and N.sChl2 are highlighted by arrows. Sequences for these chloroplasts are shown in 4.3	114
Figure 4.3 Sequence comparisons for one of the dominant chloroplasts in <i>N. stella</i> , N.sChl1 and the diatom <i>S. costatum</i> .	115
Figure 4.4 Top panel: Sequence comparisons for one of the dominant chloroplast in <i>N. stella</i> , N.sChl2 and the diatom <i>O. sinensis</i> . Bottom panel: Sequence comparisons between representative of diatoms, dinoflagellates and prymnesiophytes- the major functional groups of phytoplankton in the ocean. The sequence differences between <i>S. costatum</i> and <i>O. sinensis</i> were consistently seen between N.sChl1 and N.sChl2.	116
Figure 4.5 Digitized images from Western blots of protein extract from <i>N. stella</i> and the marine diatom <i>Thalassiosira pseudonana</i> . A. Proteins challenged with the antibody for the major light harvesting complex of Chromophyte algae, FCP and the major light harvesting complex for the chlorophyll a-b containing plant, squash. B. Proteins challenged with the antibody for the carboxylating enzyme RuBisCO. Shown is the cross reaction with the 53 kDa large subunit. C. Proteins challenged with the antibody for the 32.5 kDa, D1 component of the major structural dimer of photosystem II.	117
Figure 4.6 HPLC chromatogram for pigment extracts of <i>N. stella</i> . Peaks are labeled from the wavelength signatures of the corresponding absorption and fluorescence spectra.	118
Figure 4.7 A. Fluorescence excitation spectra scaled to 1 at 400nm (440 ex, 680 em) for <i>N. stella</i> (bold line) and Santa Barbara Basin mud (faint line). B. <i>In vitro</i> absorption spectrum for a 90% acetone extract of <i>N. stella</i> .	119
Figure 4.8 A. 77k emission spectrum (squares) of <i>N. stella</i> (440 ex) and the corresponding fit of the Gaussian peaks (smooth line). B. Gaussian curves of the 6 major components of the emission spectrum and the residuals of the fit. The major components of the spectrum are explained in the text.	120
Figure 4.9 Fast repetition rate fluorometric measurement of <i>N. stella</i> . The curve is an average of 10 measurements and shows the change in fluorescence after a series of sub-saturating blue LED flashes as described in the text.	121
Figure 4.10 A. Relationship between pH and Q (NADPH/NADP ⁺) different reducing conditions. Previously published pe's for the NADPH/NADP ⁺ couple correspond to the black line. Upper and lower error limits are presented. B. The relationship between the redox poise of a system and Q calculated from the equations in the text.	122
Figure 4.11 A. Epifluorescence micrograph of <i>Thalassiosira weissflogii</i> grown with NO ₃ ⁻ showing the location of the chloroplasts. B. As in A, except showing the labeling of the Alexa 488 tagged nitrate reductase antibody.	123
Figure 4.12 A. Epifluorescence micrograph (100x) of <i>Nonionella stella</i> showing the location of the chloroplasts. B. As in A, except showing the labeling of the Alexa 488 tagged nitrate reductase antibody.	124
Figure 4.13 A. Epifluorescence micrograph (400x) of one chamber of <i>Nonionella stella</i> showing the location of the Alexa 488 tagged nitrate reductase enzyme. B. As in A except 1000x showing individually labeled microbodies which are presumably plastids.	125

1 Introduction

1.1 General Introduction

The evolution of oxygenic photosynthesis 2.8 billion years ago altered the redox poise of the atmosphere and oceans (Blankenship 1992; Blankenship and Hartman 1998; Holland and Rye 1998). The gradual buildup of oxygen to present atmospheric levels transformed the Earth from a mildly reducing environment to a highly oxidizing one. Early Earth atmosphere was probably composed primarily of N_2 , CO_2 and H_2O and NH_3 and CH_4 were short lived due to photolysis in the optically thin atmosphere (Holland 1984; Kasting 1993). In an atmosphere and ocean with present atmospheric levels (PAL) of oxygen the dominant redox couple is:



The ultimate result of this is what we see today: complex organisms fueled by the highly energetic ($\Delta G = -119 \text{ kJ mol}^{-1}$) oxidation of organic matter by molecular oxygen. Regardless of the specific origins of life, solar energy is the only source of free energy large enough to maintain this disequilibrium for the large planet (Mauzerall 1990). For example, in the year 2001 population of Earth was over 6 billion people totaling about $31 \times 10^{13} \text{ g C}$. The energy required to fix this amount of carbon equals $3 \times 10^{11} \text{ W}$. There are four orders of magnitude more biomass than humans. Sustaining such disequilibrium requires a solar energy flux of at least $10^{-4} \text{ W cm}^{-2}$ (Mauzerall 1995).

In the cracks of the oxidizing superstructure of the Earth are organisms that have adapted to all other redox couples capable of providing free energy (Nealson and Conrad 1999; Pace 2001). For example:



is the reaction that describes anoxygenic photosynthesis and parallels oxygenic photosynthesis:



The obvious difference between the two is the latter requires an order of magnitude more free energy for the reaction to proceed to the right. The sulfur cycle reactions (eq. 1.2) have been proposed as a precursor to oxygenic photosynthesis and mitochondrial respiration (Searcy 1992). Stratified marine sediments are good ecosystems to observe the decreasing free energy yield of biological reactions as electron acceptors are successively removed from the environment (Froelich et al. 1979). The various organisms must be positioned at these gradients if they are to exploit the available electron acceptors.

In front of the backdrop of energetic disequilibrium that defines life are turbulent dynamics on smaller spatial and temporal scales. These are the processes that define ecosystems, predator-prey interactions and survival of the individual. These are the processes that require adaptation and adjustment and lead to changes in growth rate, reproductive success and ultimately are a matter of life and death. Turbulent change and major geological and environmental events (e.g. meteor impacts, snowball Earth) lead to punctuated equilibrium, rapid diversification and a new steady state after which new selective processes arise and the cycle renews. The result: the evolution of eukaryotes about 2.7 billion years ago, 10,000 species of diatoms, the diversification of angiosperms (>200,000 species) in 10 million years and the diversification of 20 orders of mammals in 12 million years (Stanley 1979; Wray et al. 1996).

The evolution of photosynthetic organisms occurred in part because of the benefits of solar energy but mostly due to the propensity of protistan organisms to ingest but not fully digest their food. This is perhaps the defining event in eukaryotic evolution (Margulis 1981). The origins of diatoms and other golden algae from secondary endosymbioses (occurring independently!!) about 250 million years ago from heterotrophic protists further emphasize the importance of these symbiotic events (Medlin et al. 1997). Diatoms are a major contributor to oceanic primary productivity and export production in the ocean (Goldman 1992). They are an important food source in many oceanic ecosystems and are a conduit for the burial and removal of CO₂ (in the form of particulate organic carbon) from the atmosphere. In recent years, biological oceanographers have sought to understand the spatial and temporal variables as well as the biological variables that drive primary productivity (Bienfang et al. 1982; Brown 1988; Coale et al. 1996b; Dugdale and Wilkerson 1998; Goldman 1992; Greene et al. 1991b; Mitchell and Holm-Hansen 1991; Smetacek 1998).

This thesis is a further means to understanding diatoms and oxygenic photosynthesis; the defining redox reaction of the last 2.8 billion years. Each chapter considers a different time scale. These scales are relevant to ecosystem function and efficiency (years to millennia), photosynthesis (microseconds to hours), and evolution (tens of thousand-billions of years). My thesis is divided into three targeted studies. Chapter 2 examines the role of diatoms in the ecosystem. I consider two relevant environmental changes; CO₂ increase and temperature increase, and their affect on CO₂ drawdown from the atmosphere and trophic transfer of carbon (the aforementioned “turbulent” changes). The third chapter examines specific changes to the efficiency of

photosynthesis in a diatom under ultra-violet light fluxes. In this chapter the mechanisms of damage to the photosynthetic apparatus under light-limiting conditions are elucidated. Finally, the fourth chapter examines the role of plastids in a deep sea inhabiting foraminifer, *Nonionella stella*. This organism is hypothesized to be an analog of photosynthetic organisms that evolved via secondary endosymbioses; the process that originated diatoms.

1.2 Summary of dissertation chapters

Here I investigate the impact of two recent phenomena on diatom productivity and the transfer of carbon to higher trophic levels. Since the beginning of the Industrial Revolution, over 200 hundred years ago, atmospheric $p\text{CO}_2$ has increased by 80 ppm (Petit et al. 1999). This has caused air and ocean temperatures to increase, on average worldwide, including the Antarctic (King 1994; Stark 1994). Two models were formulated to diagnose the impact of these phenomena on the ability of phytoplankton to fix carbon and sequester it from the atmosphere and surface ocean. An atmosphere-ocean model considered the question on geologic time scales with primary production as a function of nitrate and iron concentrations. In large parts of the open ocean and in the Southern Ocean nitrate concentrations are high and iron concentrations are low compared to the general composition of phytoplankton (Bruland et al. 1994; Martin 1990; Martin 1992; Martin et al. 1990). Therefore, in these regions, nitrate uptake and phytoplankton growth are potentially iron limited. The model, a steady state, time dependent, box model, suggests that biological production and export flux can decrease atmospheric $p\text{CO}_2$ by as much as 14 ppm, IF fluxes of iron to the surface ocean increase. Under the initial conditions particulate flux of carbon out of the surface ocean to depth equals only

5% of the maximum given our knowledge of $V_{\text{mNO}_3^-}$ (Coale et al. 1996a). Particulate flux as a fraction of $V_{\text{mNO}_3^-}$ increases to 41% when the aeolian flux of iron increases to 32 times the present input. The model uses an idealized diatom to calculate the affect of increased iron on pCO_2 . The Southern Ocean would presumably benefit from increased aeolian deposition of iron. As well, cold water increases the solubility coefficient of CO_2 . In these respects the Antarctic is an important sink for CO_2 . The increasing ocean temperatures are problematic because the Antarctic could become a source of CO_2 to the atmosphere.

The increasing temperatures are also having an impact on the size class of phytoplankton along the Antarctic peninsula (Moline et al. 2000). The second model deals with quantifying the change in trophic transfer of carbon from the phytoplankton to higher trophic levels. The Antarctic food web is centered on the krill, *Euphausia superba*. These organisms do not feed equally well on all size classes of phytoplankton, preferring the larger Antarctic diatoms to smaller cryptophytes (Quetin and Ross 1985). Cryptophytes are grazed by the gelatinous zooplankton, salps. I attempted to quantify the changes in trophic transfer efficiency given changing phytoplankton populations and varying ratios of krill and salps. The results of the work indicate that changes in the phytoplankton standing stock from diatoms to cryptophytes decrease the amount of carbon transferred to krill with a concomitant increase in carbon that either is exported out of the surface or degraded in the microbial loop. Model results from two different years of data show that when cryptophytes comprise 19 and 53% of the phytoplankton population carbon ingested by krill will decrease as much as 30% and carbon available to salps will triple. Increases in temperature also decrease the absolute

ratio of krill and salps in the population (Loeb et al. 1997). When salps dominate the grazer population only 4% of primary production is available to higher trophic levels.

The consequences of increasing Antarctic temperatures are multiplicative, changing not only the food web structure but also the potential drawdown of $p\text{CO}_2$ in the atmosphere. This is due to decreases in the solubility of the gas at warmer temperatures and in the contributions of diatoms to export production. However, there is one major caveat. Decreased diatom production and increased cryptophytes favor the grazing habits of salps and result in a tripling of carbon NOT transferred to higher trophic levels. If the fate of this carbon is export, then more particulate carbon will exit the surface ocean given increased cryptophyte biomass. However, if the salps are remineralized in the surface, ocean export production will greatly decrease.

In chapter 3 I examine the effects of ultra-violet light (280-380 nm) on photosynthetic parameters of the diatom *Thalassiosira pseudonana* (3H). Previous work on UV damage to phytoplankton concentrated on generating action spectra for damage using polychromatic wavelengths (Cullen et al. 1992). Near monochromatic wavelengths are used in an attempt to target the specific wavelengths of damage to photosystem II. These results are also compared to measurements of carbon fixation- the currency of photosynthesis. The specific weights of inhibition, ϵ , $(\text{J m}^{-2})^{-1}$ are calculated. These define the amount of damage to carbon fixation or PSII at different wavelengths. The results show that the most energetic wavelengths of light are more damaging to both PSII and carbon fixation rates. However, the function is not smooth and has wavelength specificity especially in the UVA. The results of UV treatments under both PAR light and in the dark were also compared. Damage to PSII in the dark was 30% greater than

when cells were also incubated under PAR light. This is the result of radical scavenging and the rapid light-activated response to potential damage by PSII.

Diatoms originated from the endosymbiosis of red algae about 250 million years ago (Medlin et al. 1997). This formed a photoautotrophic organism from a heterotrophic host. In the final chapter of this thesis I examine the properties of a foraminifer, *Nonionella stella* that sequesters chloroplasts in the deep sea. I hypothesize, based on experimental data that this organism is a modern analog to the early protistan host cell that formed the diatom lineage. My data suggest that it is advantageous for the organism to form an association with chloroplasts to meet the nitrogen requirements of the cell. This is analogous to the algae/coral symbiosis (Rahav et al. 1989). I present spectroscopic, protein and 16S rDNA evidence that the foraminifer hosts diatom plastids. From three years of data I conclude that the host selectively ingests or selectively digests two specific diatom species: an *Odontella sinensis*-like diatom and a *Skeletonema costatum*-like diatom. Selective maintenance of diatom endosymbioses is not unprecedented (Chai and Lee 2000). However, the fact that this organism lives at 600 m in a dysoxic, ($<5 \mu\text{M O}_2 \text{ kg}^{-1}$) sulfide rich sediment is unique.

1.3 References

- Bienfang, P. K., P. J. Harrison, and L. M. Quarmby. 1982. Sinking rate response to depletion of nitrate, phosphate and silicate in four marine diatoms. *Marine Biology* 67: 295-302.
- Blankenship, R. E. 1992. Origin and early evolution of photosynthesis. *Photosynth.Res.* 33: 91-111.
- Blankenship, R. E., and H. Hartman. 1998. The Origin and Evolution of Oxygenic Photosynthesis. *Trends in Biochemical Sciences* 23: 94-97.
- Brown, J. S. 1988. Photosynthetic pigment organization in diatoms (Bacillariophyceae). *Journal of Phycology* 24: 96-102.
- Bruland, K. W., K. J. Orians, and J. P. Cowen. 1994. Reactive trace metals in the stratified central North Pacific. *Geochimica et Cosmochimica Acta* 58: 3171-3182.
- Chai, J., and J. J. Lee. 2000. Recognition, establishment and maintenance of diatom endosymbiosis in foraminifera. *micropaleontology* 46: 182-195.
- Coale, K. H., S. E. Fitzwater, R. M. Gordon, K. S. Johnson, and R. T. Barber. 1996a. Control of community growth and export production by upwelled iron in the equatorial Pacific Ocean. *Nature* 379: 621-624.

- Coale, K. H. and others 1996b. A massive phytoplankton bloom induced by an ecosystem-scale iron fertilization experiment in the equatorial Pacific Ocean. *Nature* 383: 495-501.
- Cullen, J. J., P. J. Neale, and M. P. Lesser. 1992. Biological weighting function for the inhibition of phytoplankton photosynthesis by ultraviolet radiation. *Science* 258: 646-649.
- Dugdale, R. C., and F. P. Wilkerson. 1998. Silicate regulation of new production in the equatorial Pacific upwelling. *Nature* 391: 270-273.
- Froelich, P. N. and others 1979. Early oxidation of organic matter in pelagic sediments of the eastern equatorial Atlantic: soboxic diagenesis. *Geochem. et. cosmochem. acta* 48: 1075-1090.
- Goldman, J. C. 1992. Potential role of large oceanic diatoms in new primary production. *Deep-Sea Res.* 40: 159-168.
- Greene, R. M., R. J. Geider, and P. G. Falkowski. 1991. Effect of iron limitation on photosynthesis in a marine diatom. *Limnol. Oceanogr.* 36: 1772-1782.
- Holland, H. D. 1984. *The chemical evolution of the atmosphere and oceans*. Princeton University Press.
- Holland, H., and R. Rye. 1998. *Am. J. Sci* 298: 621-672.
- Kasting, J. F. 1993. Earth's early atmosphere. *Science* 259: 920-926.
- King, J. C. 1994. Recent climate variability in the vicinity of the Antarctic Peninsula. *International Journal of Climatology* 14: 357-369.
- Loeb, V. and others 1997. Effects of sea-ice extent and krill or salp dominance on the Antarctic food web. *Nature* 387: 897-900.
- Margulis, L. 1981. *Symbiosis in cell evolution*. Freeman and Co.
- Martin, J. H. 1990. Glacial-interglacial CO₂ change: The iron hypothesis. *Paleoceanography* 5: 1-13.
- . 1992. Iron as a limiting factor in oceanic productivity., p. 123-137. In P. Falkowski and A. Woodhead [eds.], *Primary Productivity and Biogeochemical Cycles in the Sea*. Plenum, in press.
- Martin, J. H., R. M. Gordon, and S. E. Fitzwater. 1990. Iron in Antarctic waters. *Nature* 345: 156-158.
- Mauzerall, D. C. 1990. The Photochemical Origins of Life and Photoreaction of Ferrous Ion in the Archaean Oceans. *Origins of Life and Evolution of the Biosphere* 20: 293-302.
- Medlin, L. K., W. Kooistra, D. Potter, G. W. Saunders, and R. A. Andersen. 1997. Phylogenetic Relationships of the Golden Algae (Haptophytes, Heterokont Chromophytes) and Their Plastids. *Plant Systematics and Evolution*: 187-219.
- Mitchell, B. G., and O. Holm-Hansen. 1991. Observations and modeling of the Antarctic phytoplankton crop in relation to mixing depth. *Deep Sea Res* 38: 981-1007.
- Moline, M. A., H. Claustre, T. K. Frazer, J. Grzymalski, O. M. Schofield, and M. Vernet. 2000. Changes in phytoplankton assemblages along the Antarctic Peninsula and potential implications for the Antarctic food web, p. 334. In W. Davison, C. Howard-Williams and P. Broady [eds.], *Antarctic Ecosystems: models for wider ecological understanding*. New Zealand Natural Sciences.
- Nealson, K. H., and P. G. Conrad. 1999. Life: past, present and future. *Phil. Trans. R. Soc. Lond.B* 354: 1923-1939.
- Pace, N. R. 2001. The universal nature of biochemistry. *Proc Natl Acad Sci USA* 98: 808-808.
- Petit, J. R., J. Jouzel, D. Raynaud, N. I. Barkov, J.-M. Barnola, and I. Basile. 1999. Climate and atmospheric history of the past 420,000 years from the Vostok ice core, Antarctica. *Nature* 399: 429-436.
- Quetin, L. B., and R. M. Ross. 1985. Feeding by antarctic krill, *Euphausia superba*: Does size matter?, p. 372-377. In W. R. Siegfried, P. R. Condy and R. M. Laws [eds.], *Antarctic Nutrient Cycles and Food Webs*. Springer-Verlag.
- Rahav, O., Z. Dubinsky, Y. Achituv, and P. G. Falkowski. 1989. Ammonium metabolism in the zooxanthellate coral, *Stylophora pistillata*. *Proc Roy Soc (London)* B236: 325-327.
- Searcy, D., G. 1992. Origins of mitochondria and chloroplasts from sulfur-based symbioses. In H. Hartman and K. Matson [eds.], *The origin and Evolution of cells*. World Scientific.
- Smetacek, V. 1998. Diatoms and the silicate factor. *Nature* 391: 224-225.
- Stanley, S. M. 1979. *Macroevolution. Pattern and process*. Freeman.
- Stark, P. 1994. Climate warming in the central Antarctic Peninsula. *Weather* 49.
- Wray, G. A., J. S. Levinton, and L. H. Shapiro. 1996. Molecular Evidence for Deep Precambrian Divergences Among Metazoan Phyla. *Science* 274: 568-573.

1.4 Tables

Table 1.1 Gibbs free energy changes for the oxidation of a mole of glucose ($C_6H_{12}O_6$) given various electron acceptors. Data take from Froelich et al. (1979).

Electron Acceptor	ΔG° (kJ/mole of Glucose)
O_2	-3190
MnO_2	-3090
NO_3^-	-3030
Fe_2O_3	-1400
SO_4^{2-}	-380
$2CH_2O \rightarrow CO_2 + CH_4(a)$	-350

a. This is methane formation or disproportionation.

2 Trophic transfer efficiency decreases in HNLC-like and Antarctic peninsula environments

(from Grzyski, J., Moline, M.A., and Cullen, J.T. 2002. Modeling atmosphere-ocean interactions and primary productivity. Lindholm, J. and Ruth, M. (eds) Springer Verlag. p. 125-143. and Moline, M. A., Claustre, H., Frazer, T., Grzyski, J., Schofield, O., and Vernet, M. 2000. Changes in phytoplankton assemblages and potential implications for the Antarctic food web. In: (Davidson, B. ed.) Antarctic Ecosystems: Models for Wider Ecological Understanding. Cambridge University Press, p.263-271.)

2.1 Abstract

Two models were formulated to describe potential changes in energy transfer efficiencies due to increased temperature and changes in nitrate uptake in relation to iron input. The Antarctic peninsular ecosystem undergoes changes in food web efficiencies due to increasing temperatures and the resultant increase in meltwater. In addition, portions of the Southern Ocean are considered high nutrient- low chlorophyll regions (HNLC) and have been targeted as places where increased conversion of inorganic carbon (CO₂) to sequestered organic carbon may mitigate some of the recent increase in atmospheric carbon. A food web model was constructed making assumptions about the trophic transfer efficiencies from two different size classes of phytoplankton to higher trophic levels, most especially, the Antarctic krill. We show that a decrease in the size class of phytoplankton will result in a decrease in the amount krill by as much as 30% and a decrease to 5% of the total amount of autotrophic carbon transferred to the highest trophic level in the peninsular ecosystem. This, combined with the fact that the efficiency of nitrate uptake by phytoplankton under current concentrations of iron in HNLC zones like the Southern Ocean and equatorial Pacific is very low puts further pressure on the biological pump in the Southern Ocean. However, according to our model a 64 fold increase in aeolian iron flux to the surface ocean results in a roughly 10

ppm decrease in atmospheric CO₂ concentrations *from biological activity alone*. These results agree with other recent estimates as well as emphasize the importance of physical processes in the atmosphere ocean CO₂ system. The combined impact of these two phenomena, however, would be far greater than the sum as increasing temperature not only de-stabilize the food web but result in a decrease in pCO₂ of the surface water due to off-gassing and a decrease in the formation of Antarctic bottom water.

2.2 Introduction

Food web models have been used to describe and quantify changes in resource abundance, competition, predation, biomass and stability given various environmental variables (May 1981). Marine ecosystem models are especially difficult to parameterize. Furthermore, the marine ecosystem is highly variable on seasonal, yearly, decadal and geologic timescales. Models have to properly account for these time scales.

Broad environmental concerns have become extremely popular in both scientific and media circles especially since the impact of the Industrial Revolution of the 19th century was discovered. The resultant increase in anthropogenic fossil fuel use has increased atmospheric (CO₂) from 280 to 360 ppm and warmed the Earth by approximately 0.4°C (Petit et al. 1999). “Global warming” has become a contentious buzzword. Changes in atmospheric CO₂ concentrations affect, and are affected by, interactions between the atmosphere and ocean, with potentially far-reaching implications for marine and terrestrial life. Understanding the effect of increased CO₂ on climate, biogeochemical cycles, ocean and terrestrial plant productivity has become the focus of much scientific research.

Marine ecosystems are often referred to being “top down” or “bottom up” controlled. The structure of a top down regulated ecosystem is a function of the grazer’s impact on the primary producing population while bottom up ecosystems are a function the availability of resources (phytoplankton) to the higher trophic levels. Changes in marine ecosystems from top down to bottom up or vice versa could have significant impacts on the biology and biogeochemistry of ocean regions. This is particularly significant in light of recent large scale manipulation experiments and the potential for basin wide iron fertilization experiments (Chisholm et al. 2001).

The purpose of this chapter is to diagnose the potential impact of environmental change on ecosystem function, structure and efficiency. Here we use a generalized model of the atmosphere-ocean CO₂ system and marine primary productivity to assess the potential impact of iron on nitrogen uptake and the efficiency of the biological pump. Secondly, we use an ecosystem model of the Antarctic peninsular region to assess the potential impact of changes in the size class of phytoplankton on grazers and higher trophic levels. In light of recently observed changes in the Antarctic peninsular ecosystem and Southern Ocean Iron experiments, the two models, although on different temporal and spatial scales, are remarkably inter-related. Both models show potentially large changes in the biological pump and ecosystem structure. Changes in the efficiency of the biological pump and in ecosystem structure are, in effect, changes in the conversion of inorganic carbon (CO₂) to phytoplankton biomass which is ultimately sequestered, remineralized or transferred to higher trophic levels, thus supporting a food chain. The cumulative impact of these two processes is threatening the Antarctic biogeochemical cycle.

2.2.1 Greenhouse gases and climate

Our current understanding of the ocean-atmosphere system and how anthropogenic activities will affect future climate changes relies heavily on our understanding of past perturbations of global climate detected in the geological record. Measurements of CO₂ concentrations in air bubbles trapped in polar ice cores have demonstrated that atmospheric CO₂ fluctuations of approximately 80 ppm (Petit et al. 1999) accompanied temperature fluctuations during the most recent Quaternary glacial-interglacial transition (12,000 years ago) on a time scale of 10³-10⁴ years. Whether or not present increases in atmospheric CO₂ will result in similarly drastic changes in global climate is partially dependent upon the ocean, the largest reservoir of inorganic carbon, and to what degree it will act to buffer atmospheric increases.

Because the vast majority of the combined atmosphere-ocean inorganic carbon pool resides in the sub-surface ocean (Sarmiento and Orr 1991), fluctuations in atmospheric CO₂ concentrations and the resulting shifts in global climate are thought to be forced by changes in the oceanic carbon cycle (Sundquist and Broecker 1985). Today, average surface ocean CO₂ concentrations are in equilibrium with the atmosphere while the deep ocean contains more CO₂ than could result from air-sea gas exchange alone (Broecker et al. 1980). The surplus of CO₂ in the deep ocean is in part maintained by a mechanism referred to as the biological pump (Anderson and Sarmiento 1994). The biological pump sequesters CO₂ from the atmosphere through the reduction of CO₂ by photoautotrophic organisms. In surface waters of the oceans, these organisms fix inorganic carbon (along with other nutrients) into organic molecules according to the equation for photosynthesis:



A fraction of the reduced carbon is removed from communication with the atmosphere when it sinks out of surface waters under the influence of gravity, and is remineralized in the deep ocean. The stoichiometry of the reaction represents, on average, the composition of the sinking biogenic material. Ratios of the major inorganic nutrients in the ocean interior are set by the net result of the redox reaction of carbon fixation and remineralization. The constant stoichiometry of marine export production, the Redfield ratio, is used to estimate carbon fluxes from changes in surface water nutrient concentrations (Redfield et al. 1963). In the modern ocean, the yield of this generalized reaction is thought to be limited by the supply of N (in the form of NO_3^-) to the euphotic zone because upwelled N:nutrient ratios are on average below the Redfield values (Anderson and Sarmiento 1994; Falkowski 1997). While the specific causes for variations in atmospheric CO_2 on glacial-interglacial time scales remain unknown, one way to explain the glacial increase of the oceanic carbon inventory and resulting reduction of atmospheric CO_2 levels is through increased biological pumping of carbon (increased export production) to the deep ocean (Martin 1990).

2.2.2 High nutrient low chlorophyll regions (HNLC)

In certain areas of today's ocean, such as the Southern Ocean and the Equatorial Pacific, the presence of excess surface nutrients and the virtual absence of phytoplankton biomass imply that the biological pump is not operating at its full potential (Martin 1990). These areas are referred to as high nutrient-low chlorophyll (HNLC) regions. A portion of the decrease in glacial atmospheric CO_2 could be accounted for if the biological pump were able to draw down these excess nutrients and associated inorganic carbon from the HNLC. In fact, organic carbon preserved in the sediments indicates that

export production from HNLC surface waters has co-varied with atmospheric CO₂ levels during the Quaternary (Berger et al. 1989). One way to increase the efficiency of the biological pump (export production) would be to enhance local levels of primary production.

Martin (1990) proposed that the reduction of atmospheric CO₂ during the past glaciation event was caused by increased biological production due to greater aeolian supply of Fe to ocean surface water. The “iron hypothesis” was advanced in order to address the question of why and how productivity in HNLC regions could have increased so remarkably during the last glaciation. During the last glaciation, Fe fluxes to the ocean surface were approximately 50 times higher than present day fluxes, and there is good correspondence between the supply of Fe and atmospheric CO₂ inferred from ice core records (Petit et al. 1999). The hypothesis assumes that in certain HNLC areas of the present day ocean, photosynthetic fixation of inorganic carbon is limited by low ambient Fe concentrations. Another assumption is that increased aeolian Fe supply could relax this limitation and allow excess surface nutrients to be utilized. Evidence supporting both of these assumptions comes from recent laboratory and large scale field experiments (Coale et al. 1996b; Martin et al. 1994; Martin et al. 1989; Morel et al. 1991; Sunda and Huntsman 1997). The global extent of iron limitation has also recently been extended to the Southern Ocean where presumably the potential impact on the carbon dioxide pump will be even greater (Boyd et al. 2000). Iron’s importance in the marine geochemistry of C and N stems from its central role in the physiology of marine primary producers.

Iron is an essential element for all but a few living organisms (Williams 1981).

Photoautotrophic physiology requires Fe for the production of chlorophyll, cytochromes and for the fixation and metabolism of nitrogen as a component of specific metalloenzymes. Although Fe is required in trace quantities compared to other major mineral nutrients it is largely insoluble in oxygenated seawater. Surface water concentrations of soluble, biologically available Fe are exceedingly low ($< 1 \times 10^{-9}$ mol L^{-1}) in the open ocean and depth profiles resemble those of other major plant nutrients (Bruland 1983; Martin and Gordon 1988; Martin et al. 1989). The transport of Fe into the euphotic zone as estimated from simple advective/diffusive models alone appears to be insufficient to allow marine phototrophs to deplete ambient macronutrients such as nitrate and phosphate (Martin 1990). Without additional sources of Fe, such as aeolian deposition, HNLC regions appear to be Fe limited ecosystems with low levels of phytoplankton biomass, primary productivity and export production.

2.2.3 Antarctic peninsular region

Mean air temperatures along the Antarctic Peninsula have increased significantly (2-3°C) over the past 50 years (King 1994; Smith et al. 1996; Stark 1994). Increased temperatures likely alter the spatial extent and timing of glacial meltwater runoff. Lower salinity water has direct consequences on water column stability. Five years of long-term ecosystem research (LTER) data confirm that increases in air temperature and concomitant decreases in salinity result in cryptophytes accounting for a greater proportion of phytoplankton biomass (Moline et al. 2001). The potential decrease in diatoms and export production will have multiplicative effects on atmosphere-surface ocean pCO_2 equilibrium when the physical processes CO_2 cycling are considered.

The Antarctic coastal ecosystem is dominated by a short but rapid burst of growth in summer. However, the magnitude and extent of the success of trophic transfer from phytoplankton to the highest trophic level is dependent on many environmental factors that impact the stability of the water column. Rates of primary productivity and accumulation of biomass are related to sea-ice interaction and sustained periods of water column stability (Moline 1997; Moline and Prezelin 1996). As well, the magnitude and temporal extent of favorable conditions for phytoplankton growth affects distribution and succession in both open-water and nearshore environments. Until recently, however, the effects of changing light/nutrient regimes on the structure of phytoplankton communities have received little attention (Sommer 1986; Sommer 1988; Sommer 1991; Sommer 1994; Sommer and Stabel 1986). The structure and successional dynamics of phytoplankton is important ecologically because the growing season is so short. The feeding efficiency of grazers, especially krill, the keystone species in the Antarctic ecosystem, is impacted by the phytoplankton community composition (Quetin and Ross 1985). The phytoplankton community composition and successional dynamics also have biogeochemical consequences. Diatoms significantly impact silica cycling (Leynaert et al. 1991; Nelson et al. 1991; Quéguiner et al. 1991). The size class of phytoplankton also significantly impact assimilation rates of nutrients (Boyd and Newton 1995; Claustre et al. 1997; Goeyens et al. 1991; Owens et al. 1991) and hence the flux of particulate organic carbon and nitrogen to the deep ocean. Large-scale environmental changes, therefore, that affect the size class of phytoplankton could have significant impacts on both the Antarctic food web and sequestration of organic carbon. The goal of the Antarctic food web model was to assess the potential changes in the trophic transfer of

organic carbon given observed changes in phytoplankton community composition (Moline et al. 2000). The impacts of these changes in community composition have already been observed in large-scale shifts in zooplankton communities (Loeb et al. 1997) and penguin populations (Fraser et al. 1992; Trivelpiece et al. 1990).

2.3 Atmosphere-Ocean interaction model

The model is a one-dimensional, time dependent box model that tracks the movement of carbon, nitrogen (NO_3^-), and Fe through a conceptualized open ocean ecosystem. With the exception of NO_3^- , nutrients are permitted to cycle through four major reservoirs: the atmosphere, the surface ocean, the deep ocean and the sediment. We assume that atmospheric inorganic nitrogen deposition is insignificant compared to the flux of upwelled nitrogen to the surface ocean reservoir. Vertical particulate fluxes from the surface to deep ocean in the model result from the sinking of phytoplankton cells (primarily diatoms and calcite-forming organisms).

2.3.1 Inorganic carbon fluxes

When the processes of photosynthesis and respiration are balanced in the biosphere the concentration of atmospheric CO_2 is regulated by equilibration with the ocean surface water [pCO_2]. Equilibrium between atmosphere and surface water [CO_2] is achieved through the exchange of carbon dioxide across the air-sea interface (units, $\text{M m}^{-2} \text{ day}^{-1}$) and is governed by the difference in partial pressure between the atmosphere and ocean surface waters and the piston velocity (τ , m day^{-1}) – a measure of the diffusivity of CO_2 and surface water mixing.

$$\text{Air sea exchange} = \tau (\text{pCO}_{2(\text{atm})} - \text{pCO}_{2(\text{aq})}) \quad \text{Eq.2.2}$$

While changes in the concentration of $\text{CO}_{2(\text{atm})}$ are relatively easy to model, the concentration of $\text{CO}_{2(\text{aq})}$ is a function of the carbonate chemistry of seawater. The solubility of CO_2 in seawater exceeds that for other inert gases because it can exist as three distinct species according to the following thermodynamic relationships:



The sum of these dissolved inorganic carbon species is designated C_t and is defined as

$$C_t = \text{H}_2\text{CO}_3^* + \text{HCO}_3^- + \text{CO}_3^{2-} \quad \text{Eq.2.6}$$

In order to solve for any of the inorganic carbon species two of the following four parameters must be known: pH, C_t , $\text{pCO}_{2(\text{aq})}$ and TA (total alkalinity). Total alkalinity (TA) is defined as the sum of all the bases that can accept a proton at the H_2CO_3 endpoint:

$$\text{TA} = \text{HCO}_3^- + 2(\text{CO}_3^{2-}) + \text{B(OH)}_4^- + \text{OH}^- - \text{H}^+ + \text{other bases} \quad \text{Eq.2.7}$$

When characterizing the system in terms of CO_2 alone, alkalinity can be simplified to the total carbonate alkalinity (CA):

$$\text{CA} = \text{HCO}_3^- + 2(\text{CO}_3^{2-}) \quad \text{Eq.2.8}$$

Before the concentration of $\text{CO}_{2(\text{aq})}$ can be known, we must calculate the pH ($\text{pH} = -\log [\text{H}^+]$) of the system. In order to limit the complexity of the calculations, we assume that in the pH range 7.8-8.5 the relationship is a linear function of C_t :

$$\text{pH} = -1805.4 \cdot C_t + 12.1 \quad \text{Eq.2.9}$$

Having solved for pH given C_t and CA, we can now calculate the concentration of $\text{CO}_{2(\text{aq})}$ using the ionization fractionation parameter (α_0) and the relationship

$$\text{CO}_{2(\text{aq})} = C_t \alpha_0 \quad \text{Eq.2.10}$$

where

$$\alpha_0 = (1 + 10^{-6.3}[\text{H}^+]^{-1} + 10^{-16.6}[\text{H}^+]^{-2})^{-1} \quad \text{Eq.2.11}$$

Solving equation (2.2) at each time step enables us to determine the potential flux of CO_2 from the atmosphere into the ocean (and in the reverse direction if the sign is negative). The concentration of CO_2 in a given volume of atmosphere (ppm/v) can easily be calculated from the total molar amount of CO_2 . The corresponding calculations are carried out in the CO_2 module shown in figure 2.1. In that module, the particulate C associated with sinking N is calculated using the average C/N ratio of marine plankton of 6.6 mol mol^{-1} (Redfield et al. 1963). Diffusion of CO_2 into and out of the surface ocean from and to the atmosphere is set by the concentration gradient of CO_2 between the atmosphere and the ocean and the piston velocity (τ). It should be noted that a rigorous examination of the physical influx and efflux of CO_2 from the ocean would require careful parameterization of this variable. For the purposes of the biological model the constant suffices.

2.3.2 Nutrient regulation of phytoplankton carbon fixation

The growth and sinking of marine phytoplankton represents an important conduit through which atmospheric CO_2 can enter and be sequestered in the deep ocean. The growth of marine phytoplankton requires the presence of many nutrients. Recent laboratory and field studies have shown N and Fe to be particularly important (Coale et

al. 1996a; Price et al. 1994). Nitrogen in the form of ammonium is an essential component of amino acids, the building blocks of proteins. Nitrogen limitation therefore results in a host of problems at the biochemical and biophysical level, causing reduced CO₂ fixation and ultimately reduced growth (Herzig and Falkowski 1989). In the oxygenated modern ocean the thermodynamically stable form of N is nitrate (NO₃⁻). Before nitrate can be incorporated into amino acids, for example, it must be reduced to NH₃ or NH₄⁺. This incorporation is accomplished with the two iron-containing enzymes nitrite and nitrate reductase.

Iron is an essential part of the photosynthetic apparatus. Iron limitation leads to a decrease in the efficiency of light energy conversion to reducing agents (Greene et al. 1991a; Greene et al. 1992). In areas of the ocean with high NO₃⁻ concentrations but low chlorophyll and low productivity, an addition of iron stimulates uptake of NO₃⁻ by marine phytoplankton, which is accompanied by a drawdown of atmospheric pCO₂ (Cooper et al. 1996).

Uptake of nitrate after addition of iron can be approximated (Coale et al. 1996a) by a simple Michaelis-Menten function of uptake velocity ($V_{\text{NO}_3^-}$) as a function of substrate concentration (Fe), the maximum uptake velocity (V_{max}) and the concentration of Fe supporting half saturated uptake (K_s) where $V_{\text{NO}_3^-} = 1/2 V_{\text{max}}$:

$$V_{\text{NO}_3^-} = (V_{\text{max}} N [\text{Fe}]) / (K_s + [\text{Fe}]) \quad \text{Eq. 2.12}$$

Equation (2.12) is used in Figure 2.2, to calculate NO₃⁻ uptake, or the conversion of dissolved inorganic N to particulate N that is then removed to deep water. K_s is set to 5pM and $V_{\text{max}} N$ to 0.11 mol per year.

The structure of the Fe module of this model follows that of the N and C modules and is shown in figure 2.3. Analogous to Figure 2.2, this module uses the Michaelis-Menten function to calculate particulate Fe fluxes to the deep ocean, using an average Fe:N ratio. The value for the Fe:N ratio applied in the model ($1.65 \times 10^{-4} \text{ mol mol}^{-1}$) has been determined for species of marine phytoplankton maintained in laboratory culture (Morel and Hudson 1984).

In the model, the major particulate flux of carbon from the surface water to the deep ocean and sediments occurs in the form of CaCO_3 burial. We incorporate in the model a constant background flux (i.e. independent of Fe availability) of C, N and Fe from calcite forming organisms (Broecker and Peng 1982). Calculating downward particulate flux of C, N, and Fe in this manner assumes:

- (a) ocean nutrient inventories remain constant;
- (b) the downward flux of particulate material results largely from the growth and sinking of diatoms (Goldman 1993);
- (c) the relative elemental ratios of C:N:Fe in sinking biogenic material are constant over the time scales considered in the model;
- (d) the downward flux of biogenic material or export production in this model is set by the input of Fe into the surface ocean;
- (e) when Fe concentrations are sufficient for maximum NO_3^- uptake the downward flux of particulate C and, therefore, atmospheric CO_2 concentrations are controlled by, and equal to, the upwelling flux of NO_3^- from deep water to the surface ocean. This is also the definition of new production (Dugdale and Goering 1967; Eppley and Peterson 1979).

Additionally, the model assumes that

- (f) downwelling and upwelling fluxes of the dissolved chemical species are calculated based on the concentration of the species (mol m^{-3}) and the mean ocean downwelling and upwelling rates of $0.39 \text{ m (day)}^{-1}$ (Broecker and Peng 1982);
- (g) particulate matter burial equals 1% of the flux of the particulate matter to the deep ocean;
- (h) Particulate matter remineralization that occurs on the time scale of ocean mixing ~3000 years (Broecker and Peng 1982). This implies that on these time scales there is no organic matter preservation (i.e. steady state).

Assumptions (a) – (h) link the C, N and Fe portions of the model. Despite a fixed relationship between the incorporation of C, N and Fe into particulate matter the relative drawdown of carbon from the atmosphere and surface ocean into the deep ocean is a function of the concentrations of the two major plant nutrients N and Fe. Changing either the ratio of C:N:Fe in particulate matter or the absolute uptake of N (mol yr^{-1}) does not alter the model's function – it will only change the relative drawdown or accumulation of CO_2 in the atmosphere and surface ocean. Fluxes of dissolved C, N and Fe in and out of the surface and bottom waters are a function of the concentration gradient of the nutrient and the velocity of the flux (measured in m day^{-1}). Because of deep ocean remineralization of particulate matter the concentration of C, N and Fe is higher in the deep ocean than in the surface. This results in a positive flux of nutrients into the surface water. Changes in ocean circulation patterns occurring over geologic time scales more than likely alter the magnitude of this flux (Boyle 1988).

2.4 Trophic transfer model

This model quantifies the portioning of organic carbon through the Antarctic food web (Figure 2.4). Total autotrophic carbon production serves as the model's primary input, which was partitioned into either cryptophytes or diatoms and other phytoplankton groups. Input values were based on measurements made throughout December and January of 1991-94 (Moline and Prézelin 1996). The relative fluxes from the primary carbon pool to krill, salps and other grazers (i.e. copepods) were dependent on the phytoplankton assemblage and transfer efficiencies. Transfer efficiencies of carbon (cryptophytes to krill = 10%, cryptophytes to salps= 60%, diatoms and other phytoplankton to krill=60%, and diatoms and other phytoplankton to salps= 60%) define the efficiency of ingestion for the krill and salps given different diets. The values used were mean values from previous studies relating percent retention of algae by krill based on size (MacClatchie and Boyd 1983; Meyer and El-Sayed 1983; Boyd et al. 1984; Quetin and Ross 1985) and on feeding studies of *Salpa thompsoni* (Madin and Kremer 1995), a major tunicate in the Southern ocean (Huntley et al. 1989). Partitioning of carbon to grazers was also a function of a range of previously reported krill to salp ratios (Pakhomov et al. 1994; Nishikawa et al. 1995; Loeb et al. 1997). Carbon from grazers was directed either to higher trophic levels, sedimentation or respiration. Transfer of carbon from krill to respiration was 34% (Huntley et al. 1991), from krill to higher trophic levels was 32.5% (Huntley et al. 1991), with the remainder going to sedimentation. Transfer of carbon from salps to respiration was 14.8% (Huntley et al. 1998), from salps to higher trophic levels was assumed low at 5% (Foxton 1966; Gon and Heemstra 1990), with the remaining fraction going to sedimentation.

2.5 Model results and discussion

2.5.1 HNLC

To run the model we initialize it with data for nutrient concentrations and atmospheric CO₂ that reflect modern levels. We assume an initial CO₂ concentration of the atmosphere of 10.9 μM m⁻³, which is the volumetric equivalent to a [pCO₂] of the atmosphere of 345 μATM. This conversion is necessary to calculate the flux (units, M m⁻² day⁻¹). We set C_t for surface and bottom water to 2.19 μM (= 219 mol/100 m³) and 2.31 μM (= 7854 mol/3400 m³), respectively. The model assumes a surface ocean of 100 m and an area 1m². The deep ocean is 3400m. Initial Fe in surface and bottom waters are set at 0.26 pM (= 2.6 10⁻⁸ mol/100 m³) and 1.2 pM (= 4.08 10⁻⁸ mol/3400 m³), respectively. Initial NO₃⁻ concentrations in surface and bottom waters are 12 μM (= 1.2 mol/100 m³) and 30 μM (= 102 mol/3400 m³), respectively. The results of the first scenario are derived for an aeolian Fe flux of 2.05 10⁻⁷ mol/100m³ per year and are shown as Graph 1 in figure 2.9 and table 2.1. In these figures are also plotted the results of model runs that assume, respectively, a doubling (Graph 2), four-fold (Graph 3), eight-fold (Graph 4) and sixteen-fold (Graph 5) increase in the aeolian flux of Fe.

These results presume that in HNLC regions primary productivity and the amount of CO₂ that can be removed from the atmosphere are set by the combined Fe fluxes from upwelling and aeolian deposition. An increase in the total flux of Fe into the surface waters (figure 2.9 & 2.10) will change the complex chemistry of iron in seawater. Phytoplankton are thought to only access the free ion of Fe for growth (Hudson and Morel 1993; Morel et al. 1991; Sunda 1994). The free ion concentration of Fe in solution is a function of the solubility, degree of complexation by organic ligands,

absorption/scavenging and photo-reduction/oxidation reactions in the surface and deep ocean (Johnson et al. 1997). Therefore, a realistic model of iron/ nitrate interactions should include a component that calculates the various pools of iron, both bio-available and refractory. On longer time scales considered in this model, we assume that the free ion activity of Fe is a linear, increasing function of total Fe in the system, so that any increase of ambient Fe will lead to an increase in production. Increasing the complexity of the model with respect to Fe speciation does not change the qualitative behavior of the model.

Because open ocean HNLC regions are far removed from terrestrial sources of Fe and continental shelf sediments, riverine Fe fluxes and advective Fe inputs to surface waters are extremely low. Therefore, the primary inputs of Fe required to promote photosynthesis in these ecosystems must come from either upwelled water or the aeolian flux (Coale et al. 1996a; Martin 1990). As mentioned above, Fe is extremely insoluble in oxygenated seawater resulting in very low amounts of bioavailable Fe (available for uptake by phytoplankton). In fact, bioavailable Fe in HNLC regions is below the best estimates of K_s (where Fe uptake is half saturated) for marine diatoms. This suggests that Fe uptake may be diffusion limited for all but the smallest phytoplankton (Hudson and Morel 1993).

Figure 2.9 shows that higher aeolian Fe fluxes reduce the steady-state levels of atmospheric $[pCO_2]$, with a four-fold increase resulting in long-run $[pCO_2]$ that is nearly the same as the initial conditions. Figure 2.10 shows the temporary downward adjustments in Surface C_t and ultimate rise to the steady-state level that accompany

initially high levels in surface Fe. The exception is the case in which there is a sixteen-fold increase in Fe, and a continuous reduction of surface C_t .

A basic simplification of the model is that the size structure of the phytoplankton community is not considered, which can have important implications for the biogeochemical cycling of carbon and the productivity of the ecosystem. A defining feature of HNLC regions is the absence of large phytoplankton ($>5 \mu\text{m}$) and the predominance of small primary producers (Chavez 1989; Price et al. 1994). However, upon relief of iron limitation (and the diffusion barrier) larger diatoms can rapidly dominate the biomass of primary producers (Price et al. 1994; Price et al. 1991). This shift in the size of primary producers affects both the kinetics of nutrient uptake – largely through changes in surface area to volume ratio (Morel et al. 1991) – and the amount of export production from the ecosystem (removal of CO_2 from surface to deep water).

A constant relationship is assumed between surface water $[\text{Fe}]$ and uptake rate of NO_3^- in the model that is characteristic of large, rapidly growing phytoplankton. In HNLC regions, where Fe concentrations are limiting, small cells predominate which have lower K_s , $V_{\max\text{NO}_3}$, and absolute growth rates than larger diatoms. Under Fe limiting conditions the phytoplankton community is unable to remove all upwelled NO_3^- and a surplus is observed to exist in surface waters. Each unutilized mole of NO_3^- represents 6.6 moles of potential atmospheric CO_2 drawdown if the biological pump was operating efficiently. When Fe is added to the system large phytoplankton proliferate and deplete NO_3^- with a concomitant drawdown of atmospheric CO_2 . Because the model underestimates the utilization of nutrients (C and N) under Fe limiting conditions the

difference in atmospheric CO₂ concentrations between Fe depleted and replete scenarios is a conservative estimate.

Over the geologic time scales of the model, the simplification to a homogenous population of phytoplankton still enables us to represent this system. The model shows that under the initial conditions the supply of NO₃⁻/Fe to the surface ocean is significantly higher compared to the Redfield ratios of particulate matter, indicating iron limitation. This is also represented by plots of the relationship between surface iron inventory and NO₃⁻ incorporated into particulate matter (figure 2.6). The result is that under the initial conditions maximal particulate nitrate fluxes equal less than 0.25 mol N m⁻² yr⁻¹. The amount of Fe input to the surface can only support a downward flux of particulate carbon that equals 5% of the potential given NO₃⁻ inputs. Under these conditions the ocean is a source of CO₂ to the atmosphere (Figure 2.5). This phenomenon is typical of warm water upwelling systems where high Ct, nutrient rich bottom water reaches the surface, is warmed, decreasing the solubility of CO₂ in water and diffuses into the atmosphere (Cooper et al. 1996). To a certain extent the HNLC ocean can become a sink for atmospheric carbon if surface concentrations of iron increase. Under such conditions the efficiency of the biological pump increases because nitrate uptake efficiencies increase resulting in more particulate organic carbon (figure 2.8). This reverses the sign of air-sea exchange making the ocean a sink, thereby decreasing atmospheric pCO₂ by as much as 12 ppm (figure 2.9).

2.5.2 Antarctic peninsular ecosystem

The recurrent transition from diatoms to cryptophytes in a multi-year study is strongly correlated to both decreases in salinity and increasing temperatures along the

Antarctic Peninsula (Moline and Prézelin 1996; Moline 1998). With regards to the overlying food web this means a decrease in the size-class of phytoplankton. Bloom-forming diatoms range in size from 15-270 μm (Krebs 1983; McMinn and Hodgson 1993), while cryptophytes at this study site were measured at $8 \pm 2 \mu\text{m}$ (see McMinn and Hodgson 1993; Kang and Lee 1995). This size difference can impact the grazing efficiencies of key zooplankton species. Antarctic krill, *Euphausia superba*, for example, does not feed equally well on all sizes classes of phytoplankton; cells $< 20 \mu\text{m}$ are retained with $< 50\%$ efficiency (MacClatchie and Boyd 1983; Meyer and El-Sayed 1983; Boyd et al. 1984; Quetin and Ross 1985; Granéli et al. 1993). Moreover, recent field evidence suggests that adult krill selectively graze larger phytoplankton cells resulting in a relative increase in the abundance of smaller cells including cryptophytes (Kopczynska 1992). In contrast, salps are capable of feeding on a large range of particle sizes and have been shown to effectively graze on phytoplankton in the size range of cryptophytes (Madin and Kremer 1995).

Phytoplankton assemblages can also influence the distribution of krill (Daly and Macauley 1991; Madin and Kremer 1995; Quetin et al. 1996). Increased cryptophyte dominance may cause adult krill to exhibit a directed offshore movement, independent of hydrography (Kanda et al. 1982), to more effectively graze larger diatom populations. Krill is considered the keystone species in the Antarctic marine food web and shifts in its spatial distribution during summer will affect numerous organisms, particularly penguins and some seals/whales. As an example, the foraging distances for land-based species such as the Adelie penguin would likely increase with a negative feedback to its growth and reproduction (Fraser and Trivelpiece 1996). The impact on higher trophic levels may

be especially significant, as cryptophyte dominance occurs during summer months when feeding activities and growth of most species are maximal (Laws 1985).

High concentrations of cryptophytes and the absence of krill in nearshore waters may allow for a proliferation of salps, which reproduce rapidly in response to favorable environmental conditions via asexual reproduction (see Alldredge 1984 for relevant review). In fact, *Salpa thompsoni* was abundant in coastal areas, including the Palmer basin, and less prevalent offshore during the summer months of 1993-94 (Ross et al. 1996), coincident with a peak occurrence of cryptophytes.

A recent report documents a long-term shift in the zooplankton community near Elephant Island in response to fluctuations in sea-ice cover and changes in mean air temperature (Loeb et al. 1997). Colder years with extensive sea-ice development were found to favor reproduction and survival of Antarctic krill, *Euphausia superba*, while warmer years, where mean yearly air temperatures occasionally exceeded -1°C , reduced the extent of sea-ice and showed *Salpa thompsoni* was the dominant herbivore (Loeb et al. 1997). Other studies have also quantified this inverse distribution of krill versus salps near the Antarctic Peninsula (Huntley et al. 1989; Nishikawa 1995) and frontal regions (Pakhomov et al. 1994). The food web model was developed to quantify the potential effects of changing phytoplankton size class and zooplankton assemblage on the flow of carbon through the Antarctic food web (figure 2.4). Model results revealed that both a shift in the phytoplankton community composition and in the ratio of krill to salp biomass significantly altered the amount of carbon available to higher trophic levels and increased sedimentation/microbial loop (figure 2.11). From 1991 to 1994, the percent of total carbon production from cryptophytes during summer months increased from 19% to

53%. The direct effect of this change in phytoplankton productivity was to decrease the amount of carbon flow through krill by 32% (figure 2.11a). The decreased phytoplankton size and decreased grazing efficiencies by krill caused a threefold increase in the carbon available to salps. Salp dominated grazer systems transfer less carbon to higher trophic levels (4%) and more carbon (62%) that is either exported out of the system or contained in the microbial loop. Sedimentation as a result of salp feeding activities increased fivefold. Similarly, Boyd and Newton (1995) have shown that between years of similar biomass and productivity, the changes in the community structure can alter the flux of particulate organic carbon by two fold. The increased abundance of cryptophytes would decrease the biogenic silica production in the upper water column and decrease the rate and quantity of biogenic silica accumulation in the sea-bed.

In response to a relative decrease in krill abundance, the model revealed that 75% of fixed carbon originally transferred to higher trophic levels would be redirected to the sediments or the microbial loop (figure 2.11b). The decreased krill to salp ratio was also shown to double the carbon sedimented or available to the microbial loop. This is in part caused by decreased krill fecal pellet production and the fact that salps are not efficiently utilized as a carbon source by other predators (Foxton 1966; Gon and Heemstra 1990). These outputs should also be viewed as conservative, given that the model does not incorporate the 7:1 ratio of the longevities of krill and salps, respectively. Model results illustrate that the influence of cryptophytes and the change in zooplankton community has the potential of altering the structure of the food web and directing carbon away from

use by top vertebrate predators of the Antarctic ecosystem, such as fishes, birds, seals and whales.

2.6 Conclusions

These models represent physical processes very simply: heat exchange is not represented, mixing rates are constant, and in the one-dimensional model no lateral advection occurs. The temperature of surface waters has a profound effect on the solubility of CO_2 and the resulting equilibrium concentration of dissolved CO_2 (Millero 1995). Because cold water holds much more CO_2 , the high latitude HNLC regions (Subarctic Pacific and Southern Ocean) are more likely to act as sinks for atmospheric CO_2 despite inefficient surface nutrient utilization. Thus, the increasing temperatures are having a negative impact on the solubility of CO_2 in water (K_h decreases). In addition, the Southern Ocean is an important area of deepwater formation where cold surface waters and inorganic and organic carbon effectively and rapidly communicate with the ocean interior. Decreases in deep water formation will have a similar negative impact on removing CO_2 from communication with the atmosphere. Regionally specific models that incorporate temperature dependent equilibrium constants for the carbonate system may allow for more accurate calculation of CO_2 fluxes. We expect that the equilibrium constants used for this model (20°C) lead to a conservative estimate of air-sea CO_2 exchange. Including cold surface waters with increased production in response to Fe additions should lead to a much greater effect on the atmospheric pCO_2 .

Other simplifications in this model that would otherwise contribute to the remineralization of nutrients and export flux in marine ecosystems are the exclusion of higher trophic level grazers and the microbial loop. These trophic levels effect the

recycling of nutrients in surface waters and therefore, the amount of export production. However, we assume that the overall production in oligotrophic waters (and hence, the maximal drawdown of CO_2) is regulated by the upwelling flux of NO_3^- and, more importantly in the HNLC, the combined upwelling and aeolian inputs of Fe. Therefore, the effects of these annual and inter-annual processes are minimal compared to the *a priori* knowledge of iron limitation in this system. The failure to consider the microbial loop in the food web limits our ability to quantify changes in the biological pump based on changing phytoplankton functional groups and subsequent changes in krill and salps. However, the importance of phytoplankton size class on the grazing efficiency of krill and salps has been demonstrated. The synergistic impact of increasing temperature, low nutrients and a short growing season is a fundamental change in the ecosystem structure of the Antarctic peninsular region.

Because the HNLC model is in steady state the sources and sink terms are constant; on geologic time scales this is not true. The model could be easily modified to incorporate changes in the NO_3^- inventory driven by Fe availability by adding a sink and source term sensitive to surface Fe concentrations. Increasing the Fe flux to surface water has the potential to affect the relative rates of nitrogen fixation and denitrification. These interactions have been hypothesized to regulate the oceanic inventory of oxidized nitrogen on geologic time scales (Falkowski 1997). In essence, an increase in Fe and the concomitant increase in nitrogen fixation would have the eventual effect of increasing the upwelling concentration of NO_3^- in the world's oceans. This creates another potential positive feedback between iron supply and primary production. If, on the other hand, the

relative ratio of nitrogen fixation/denitrification decreases, NO_3^- is consumed and the maximum potential for primary production decreases.

2.7 References

- Anderson, L. A., and J. L. Sarmiento. 1994. Redfield ratios of remineralization determined by nutrient data analysis. *Global Biogeochemical Cycles* **8**: 65-80.
- Berger, W. H., V. S. Smetacek, and G. Wefer. 1989. Productivity of the ocean: present and past. Wiley.
- Boyd, P., and P. Newton. 1995. Evidence of the potential influence of planktonic community structure on the interannual variability of particulate organic carbon flux. *Deep-Sea Res.* **42**: 619-639.
- Boyd, P. and others 2000. A mesoscale phytoplankton bloom in the polar Southern Ocean stimulated by iron fertilization. *Nature* **407**: 695-702.
- Boyle, E. A. 1988. Cadmium: chemical tracer of deepwater paleoceanography. *Paleoceanography* **3**: 471-489.
- Broecker, W. S., and T.-H. Peng. 1982. Tracers in the Sea. Eldigio Press.
- Broecker, W. S., T.-H. Peng, and R. Engh. 1980. Modelling the carbon system. *Radiocarbon* **22**: 565-598.
- Bruland, K. W. 1983. Trace Elements in Sea-water, p. 157-220, Chemical Oceanography. Academic Press.
- Chavez, F. P. 1989. Size distribution of phytoplankton in the central and eastern tropical Pacific. *Global Biogeochemical Cycles* **3**: 27-35.
- Chisholm, S. W., P. G. Falkowski, and J. J. Cullen. 2001. Dis-crediting ocean fertilization. *Science* **294**: 309-310.
- Claustre, H., M. A. Moline, and B. B. Prezelin. 1997. Sources of variability in the column photosynthetic cross section for Antarctic coastal waters. *Journal of Geophysical Research-Oceans* **102**: 25047-25060.
- Coale, K. H., S. E. Fitzwater, R. M. Gordon, K. S. Johnson, and R. T. Barber. 1996a. Control of community growth and export production by upwelled iron in the equatorial Pacific Ocean. *Nature* **379**: 621-624.
- Coale, K. H. and others 1996b. A massive phytoplankton bloom induced by an ecosystem-scale iron fertilization experiment in the equatorial Pacific Ocean. *Nature* **383**: 495-501.
- Cooper, D. J., A. J. Watson, and P. D. Nightingale. 1996. Large decrease in ocean-surface CO_2 fugacity in response to *in situ* iron fertilization. *Nature* **383**: 511-513.
- Dugdale, R. C., and J. J. Goering. 1967. Uptake of new and regenerated forms of nitrogen in primary productivity. *Limnology and Oceanography* **12**: 196-206.
- Eppley, R. W., and B. J. Peterson. 1979. Particulate organic matter flux and planktonic new production in the deep ocean. *Nature* **282**: 677-680.
- Falkowski, P. G. 1997. Evolution of the nitrogen cycle and its influence on the biological sequestration of CO_2 in the ocean. *Nature* **387**: 272-275.
- Fraser, W. R., W. Z. Trivelpiece, D. G. Ainley, and S. G. Trivelpiece. 1992. Increases in Antarctic penguin populations: reduced competition with whales or a loss of sea ice due to environmental warming? *Polar Biology* **11**: 525-531.
- Goeysens, L., F. Sorensson, P. Tréguer, J. Morvan, M. Panouse, and F. Dehairs. 1991. Spatiotemporal variability of inorganic nitrogen stocks and uptake fluxes in the Scotia-Weddell Confluence area during November and December 1988. *Mar. Ecol. Prog. Ser.* **77**: 7-19.
- Greene, R. M., R. J. Geider, and P. G. Falkowski. 1991. Effect of iron limitation on photosynthesis in a marine diatom. *Limnology and Oceanography* **36**: 1772-1782.
- Greene, R. M., R. J. Geider, Z. Kolber, and P. G. Falkowski. 1992. Iron-Induced Changes in Light Harvesting and Photochemical Energy-Conversion Processes in Eukaryotic Marine-Algae. *Plant Physiology* **100**: 565-575.
- Hudson, R. J. M., and F. M. M. Morel. 1993. Trace metal transport by marine microorganisms: implications of metal coordination kinetics. *Deep-Sea Research* **40**: 129-150.
- Johnson, K. S., R. M. Gordon, and K. H. Coale. 1997. What controls dissolved iron concentrations in the world ocean? *Marine Chemistry* **57**: 137-161.
- King, J. C. 1994. Recent climate variability in the vicinity of the Antarctic Peninsula. *International Journal of Climatology* **14**: 357-369.

- Leynaert, A., P. Tréguer, B. Quéguiner, and J. Morvan. 1991. The distribution of biogenic silica and the composition of particulate organic matter in the Weddell-Scotia Sea during spring 1988. *Mar. Chem.* **35**: 435-447.
- Loeb, V. and others 1997. Effects of sea-ice extent and krill or salp dominance on the Antarctic food web. *Nature* **387**: 897-900.
- Martin, J. H. 1990. Glacial-interglacial CO₂ change: The iron hypothesis. *Paleoceanography* **5**: 1-13.
- Martin, J. H. and others 1994. Testing the iron hypothesis in ecosystems of the equatorial Pacific Ocean. *Nature* **371**: 123-129.
- Martin, J. H., and R. M. Gordon. 1988. Northeast Pacific iron distributions in relation to phytoplankton productivity. *Deep-Sea Research* **35**: 177-196.
- Martin, J. H., R. M. Gordon, S. Fitzwater, and W. W. Broenkow. 1989. VERTEX: phytoplankton/iron studies in the Gulf of Alaska. *Deep-Sea Research* **36**: 649-680.
- May, R. M. 1981. Patterns in multi-species communities, p. 197-227. *In* R. M. May [ed.], *Theoretical ecology*. Sinauer.
- Millero, F. J. 1995. Thermodynamics of the carbon dioxide system in the oceans. *Geochim. Cosmochim. Acta* **59**: 661-677.
- Moline, M., Prézelin, B. B., Schofield, O., Smith, R. C. 1997. Temporal dynamics of coastal Antarctic phytoplankton: physical/chemical/biological linkages through a summer diatom bloom., p. 67-72. *In* J. V. B. Battaglia, and D. W. H. Walton [ed.], *Antarctic Communities*. Cambridge University Press.
- Moline, M. A., H. Claustre, T. K. Frazer, J. Grzyski, O. M. Schofield, and M. Vernet. 2000. Changes in phytoplankton assemblages along the Antarctic Peninsula and potential implications for the Antarctic food web, p. 334. *In* W. Davison, C. Howard-Williams and P. Broady [eds.], *Antarctic Ecosystems: models for wider ecological understanding*. New Zealand Natural Sciences.
- . 2001. Changes in phytoplankton assemblages along the Antarctic Peninsula and potential implications for the Antarctic food web, p. 334. *In* P. Broady [ed.], *Antarctic Ecosystems: models for wider ecological understanding*. New Zealand Natural Sciences.
- Moline, M. A., and B. B. Prézelin. 1996. Long-term monitoring and analyses of physical factors regulating variability in coastal Antarctic phytoplankton biomass, in situ productivity and taxonomic composition over subseasonal, seasonal and interannual time scales. *Marine Ecology-Progress Series* **145**: 143-160.
- Morel, F. M. M., and R. J. M. Hudson. 1984. The geobiological cycle of trace elements in aquatic systems: Redfield revisited, p. 251-281.
- Morel, F. M. M., J. G. Rueter, and N. M. Price. 1991. Iron nutrition of phytoplankton and its possible importance in the ecology of ocean regions with high nutrient and low biomass. *Oceanography* **4**: 56-61.
- Nelson, D. M., J. A. Ahern, and L. J. Herlihy. 1991. Cycling of biogenic silica within the upper water column of the Ross Sea. *Mar. Chem.* **35**: 461-476.
- Owens, N. J. P., J. Priddle, and M. J. Whitehouse. 1991. Variations in phytoplanktonic nitrogen assimilation around South Georgia and in the Bransfield Strait (Southern Ocean). *Mar. Chem.* **35**: 287-304.
- Petit, J. R., J. Jouzel, D. Raynaud, N. I. Barkov, J.-M. Barnola, and I. Basile. 1999. Climate and atmospheric history of the past 420,000 years from the Vostok ice core, Antarctica. *Nature* **399**: 429-436.
- Price, N. M., B. A. Ahner, and F. M. M. Morel. 1994. The equatorial Pacific Ocean: Grazer-controlled phytoplankton populations in an iron-limited ecosystem. *Limnology and Oceanography* **39**: 520-534.
- Price, N. M., L. F. Andersen, and F. M. M. Morel. 1991. Iron and nitrogen nutrition of equatorial Pacific plankton. *Deep-Sea Research* **38**: 1361-1378.
- Quéguiner, B., P. Tréguer, and D. M. Nelson. 1991. The production of biogenic silica in the Weddell and Scotia Seas. *Mar. Chem.* **35**: 449-459.
- Quetin, L. B., and R. M. Ross. 1985. Feeding by antarctic krill, *Euphausia superba*: Does size matter?, p. 372-377. *In* W. R. Siegfried, P. R. Condy and R. M. Laws [eds.], *Antarctic Nutrient Cycles and Food Webs*. Springer-Verlag.
- Redfield, A. C., B. H. Ketchum, and F. A. Richards. 1963. The influence of organisms on the chemical composition of seawater, p. 26-77. *In* M. N. Hill [ed.], *The Sea*. Interscience.

- Sarmiento, J. L., and J. C. Orr. 1991. Three dimensional simulations of the impact of Southern Ocean nutrient depletion on atmospheric CO₂ and ocean chemistry. *Limnol. Oceanogr.* **36**: 1928-1950.
- Smith, R. C., S. E. Stammerjohn, and K. S. Baker. 1996. Surface air temperature variations in the western Antarctic Peninsula region, p. 105-121. *In* R. Ross, E. Hofmann and L. Quetin [eds.], *Foundation for Ecosystem Research in the Western Antarctic*. Antarctic Research Series. American Geophysical Union.
- Sommer, U. 1986. Nitrate- and silicate-competition among antarctic phytoplankton. *Mar. Bio.* **91**.
- . 1988. The species composition of Antarctic phytoplankton interpreted in terms of Tilman's competition theory. *Oecologia* **77**: 464-467.
- . 1991. Comparative nutrient status and competitive interactions of two Antarctic diatoms (*Corethron criophilum* and *Thalassiosira antarctica*). *J. Plank. Res.* **13**.
- . 1994. The impact of light intensity and daylength on silicate and nitrate competition among marine phytoplankton. *Limnology and Oceanography* **39**: 1680-1688.
- Sommer, U., and H.-H. Stabel. 1986. Near surface nutrient and phytoplankton distribution in the Drake Passage during early December. *Polar Biology* **6**: 107-110.
- Stark, P. 1994. Climate warming in the central Antarctic Peninsula. *Weather* **49**.
- Sunda, W. G. 1994. Trace metal/phytoplankton interactions in the sea, p. 213-247. *In* W. Stumm [ed.], *Chemistry of Aquatic Systems: Local and Global Perspectives*. ECSC, EEC, EAEC.
- Sunda, W. G., and S. A. Huntsman. 1997. Interrelated influence of iron, light and cell size on marine phytoplankton growth. *Nature* **390**: 389-392.
- Sundquist, E. T., and W. S. Broecker. 1985. The carbon cycle and atmospheric CO₂: natural variations from Archean to present. *Geophys. Monogr.* **32**: 627.
- Trivelpiece, W. Z., S. G. Trivelpiece, G. R. Geupel, J. Kjelson, and N. J. Volkman. 1990. Adelie and Chinstrap penguins: Their potential as monitors of the southern ocean marine ecosystem, p. 191-202. *In* K. Kerry and G. Hempel [eds.], *Antarctic Ecosystems: Ecological Change and the Conservation*. Springer-Verlag.
- Williams, R. J. P. 1981. Natural selection of the chemical elements. *Proceedings of the Royal Society of London* **213**: 361-397.

Table 2.1 Variables for the Open Ocean Iron/Nitrate Model

Variable	CASE A- HNLC		Case B	Case C	Case D	Case E
	Initial conditions	3000 years	2x Fe to Surface	4x Fe to Surface	8x Fe to Surface	32x Fe to Surface
[CO ₂] Atmosphere	10.9 mM (m ⁻³)	11.1	11.0	11.0	10.9	10.6
pCO ₂ Atmosphere	345 μATM	350.2	348.8	347.5	345.1	335.8
τ (piston velocity)	3e ³ m yr ⁻¹	n/a	n/a	n/a	n/a	n/a
C _i Surface Water	2.19 mM	2.2	2.2	2.2	2.2	2.2
C _i Bottom Water	2.31 mM	2.3	2.3	2.3	2.3	2.3
pCO ₂ Surface Water	345 μAtm	350.8	349.2	347.7	345.1	334.8
upwelling rate	130 m yr ⁻¹	n/a ^a	n/a	n/a	n/a	n/a
[Fe] Surface	0.21 pM	0.3	0.5	0.7	1.1	3.5
[Fe] Bottom	1.3 pM	2.0	1.9	1.9	1.9	1.7
[NO ₃] Surface	12.0 μM	12.3	12.2	12.0	11.8	10.8
[NO ₃] Bottom	30.0 μM	30.0	30.0	30.0	30.0	30.0
C:NO ₃ (mol:mol)	6.6	n/a	n/a	n/a	n/a	n/a
NO ₃ :Fe (mol:mol)	6.06 e ³	n/a	n/a	n/a	n/a	n/a
K _d (Fe)	5 pM	n/a	n/a	n/a	n/a	n/a
V _{max} N	0.11 mol yr ⁻¹	n/a	n/a	n/a	n/a	n/a
Particulate Carbon to depth as % of V _{max} N	n/a	4.8	8.4	11.6	17.5	41.1

^a. N/A not applicable or constant

2.9 Figures

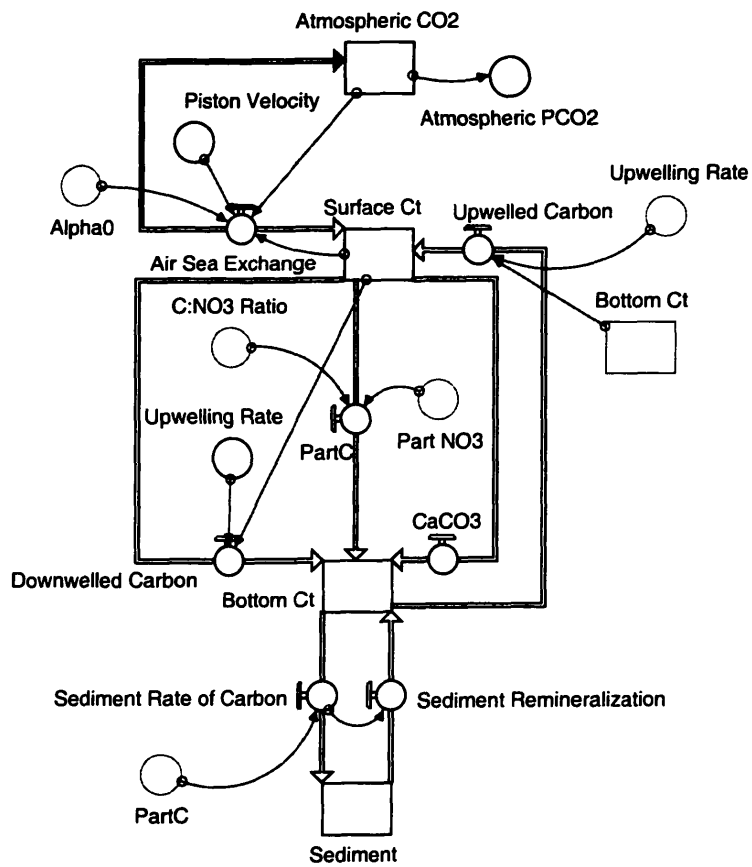


Figure 2.1 Schematic of the relationship between CO₂ in the four sections of the model: atmosphere, surface ocean, deep ocean and sediment.

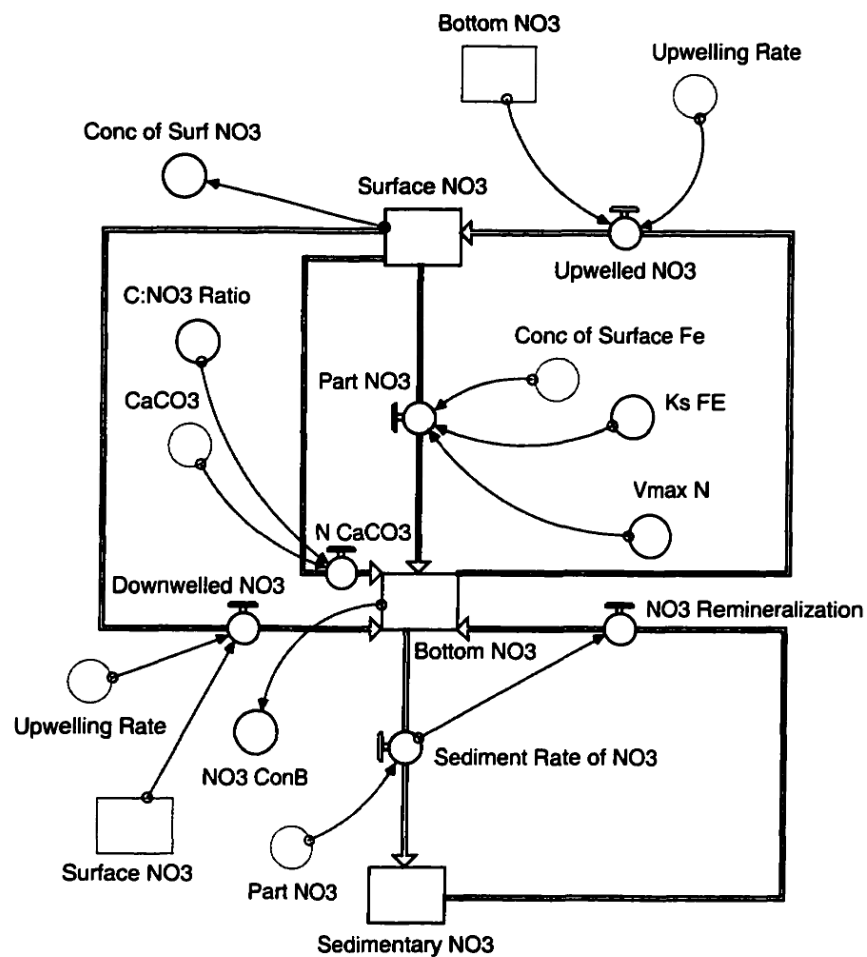


Figure 2.2 Schematic of the nitrate flow in the three sections of the model: surface ocean, deep ocean and sediment.

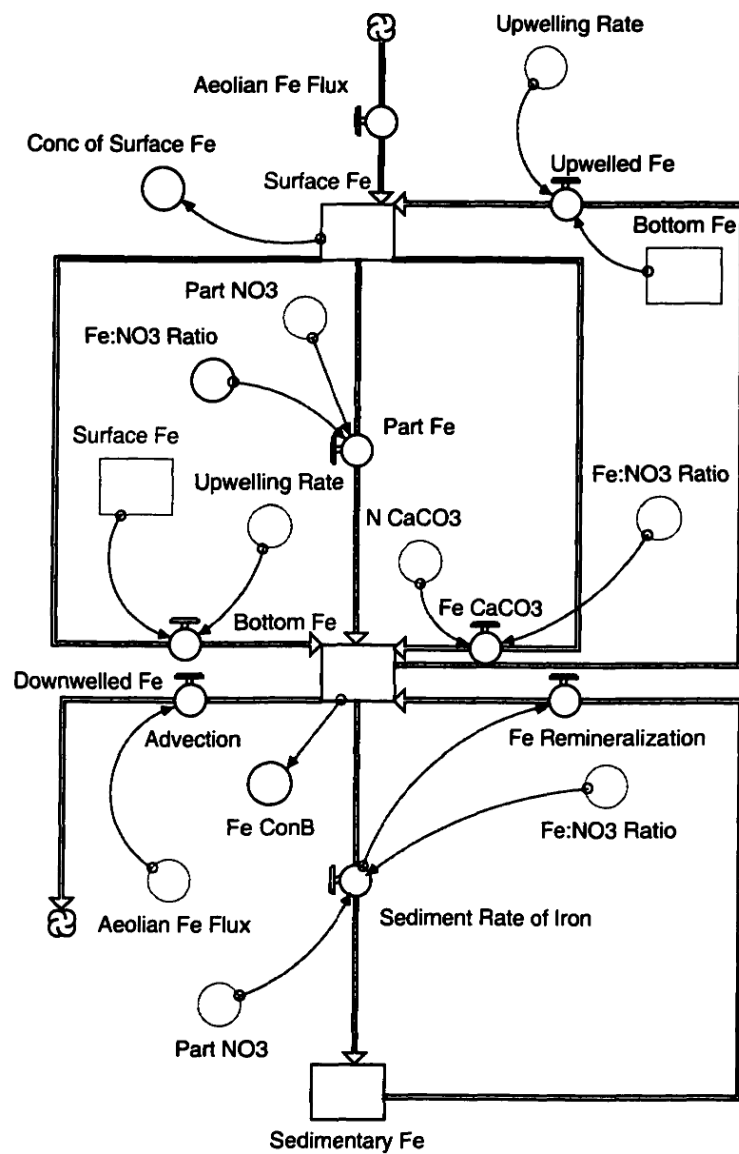


Figure 2.3 Schematic of the iron flow in the three sections of the model: surface ocean, deep ocean and sediment. Note that iron can also enter the system from aeolian sources but not exit the surface ocean to the atmosphere.

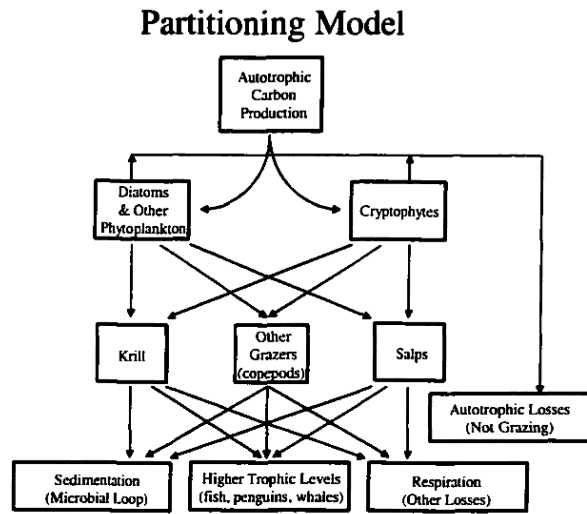


Figure 2.4 Schematic of the Antarctic food web model where primary production is divided into two relative size classes of phytoplankton, diatoms and other phytoplankton and cryptophytes.

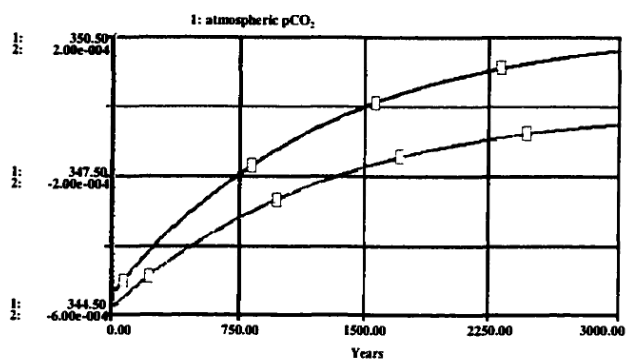


Figure 2.5 Model output of atmospheric $p\text{CO}_2$ (ppm) and air-sea exchange under the initial conditions (Case A, table 2.1). The model runs for 3000 years after which the atmosphere and surface ocean are in equilibrium.

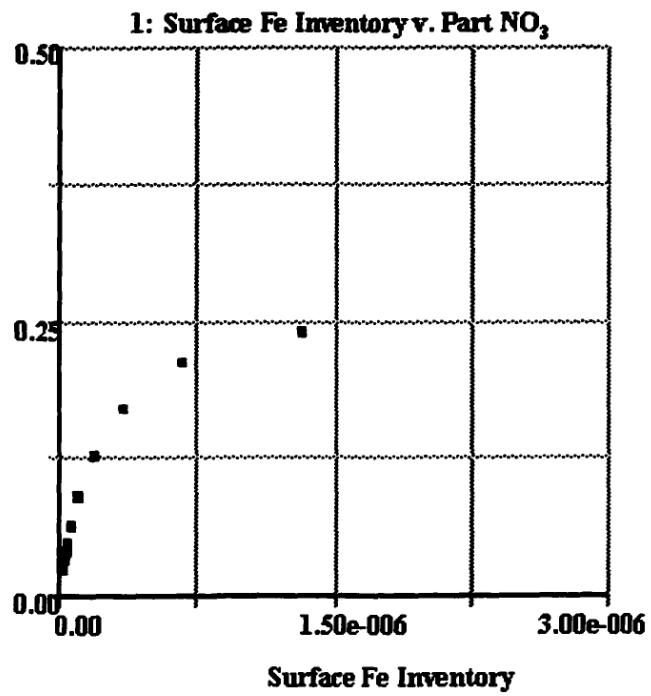


Figure 2.6 Model output of surface Fe inventory (mol) versus particulate N ($\text{mol N m}^{-2} \text{yr}^{-1}$) under the initial conditions (table 2.1).

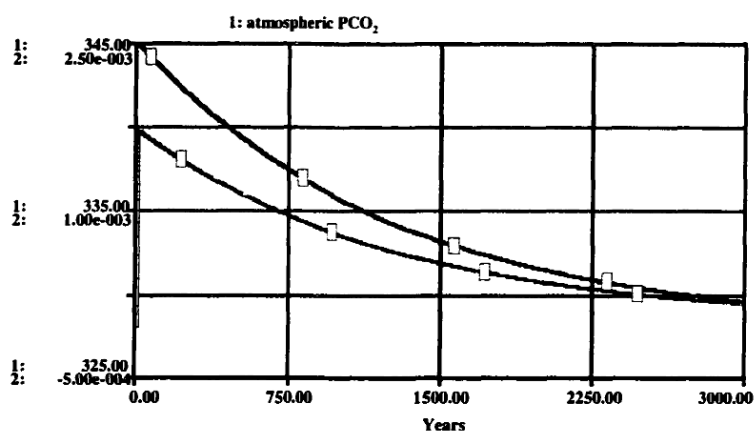


Figure 2.7 Model output of atmospheric pCO_2 (ppm) and air-sea exchange under Case E (table 2.1). The model runs for 3000 years after which the atmosphere and surface ocean are in equilibrium. Note the different scales compared to figure 2.5.

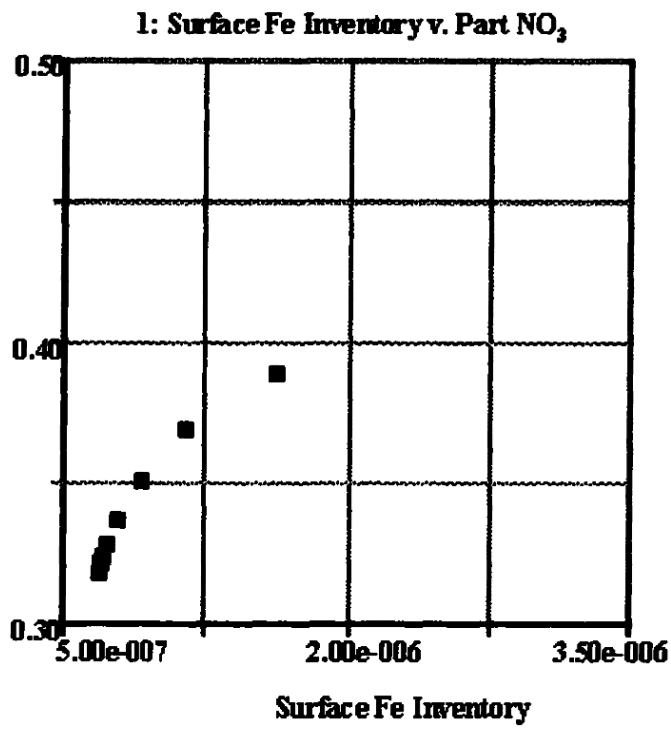


Figure 2.8 Model output of surface Fe inventory (mol) versus particulate N (mol N m⁻² yr⁻¹) under Case E (table 2.1). Note the different scales compared to figure 2.6.

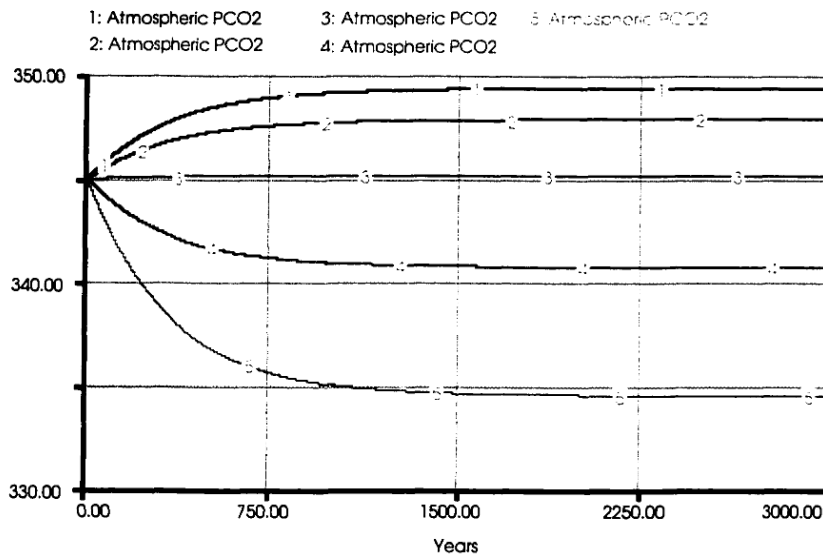


Figure 2.9 Model output of atmospheric $p\text{CO}_2$ (ppm) and air-sea exchange under the model conditions specified in table 2.1. The model runs for 3000 years after which the atmosphere and surface ocean are in equilibrium.

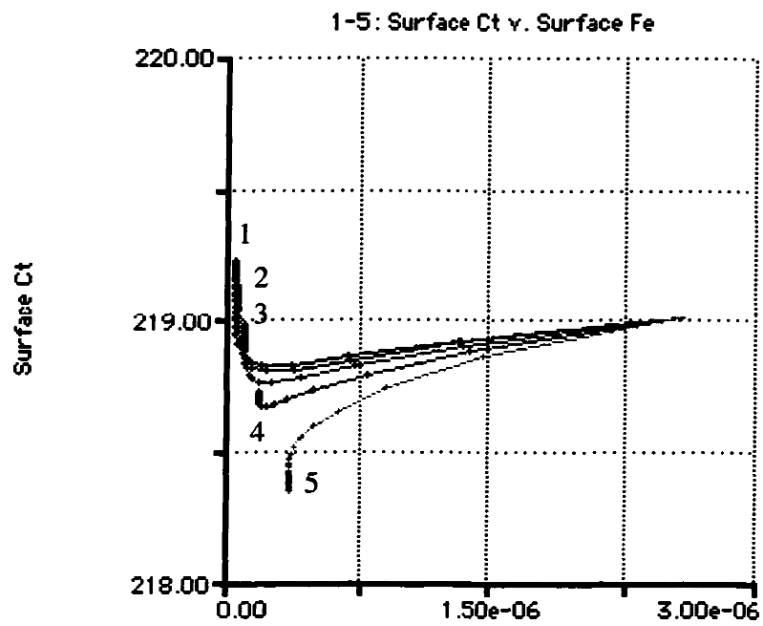


Figure 2.10 Schematic of the iron flow in the three sections of the model: surface ocean, deep ocean and sediment. Note that iron can also enter the system from aeolian sources but not exit the surface ocean to the atmosphere.

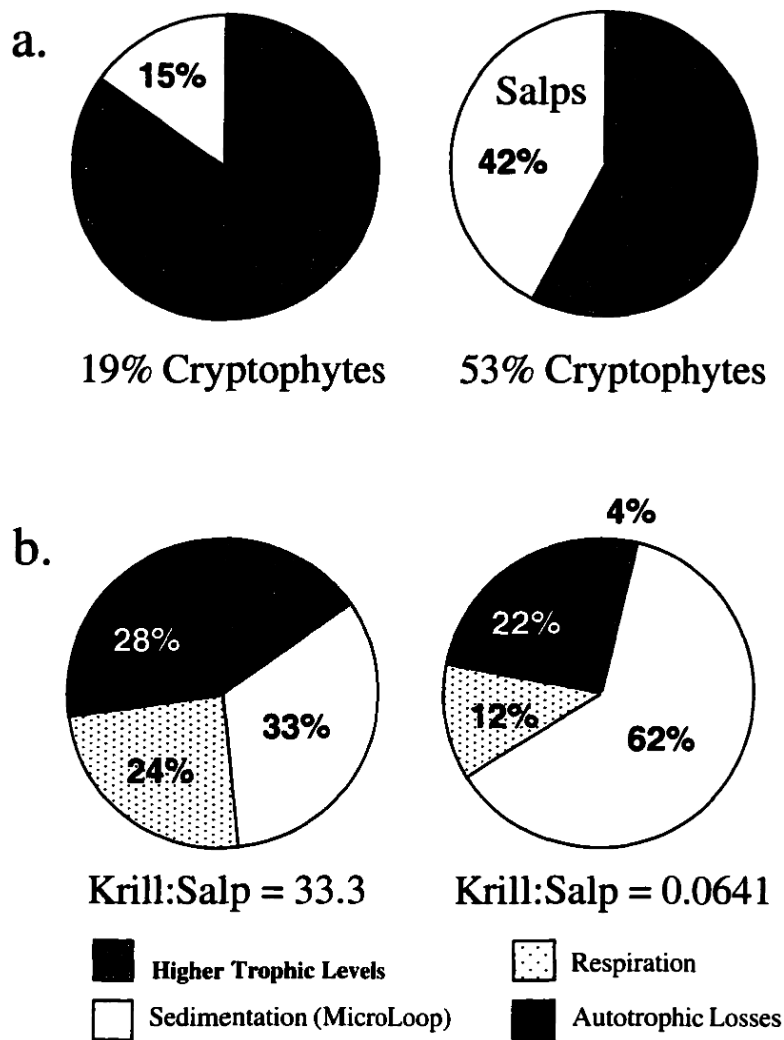


Figure 2.11 Results from the model used to calculate the portioning of energy throughout the Antarctic food web. A). The calculated flow of carbon through either krill (shaded) or salps (open) based on the percentage of cryptophyte primary production. The percent of cryptophyte primary production ranged from 19% in 1991-92 to 53% in 1993-94. B). the partitioning of carbon into higher trophic levels (light shade), respiration (stippled), sedimentation or microbial loop (open) and autotrophic losses (dark shade) was calculated based on changing krill to salp ratios. Krill to salp ratios ranging from 0.0641 to 33.3 (Loeb et al 1997) were used and corresponded to 19 and 53% cryptophytes, respectively.

2.10 Atmosphere-ocean interaction model

Calculation of pCO₂ in Surface Waters

$\text{Alpha0} = 1/(1+(1.28825\text{E-}06/(10^{\wedge}\text{-pH}))+ (9.77237\text{E-}16/((10^{\wedge}\text{-pH})^2)))$

$\text{Alpha1} = ((\text{pH}/10^{\wedge}\text{-6.3})+1+(10^{\wedge}\text{-10.3}/\text{pH}))^{\wedge}\text{-1}$

$\text{Alpha2} = (((\text{pH})^2/10^{\wedge}\text{-16.6})+(\text{pH}/10^{\wedge}\text{-10.3})+1)^{\wedge}\text{-1}$

$\text{Ct_molar} = \text{Surface_Ct}/1\text{e5}$

$\text{pCO2_Surface} = (\text{Surface_Ct}/1\text{e5}*\text{Alpha0}/3.16\text{e-}2)*1\text{e6}$

$\text{pH} = -1805.4*\text{Ct_molar}+12.1$

CO₂ Module

$\text{Atmospheric_CO2}(t) = \text{Atmospheric_CO2}(t - dt) + (-\text{Air_Sea_Exchange}) * dt$

INIT Atmospheric_CO2 = 10.9

OUTFLOWS:

$\text{Air_Sea_Exchange} = \text{Piston_Velocity}*((\text{Atmospheric_CO2}/1\text{e6})-((\text{Surface_Ct}/1\text{e5})*\text{Alpha0}))$

$\text{Bottom_Ct}(t) = \text{Bottom_Ct}(t - dt) + (\text{Downwelled_Carbon} + \text{PartC} + \text{Sediment_Remineralization} + \text{CaCO3}$
 $- \text{Upwelled_Carbon} - \text{Sediment_Rate_of_Carbon}) * dt$

INIT Bottom_Ct = 7854

INFLOWS:

$\text{Downwelled_Carbon} = (\text{Surface_Ct}/100)*\text{Upwelling_Rate}$

$\text{PartC} = (\text{Part_NO3}*\text{C:NO3_Ratio})$

$\text{Sediment_Remineralization} = \text{Delay}(\text{Sediment_Rate_of_Carbon}, 2, 0)$

$\text{CaCO3} = 15$

OUTFLOWS:

$\text{Upwelled_Carbon} = (\text{Bottom_Ct}/3400)*\text{Upwelling_Rate}$

$\text{Sediment_Rate_of_Carbon} = \text{PartC}*.01$

$\text{Sediment}(t) = \text{Sediment}(t - dt) + (\text{Sediment_Rate_of_Carbon} - \text{Sediment_Remineralization}) * dt$

INIT Sediment = 0.44

INFLOWS:

$\text{Sediment_Rate_of_Carbon} = \text{PartC}*.01$

OUTFLOWS:

$\text{Sediment_Remineralization} = \text{Delay}(\text{Sediment_Rate_of_Carbon}, 2, 0)$

$\text{Surface_Ct}(t) = \text{Surface_Ct}(t - dt) + (\text{Air_Sea_Exchange} + \text{Upwelled_Carbon} - \text{Downwelled_Carbon} -$
 $\text{PartC} - \text{CaCO3}) * dt$

INIT Surface_Ct = 219

INFLOWS:

$\text{Air_Sea_Exchange} = \text{Piston_Velocity}*((\text{Atmospheric_CO2}/1\text{e6})-((\text{Surface_Ct}/1\text{e5})*\text{Alpha0}))$

$\text{Upwelled_Carbon} = (\text{Bottom_Ct}/3400)*\text{Upwelling_Rate}$

OUTFLOWS:

$\text{Downwelled_Carbon} = (\text{Surface_Ct}/100)*\text{Upwelling_Rate}$

$\text{PartC} = (\text{Part_NO3}*\text{C:NO3_Ratio})$

$\text{CaCO3} = 15$

$\text{Atmospheric_PCO2} = (\text{Atmospheric_CO2}/1\text{e6}/3.16\text{e-}2)*1\text{e6}$

$\text{Piston_Velocity} = 3\text{e3}$

$\text{Upwelling_Rate} = 130$

Fe Module

$\text{Bottom_Fe}(t) = \text{Bottom_Fe}(t - dt) + (\text{Downwelled_Fe} + \text{Part_Fe} + \text{Fe_Remineralization} + \text{Fe_CaCO3} -$
 $\text{Upwelled_Fe} - \text{Sediment_Rate_of_Iron} - \text{Advection}) * dt$

INIT Bottom_Fe = 4.08e-8

INFLOWS:

```

Downwelled_Fe = (Surface_Fe/100)*Upwelling_Rate
Part_Fe = Part_NO3*Fe:NO3_Ratio
Fe_Reminerlization = delay(Sediment_Rate_of_Iron,2,0)
Fe_CaCO3 = N_CaCO3*Fe:NO3_Ratio
OUTFLOWS:
Upwelled_Fe = (Bottom_Fe/3400)*Upwelling_Rate
Sediment_Rate_of_Iron = (Part_NO3*Fe:NO3_Ratio)*.01
Advection = Aeolian_Fe_Flux
Sedimentary_Fe(t) = Sedimentary_Fe(t - dt) + (Sediment_Rate_of_Iron - Fe_Reminerlization) * dt
INIT Sedimentary_Fe = 0

INFLOWS:
Sediment_Rate_of_Iron = (Part_NO3*Fe:NO3_Ratio)*.01
OUTFLOWS:
Fe_Reminerlization = delay(Sediment_Rate_of_Iron,2,0)
Surface_Fe(t) = Surface_Fe(t - dt) + (Upwelled_Fe + Aeolian_Fe_Flux - Downwelled_Fe - Part_Fe -
Fe_CaCO3) * dt
INIT Surface_Fe = 2.6e-8

INFLOWS:
Upwelled_Fe = (Bottom_Fe/3400)*Upwelling_Rate
Aeolian_Fe_Flux = 16*2.048835e-7
OUTFLOWS:
Downwelled_Fe = (Surface_Fe/100)*Upwelling_Rate
Part_Fe = Part_NO3*Fe:NO3_Ratio
Fe_CaCO3 = N_CaCO3*Fe:NO3_Ratio
Conc_of_Surface_Fe = Surface_Fe/100000
Fe:NO3_Ratio = 1.65e-4
Fe_ConB = Bottom_Fe/3400000

Nitrate Module
Bottom_NO3(t) = Bottom_NO3(t - dt) + (Part_NO3 + Downwelled_NO3 + NO3_Reminerlization +
N_CaCO3 - Sediment_Rate_of_NO3 - Upwelled_NO3) * dt
INIT Bottom_NO3 = 102

INFLOWS:
Part_NO3 = (Vmax_N*Conc_of_Surface_Fe/(Ks_FE+Conc_of_Surface_Fe))
Downwelled_NO3 = (Surface_NO3/100)*Upwelling_Rate
NO3_Reminerlization = delay(Sediment_Rate_of_NO3,2,0)
N_CaCO3 = CaCO3/C:NO3_Ratio
OUTFLOWS:
Sediment_Rate_of_NO3 = Part_NO3*.01
Upwelled_NO3 = (Bottom_NO3/3400)*Upwelling_Rate
Sedimentary_NO3(t) = Sedimentary_NO3(t - dt) + (Sediment_Rate_of_NO3 - NO3_Reminerlization) * dt
INIT Sedimentary_NO3 = 0.07

INFLOWS:
Sediment_Rate_of_NO3 = Part_NO3*.01
OUTFLOWS:
NO3_Reminerlization = delay(Sediment_Rate_of_NO3,2,0)
Surface_NO3(t) = Surface_NO3(t - dt) + (Upwelled_NO3 - Part_NO3 - Downwelled_NO3 - N_CaCO3) *
dt
INIT Surface_NO3 = 1.2000

INFLOWS:
Upwelled_NO3 = (Bottom_NO3/3400)*Upwelling_Rate

```

OUTFLOWS:
Part_NO3 = (Vmax_N*Conc_of_Surface_Fe/(Ks_FE+Conc_of_Surface_Fe))
Downwelled_NO3 = (Surface_NO3/100)*Upwelling_Rate
N_CaCO3 = CaCO3/C:NO3_Ratio
C:NO3_Ratio = 6.6
Conc_of_Surf_NO3 = Surface_NO3/100000
Ks_FE = 5e-12
NO3_ConB = Bottom_NO3/3400000
Vmax_N = .11

3 Monochromatic ultraviolet light induced damage to photosystem II efficiency and carbon fixation in the marine diatom *Thalassiosira pseudonana* (3H)

(from, Grzyski, J., Orrico, C., Schofield, O. 2000. Monochromatic ultraviolet light induced damage to photosystem II efficiency and carbon fixation in the marine diatom *Thalassiosira pseudonana* (3H). Photosynthesis Research)

3.1 Abstract

Low light adapted cultures of the marine diatom *Thalassiosira pseudonana* (3H) were cultured and incubated for 30 minutes under different ultraviolet (UV) wavelengths of near monochromatic light with and without background photosynthetically active radiation (PAR, 380-700nm). Maximum damage to the quantum yield for stable charge separations was found in the UVB (280-320nm) wavelengths without background PAR light while the damage under PAR was 30% less. UV induced damage to carbon fixation in the cells was described by a function similar to non-linear functions of inhibiting irradiance previously published with the exception that damage was slightly higher in the UVA (320-380). Various measurements of fluorescent transients were measured and the results indicate localised damage most likely on the acceptor side of the photosystem II reaction center. However, dark adapted measurements of fluorescence transients with and without DCMU do not result in similar functions. This is also true for the relationships between fluorescence transients and carbon fixation for this species of marine diatom. The correlation between the weightings ϵ_H from measurements of carbon fixation and the quantum yield for stable charge separation as calculated from induction curves without DCMU and with DCMU is R^2 0.44 and R^2 0.78 respectively. The slopes of the two measurements are 3.8 and 1.4 respectively. The strong correlation between the weightings of the induction curves without DCMU and carbon fixation are due to a loss

of electron transport from the reaction center to plastoquinone. Under these experimental conditions of constant photon flux density (PFD) this is manifested as a strong linear relationship between the decrease in the operational quantum yield of photosystem II and carbon fixation.

3.2 Introduction

The discovery of the ozone hole in Antarctica (Farman et al. 1985) has resulted in concerted efforts to determine the potential impact of elevated levels of ultraviolet-B radiation (UVB, 280-320 nm) on photoautotrophic activity (Smith et al 1992) and marine organisms, in general (Calkins 1980). The enhancement of UVB can significantly depress both higher plant and microalgal photosynthetic rates (Iwanzik et al. 1983; El-Sayed et al. 1990; Teramura et al. 1991; Helbing et al. 1992; Smith et al. 1992). The magnitude of UV inhibition depends on UV dose and UV dose rate (Cullen and Lesser 1991), and on the measurement techniques utilized (Coohill 1994; Prézelin et al. 1994a). There are also important physiological and structural differences between higher plants and single celled algae. Therefore species-specific differences in sensitivity to UV radiation must be considered (Jokiel and York 1984, Karentz et al. 1991, Karentz 1994, Helbing et al. 1992, Smith et al. 1992, Vernet et al. 1994). Inhibition rates are difficult to interpret especially if the specific target sites of damage are not known. Action spectra (or biological weighting factors) can provide a quantitative means to estimate the impact of elevated ultraviolet light on natural communities (Smith et al. 1980, Cullen et al. 1992, Quate et al. 1992) if the underlying processes influencing the photoinhibition are characterized (Coohill 1991).

Action spectra describe the wavelength dependent sensitivity of a process to light-induced damage (Smith et al. 1980, Rundel 1983, Caldwell et al. 1986, Coohill 1989, Cullen et al. 1992). They can be used to discriminate between the photoinhibition due to UVB, ultraviolet-A (UVA, 320-400 nm), and photosynthetically available radiation (PAR, 400-700 nm), all of which impact photosynthetic activity in a differential manner (cf. Baker and Bowyer 1994, Helbing et al. 1992, Prezelin et al. 1994b). Defining processes that influence the spectral variability in action spectra would allow for a mechanistic interpretation of the variability in UVB-induced damage (Coohill 1991). Photoinhibition is a function of both damage and repair processes. Therefore, biological responses to UV are sensitive to dose and dosage rate (i.e. reciprocity does not hold, Cullen & Lesser 1991, Lesser et al. 1994, Neale et al. 1994). This, and that UVB impacts numerous targets contribute to the significant variability observed in the polychromatic action spectra for photosynthesis (Neale et al. 1994, Boucher & Prezelin 1996). Our ability to mechanistically describe this variability will require an understanding of: the specific target sites for UV inhibition within the photosynthetic machinery, the UVB-damage repair rates and the action spectra of repair (within and between species of phytoplankton), and the impact of photoacclimation processes.

Laboratory studies on higher plants and green algae suggest that UVB is most damaging to photosystem II (PS II) within the photosynthetic machinery (Kulandaivelu & Noorudeen 1983; Iwanzik et al. 1983; Greenberg et al. 1989; Renger et al. 1989). The UVB radiation appears to degrade the D1 protein, part of the D1/D2 heterodimer; the major structural complex within PSII (Greenberg et al. 1989; Richter et al. 1990; Melis et al. 1992; Jansen et al. 1993). Damage to PSII reduces the ability of algae to generate

stable charge separations, which results in an overall lowering of carbon fixation rates. Ultra-violet light inhibition of PSII quantum yields has been observed in field communities under the ozone hole (Schofield et al. 1995). These results are to be expected if damage occurs at the primary (Q_A) and/or secondary (Q_B) electron acceptor because the quinones absorb UV wavelengths of radiation (Greenberg et al. 1989; Melis et al. 1992; Jansen et al. 1993). The donor side of PSII is also a possible target as tyrosine residues absorb at 280 nm in their reduced form and 310 in their oxidized radical form (Diner and deVity 1985; Vass et al. 1996). Other studies have demonstrated decreases in the pool size of carbon fixation enzymes such as carbonic anhydrase (Dionisio et al. 1989) and ribulose-1,5-bisphosphate carboxylase/oxygenase (rubiscO) (Strid et al. 1990; Neale et al. 1993). However, the primary targets for the UV-suppression of photosynthetic activity are still debated (Baker et al. 1997).

Our goals in characterizing monochromatic action spectra for a low light adapted culture of *Thalassiosira pseudonana* were to better measure wavelengths of sensitivity to ultraviolet light and to compare the measurements of damage to photosystem II to depressions to carbon fixation. In areas of the ocean characterized by high mixing rates and potentially high ultraviolet fluxes like the Southern Ocean phytoplankton damage and repair rates are not in steady state (Neale et al 1998). The ultimate goal of ocean photo-biology is to reconcile depressions in photosystem II activity and depressions in carbon fixation and the subsequent impact on cellular growth rates. As part of that effort this paper will relate the ultraviolet light impact on non-invasive active fluorescence measurements and carbon fixation.

3.3 Materials and methods

3.3.1 Culture conditions

Cultures of the marine diatom *Thalassiosira pseudonana* were grown in temperature controlled incubators at 20 °C. Two identical cultures were grown in 2.8 L fennbach flasks at a light intensity of $80 \mu\text{mol m}^{-2} \text{s}^{-1}$ and were maintained in exponential growth phase by serial dilution with fresh f/2 media (Guillard 1975). Light was provided by Phillips 40CW • RS • WM cool white lamps on a 12:12h light:dark cycle. Cell numbers and growth rates were determined by cell counting with a Bright Line hemacytometer. The growth rates of the two cultures were the same (table 3.2).

3.3.2 Ultraviolet light incubations

Measurements of the spectral sensitivity to ultraviolet light were performed using high intensity light provided by 1000W xenon arc lamp. Light was directed through a quartz condensing lens and a 1/4 meter monochromator (Oriel Systems). A computer using a stepper interface controlled the monochromator. Light (2.5 nm full width- half maximum) exiting the monochromator was filtered through a short pass filter (Corion UG 11s) to remove any stray visible light. Experiments on the susceptibility of photosystem II to ultraviolet light only, were conducted in the absence of visible light. For all incubations, a 1 cm^2 beam of light was focused on a 1 cm quartz cuvette containing 1 ml of culture. The flux of light was measured using a high sensitivity UV-visible 1 cm^2 silicon light detector (Oriel Systems). Cumulative exposure was calculated based on the absorbance at each wavelength and varied between 100 and 200 J m^{-2} . Calibrations of the lamp were repeated throughout the experiment. The sample chamber was also temperature controlled by a circulating water bath.

3.3.3 Fluorescence parameters of *Thalassiosira pseudonana*

Baseline measurements of the fluorescence parameters of the phytoplankton cultures were performed in triplicate on the cultures throughout the day. The cultures were probed for photosystem II efficiency using a Pulse Amplitude Modulated (PAM) fluorometer (Heinz Walz, Effeltrich, Germany). This provided a robust baseline and ensured that changes in PSII efficiency of UV irradiated cells were not a product of growth conditions or changes in light acclimation. Aliquots of the cultures were dark adapted for 5 minutes, then fluorescence induction curves with and without 3-(3,4-dichlorophenyl)-1,1-dimethyl urea (DCMU, 20 μ M final concentration) and fluorescence decay curves were measured. Calculations of the maximum quantum yield of photosystem II for stable charge separations are made from measurements of F_o (Q_A , completely oxidised) and F_m (Q_B , completely reduced). The quantum yield as calculated from DCMU induction curves is denoted ϕ_{IIc}^o (DCMU); while the calculation from Kautsky curves without DCMU is denoted ϕ_{IIc}^o (Kaut) (table 2.1).

3.3.4 Measurements of UV effects without PAR light

One ml samples of the diatom containing approximately 0.4 μ g Chl *a*/ml were incubated for 30 minutes under 9 wavelengths in the UVB (every 5 nm between 280-320nm) and 4 wavelengths in the UVA (330, 340, 350, 360). After irradiation, each sample was probed for photosynthetic activity using the PAM fluorometer. Kautsky induction curves without DCMU were measured after triggering a light-emitting diode (665 nm, 30 μ mol photons \cdot m $^{-2}$ \cdot s $^{-1}$) and a 600ms flash from a flash lamp (Schott KL-1500). The fluorescence rise was sampled every 300 μ s for 4.8 s. The fluorescence transients (O,I,D,P) were determined after smoothing all curves with a 23 point least

squares convolution integral (Savitsky and Golay, 1964). F_0 is the minimum fluorescence level when all the reaction centers are open (Q_A oxidised). F_i is the level corresponding to the reaction centers unable to reduce plastoquinone (Cao and Govindjee, 1990). F_d is the subsequent dip in fluorescence and F_p is the maximum level of fluorescence level when all of Q_A , the primary electron acceptor has been reduced (Lavorel 1959, Munday and Govindjee 1969, Govindjee 1995). After the measurements without DCMU samples were dark adapted for two minutes and then incubated for one minute with DCMU. The induction curve was measured after triggering a 600 ms pulse from a red LED at a sampling rate of 100 μ s for 1.6s. These curves were similarly smoothed and then deconvolved using an exciton-radical pair equilibrium model adapted from Trissl and Lavergne (1994). Examples of both induction curves are presented in figure 3.2. Changes in σ_{psII} were calculated from the exciton-radical pair equilibrium model. Briefly, the magnitude of fluorescence can be described as a function of open reaction centers (q):

$$\frac{F}{F_0} = \frac{\frac{F_m}{F_0} - \left(\frac{F_m}{F_0} - (1 + J_{con}) \right) \cdot q}{1 + J_{con} \cdot q} \quad \text{Eq. 3.1}$$

The change in open reaction centers over time can further be described by:

$$\frac{dq}{dt} = -\sigma_{II} \cdot q \cdot (1 + J_{con}) / (1 + J_{con} \cdot q) \quad \text{Eq. 3.2}$$

Fluorescence decay curves were measured at a resolution of 10 μ s for 0.16s after applying a single turnover flash (Walz, Single Turnover Flash Lamp, XST-103). The fluorescence decay curves describe the reoxidation of Q_A^- by either Q_B or Q_B^- and were quantified by an offset double exponential decay equation:

$$F = A e^{-k_a t} + B e^{-k_b t} + F_0 \quad \text{Eq. 3.3}$$

In this equation A and B are amplitudes and k_a and k_b are rate constants for the fast and slow phases respectively. The existence of a slower ($t_{1/2}$ of ~1.5s) component could not be resolved by the short acquisition time of our setup (0.16s). Five curves taken 20s apart were averaged for all decay measurements. The fluorescence induction curves without the addition of DCMU were analyzed for changes in the rise time to the I, D, and P components of the curve as well as the ϕ_I , ϕ_D and ϕ_P . All wavelengths reported were done at least in triplicate.

3.3.5 Analytical measurements in the presence of PAR light

Incubations at 5 wavelengths of UVR (280, 300, 320, 340, 360) and the growth irradiance of the cultures were performed to assess the effect UVR on both PSII efficiency and carbon fixation rates. Aliquots of culture were incubated as described above with one modification: a fiber optic arm providing PAR light (intensity same as growth conditions) was connected to the incubation chamber. At the beginning of each day and periodically throughout the day controls without UV light were measured in both the incubator and the incubation chamber to assure that deviations were caused by the experimental treatments and not any biological rhythms or changes in the experimental conditions. All fluorescence measurements were also carried out on the controls.

Productivity rates were measured by adding aqueous $\text{NaH}^{14}\text{CO}_3$ (final concentration of 185 Becquerels L^{-1}) to an aliquot of culture and then irradiating 1 ml samples for the 30 minute incubation period. At the end of the incubation period fluorescence measurements in the presence of PAR were made. These included F_o' , F_m' and F_t . These values can be used to calculate the efficiency of photon trapping by open PSII centers:

$$\phi_{exc} = \frac{F_m' - F_o'}{F_m'} \quad \text{Eq. 3.4}$$

The operational quantum yield of PSII can be calculated as:

$$\phi_{PSII} = \frac{F_m' - F_t}{F_m'} \quad \text{Eq. 3.5}$$

After 5 minutes of dark adaptation the same suite of dark-adapted fluorescence measurements were made as previously described. Samples were then fixed with 10 μl of glacial acetic acid and counted the following day in a scintillation counter (Beckman LS 6000IC). In order to correct for small increases in the chl- a content of the sample that occurred during long experiments multiple samples were taken throughout the day. Chlorophyll- a content of the cultures was measured in a spectrophotometer (Perkin Elmer, Lambda-12) after an overnight extraction in 100% acetone and dilution with water

to a final concentration of 90% acetone. Chlorophyll-*a* content was calculated using the tri-chromatic equation of Jefferies and Humphrey (1975)(n=3).

3.3.6 Calculation of ϵ_H ($J\ m^{-2}$)⁻¹

Our short term measurements of the average photosynthetic rate or quantum yield after a specific exposure period of UV with or without PAR light assume no active repair. Therefore the specific weight of inhibition, ϵ ($J\ m^{-2}$)⁻¹ can be calculated from the cumulative exposure and the average photosynthetic rate (Neale and Kieber, 2000):

$$P(t) = P(0) \exp - H_{inh} \quad \text{Eq. 3.6}$$

where:

$$H_{inh} = \epsilon(\lambda) H(\lambda) \quad \text{Eq. 3.7}$$

and,

$$\epsilon(\lambda) = -\log \left(\frac{P(t)}{P(0)} \right) H(\lambda)^{-1} \quad \text{Eq. 3.8}$$

$P(t)$ is either the measure of photosystem II activity or carbon fixation initially at the level $P(0)$. H represents the radiant exposure ($J\ m^{-2}$) and is calculated based on the measurements of radiant flux in the cuvette filled with water multiplied by the optical density of the sample at the specific wavelength measured.

3.4 Results

3.4.1 Acclimation state of *T. pseudonana*

The cultures of *T. pseudonana* were acclimated to a sub-saturating irradiance (table 3.2). Therefore, the maximum rate of light-limited photosynthesis is defined by the

ability of the reaction centers and antenna to absorb incoming photons according to a linear function of irradiance with a slope α :

$$\alpha = \sigma_{psII} \cdot n \cdot \phi_m \quad \text{Eq. 3.9}$$

where ϕ_m :

$$\phi_m = \sigma_{psII} (\sigma_{psu})^{-1} \quad \text{Eq. 3.10}$$

Changes therefore, in either σ_{psII} or n , the number of reaction centers, will lead to changes in the maximum rate of light limited photosynthesis at any given light level below I_k (cf. Sakshaug et. al., 1997, table 3.1). The experimental protocol allowed for close monitoring of changes in σ_{psII} as well as changes in the overall efficiency of generating a stable charge separation, ϕ_{II} . The overall variability in the size of σ_{psII} was 28% and ϕ_{II} varied by less than 10% over the time course of the experiment. Daily variability of σ_{psII} was less than 10%, allowing good resolution in measuring whether or not UVR induced changes in the size of σ_{psII} during experimental treatments.

3.4.2 Signature of photosystem II damage without PAR

The maximum quantum yield of stable charge separations (ϕ_{IIc}^0) declined for both Kautsky and DCMU induction curves after a 30 minute treatment with UVR (Figure 3.1). Both spectra indicate that as wavelength decreases into the UVB damage increases. As well, both spectra also indicate significantly more damage at wavelengths less than 295 nm than in the UVA part of the spectrum ($p < 0.05$); though significant inflections exist in

both curves. The decrease in ϕ_{IIc}^0 is between 2 and 5 times greater for measurements made without the inhibitor DCMU. These differences are most evident at the lowest wavelengths in the UVB. The differences between the two measurements are obvious when the actual measured curves are overlaid (Figure 3.2).

3.4.3 Signature of photosystem II damage with PAR

Although there is less spectral resolution in the PSII damage curves generated under both UVR and PAR the results were highly repeatable (Table 3.3). Damage as measured by induction curves with and without DCMU was less in the presence of PAR and UVR than under UVR alone. Maximum values of damage under PAR and UVR were 0.0007 and 0.00014 (J m^{-2})⁻¹ for Kautsky curves and DCMU induction curves respectively (3.3), whereas values were 0.0009 and 0.0004 (J m^{-2})⁻¹ for the same measurements under UVR alone. The sensitivity to damage was still greater in the Kautsky curves with the largest difference at 280 nm. Damage to PSII as calculated from DCMU induction curves was minimal at all wavelengths and in some instances the addition of UVA light actually enhanced ϕ_{IIc}^0 ; even though the Kautsky measurements indicated damage. Subsequent changes in the σ_{psII} because of either decreases or increases in ϕ_{IIc}^0 were outside of the resolution of the measurements (Table 3.3).

3.4.4 UVR induced changes in photosynthetic function. Carbon Fixation

The measurements of ϵ_H for carbon fixation after exposure to UV and PAR was wavelength dependent but not an exponentially decreasing function (3.4). Decreased rates of carbon fixation to *T. pseudonana* were maximal at 280 nm. Unlike polychromatic spectra of damage to carbon fixation no significant differences between

the wavelengths 300 and 320 were found. The wavelength that induced the least damage was 360 nm. As was noted in the DCMU measurements under PAR and UVA there were occasional instances of enhancement in carbon fixation rates under UVA wavelengths.

3.4.5 Connectivity between reaction centers

Besides changes in ϕ_{IIc}^0 , exposure to UVR induced highly significant changes in the connectivity (J_{con}) between PSII reaction centers. Changes in J_{con} mimic the changes reported in measurements of ϕ_{IIc}^0 ; connectivity between reaction centers declines as damage increases. The most significant changes in J_{con} were induced by UVR alone at 285 and 295 nm, where there was no connectivity (3.5). This is also similar to the results found for decreases in ϕ_{IIc}^0 where the greatest change was in the treatment with UVR only. In UVR and PAR treatments changes in J_{con} were minimal except at 280 and 300 nm.

3.4.6 Photosystem II light utilization

The effects of UV light on PSII function in the presence of PAR and its possible relationship to changes in carbon fixation were assessed. Changes in the absolute values of both the operational quantum yield (ϕ_{II}) and the efficiency of photon trapping (ϕ_{exc}) are shown (Figure 3.6.a). Decreases in both ϕ_{II} and ϕ_{exc} were consistent with the other measurements; damage increased as wavelength decreased. However significant differences in the amount of damage between the two measurements exist. At all wavelengths damage as indicated by ϕ_{II} was greater than that indicated by ϕ_{exc} with the greatest differences at 320 and 340 nm.

In order to compare the relationship between ϕ_{II}^o (kaut), ϕ_{II}^o (DCMU), ϕ_{II} , ϕ_{exc} , and the changes in carbon fixation, all of the data are plotted according to the measurements of ϵ_H ($J\ m^{-2}$)⁻¹ and the linear equations of the lines of best fit are shown in table 3.4 (Figure 3.6.b). The type II linear regression between ϕ_{II} and carbon fixation gives the line of best fit ($R^2 = 0.81$). While all of the linear regressions except for measurements with DCMU were good the slopes indicate that while damage to PSII and depressions in carbon fixation are linearly related they don't occur with a slope of one.

Changes in other fluorescence variables (σ_{psII} , Ka, Kb, a, and b) were highly variable and were generally not statistically significant from non-treated samples (table 3.3). However, this can be assumed to be both a product of any effect the treatment had on the sample and a loss of computing power due to noise in the curves. Both are manifested in larger errors as wavelength decreases and damage increases.

3.5 Discussion

The difficulty in assessing actual targets of damage in the photosynthetic apparatus is caused both by multiple potential target sites and, over time, by an active repair cycle. We avoided some of the multiple potential target sites by using near monochromatic light. However, it is possible that different target sites have the same absorption maximum. As well, damage to the photosynthetic apparatus is often the result of cumulative dose affecting multiple processes simultaneously (Jones and Kok 1966, Baker and Bowyer 1994).

Photosynthesis, below the level of light saturation, is a product of irradiance, the number of reaction centers and the optical cross sections of PSII. We would expect damage to be a function of the efficiency of the wavelength at altering n or σ_{psII} and not a

situation similar to that of dosage rate or bright light photoinhibition. In dosage rate photoinhibition, the efficiency and magnitude of damage is masked by repair and/or xanthophyll induced quenching so that in time a steady state is reached. During bright light photoinhibition, the incident flux, which is disproportionately high compared to the dissipative capacity of PSII, causes damage that is independent of the wavelength (Jones and Kok 1966). These phenomena will be species, time and acclimation state dependent. Given the monochromatic light regimes and the relatively low output at each wavelength ($\sim 150 \text{ J m}^{-2}$), dosage rate photoinhibition and bright light photoinhibition could be overlooked. Instead the efficiency of damage could be investigated with the initial assumption that the plastoquinone pool would never be fully reduced and that any target sites impacting α would overwhelmingly be associated with PSII.

Although the increase in damage with decreasing wavelengths is not surprising (cf. Coohill 1991; Baker and Bowyer 1994 and Lumsden 1997) the discrepancy between the various measurements can not simply be explained by the mechanics of the different measurements (Schreiber 1995, Kolber et al. 1998). The measurements were independent, highly repeatable and showed wavelength-specific features. It is clear from figure 3.6 that the fluorescence measurements agree well with the measurements of damage to carbon fixation even though the slopes of both lines indicate that the damage to PSII underestimates the overall damage to carbon fixation. An underestimation implies that not all of the damage to carbon fixation originates from PSII targets. However both the theoretical (as defined by equations 3.5 & 3.6) and measured correlation ($R^2 \sim 0.77$) between damage to PSII and carbon fixation are robust. Discrepancies between PSII and carbon fixation damage would likely increase during

light-saturated photosynthesis when the re-oxidation of the plastoquinone pool becomes a limiting factor to the maximum rate of photosynthesis. In addition, if targets are located outside of PSII, the damage measured here is a low estimate of damage. It is also very clear from the comparisons of the damage to the quantum yield under UVR alone and under both UV and PAR that PAR alleviates the damage to PSII. This is perhaps due to the reduction of molecules involved in radical scavenging. The comparisons of the yields of UV and UV/PAR treated phytoplankton demonstrate the rapid response to potential damage notwithstanding the effects of photoactivation or active repair.

Changes in the quantum yield alone do not elucidate the mechanisms of damage associated with UVR. In fact studies have been done showing little or no change in the quantum yield of PSII despite a large plant and microalgal literature implicating the D1 protein site as a potential target of damage (Neale et al. 1993, Lesser et al 1994). This is because the correct interpretation of fluorescence measurements requires considering both the time constants of the measurements and the specificity of the target site (Butler 1978; Geacintov and Breton 1987; Govindjee 1995). For example, the herbicide DCMU competes with plastoquinone for binding to the Q_B site, blocking electron transport from Q_A to Q_B . The DCMU induction curve therefore, gives information on the fraction of reduced Q_A (Melis and Schreiber, 1979; Melis and Duysens, 1979); it is not a good indicator of changes in either $[Q_A]$ or $[PQ]$. The data show poor relationships between the damage as estimated from Kautsky curves with DCMU and without DCMU. The significant inconsistencies between damage to carbon fixation and changes in the quantum efficiency of PSII as calculated from the different fluorescent measurements suggest damage beyond the site of DCMU binding. Simply described the damage to PSII

as indicated by the fluorescence transients reduces the electron flow from the reaction centre to plastoquinone.

Analysis of the DCMU induction rise shows significant wavelength dependency in the connectivity parameter J_{con} despite not seriously altering both $\phi_{\text{IIc}}^{\circ}(\text{DCMU})$ and the optical cross section of PSII. If a change in the concentration of oxidised Q_A was an important component of UV damage this should have been manifested as a change in either the amplitudes of the slow or fast components of the fluorescence decay curves after a single turnover saturating flash. However, no significant changes were found. Furthermore, we would have expected considerable variability in both $\phi_{\text{IIc}}^{\circ}(\text{DCMU})$ and the optical cross section of PSII if the D1 protein were a major UV target. Perhaps a change in the connectivity is a discrete mechanism that while not seriously altering σ_{psII} , provides oxidative relief through non-photochemical quenching (ie. heat dissipation).

Despite small decreases in $\phi_{\text{IIc}}^{\circ}(\text{DCMU})$ and σ_{psII} these data show that exciton movement is impacted by UV, especially UVB. Unlike the cases of no UVR or when there is free exciton movement, an increase in UVR inhibits free distribution of energy among the reaction centers in a domain. The competition for excitation energy decreases because exciton movement is related to the functional distance between pigments (Paillotin 1976). These data suggest that high energy UVB causes a conformational change in the reaction center structure. This change results in either a small loss of efficiency of stable charge separation or an inability of the reaction center to dissipate exciton energy. Under low or no light conditions UV photons cause instability of Q_B^- . Our data on the differences in induction curve damage with and without DCMU would indicate that this causes a reduction in the rate of electron flow to PQ. This is also

consistent with the increase in damage seen under no PAR light. In this case the potential of Q_B^- to become reduced again, protonated and then exchanged with PQ is low. In other words, the addition of UVR makes damage by light more efficient even under light-limiting conditions by altering the function (ability to generate stable charge separation) but more importantly the physical structure of reaction centers (where the eventual result is decrease in the probability of reducing PQ).

The distinction between ϕ_{II} and ϕ_{exc} is based on the redox state of Q_A with ϕ_{exc} calculated from the maximum variable fluorescence under actinic light while ϕ_{II} is strongly influenced by the PFD (Kroon 1994). However, in the case of our measurements the PFD did not change so the increase in Ft is the result of UV light induced quenching (equation 3.4, Figure 3.6a). The discrepancy between ϕ_{exc} and either carbon damage or ϕ_{IIc}^0 (K_{aut}) indicates that damage is greater to Fm than Fm'. The net result is a decrease in the total electron transport as wavelength decreases. The light-limited, carbon fixation rate is dependent on this flow of electrons from PSII. Electron transport is the product of σ_{psII} , photon flux density (PFD) and ϕ_{II} . Our experimental setup held PFD constant and only small changes in σ_{psII} are reported. This would explain the robust relationship between ϕ_{II} and carbon damage. It should therefore be possible to draw conclusions about decreases in carbon fixation and potentially growth rate from measurements of ϕ_{II} and PFD. Furthermore, this non-invasive measurement is amenable to *in situ* studies of UV damage.

In conclusion, damage from UVR to either PSII or carbon fixation shows a wavelength dependency. Damage to the PSII quantum yields is robustly and linearly related to carbon fixation on short time scales. This relationship reflects damage at target

sites on both the donor and acceptor side of PSII and can be explained by comparing the discrepancies between the different measurements of photosystem II fluorescence.

Ultraviolet light decreases the electron flow from reaction centers to plastoquinone.

Under light limiting conditions like those found in the oceans, this is significant.

3.6 References

- Baker NR, Noguez, S, Allen, DJ (1997) Photosynthesis and photoinhibition. In Lumsden, P(ed) *Plants and UVB: responses to environmental change*. Cambridge University Press pp 95-111.
- Baker NR, Bowyer, JR (1994) Photoinhibition of photosynthesis from molecular mechanisms to the field. BIOS scientific, Oxford, 471 pp.
- Boucher NP, Prezelin BB (1996) An in situ biological weighting function for UV inhibition of phytoplankton carbon fixation in the Southern Ocean. *Mar Ecol-Prog Ser* 144: (1-3) 223-236 DEC 1996
- Butler, WL. 1978. Energy distribution in the photochemical apparatus of photosynthesis. *Annu. Rev. Plant Physiol.* 29: 345-378.
- Caldwell, MM., Camp, LB., Warner, CW., Flint, SD. 1986. Action spectra and their key role in assessing biological consequences of solar UV-B radiation change. In R. C. Worrest & M. M. Caldwell (eds). *Stratospheric Ozone Reduction, Solar Ultraviolet Radiation and Plant Life.* Springer Verlag, New York pp: 87-111.
- Calkins, J., Thordardottir, T. 1980. The ecological significance of solar UV radiation on aquatic organisms. *Nature.* 283: 563-566.
- Cao J. & Govindjee. 1990. Chlorophyll a fluorescence transient as an indicator of active and inactive Photosystem II in thylakoid membranes. *Biochim. Biophys. Acta.* 1015: 180-88.
- Coohill, T. P. 1989. Ultraviolet action spectra for higher plants. *Photochem. Photochem.* 50: 451-457.
- Coohill, T. P. 1991. Action spectra again? *Photochem. Photobiol.* 54: 859-870.
- Cullen, J. J., & Lesser, M. P. 1991. Inhibition of photosynthesis by ultraviolet radiation as a function of dose and dose rate: results for a marine diatom. *Mar. Biol.* 111: 183-190.
- Cullen, J. J., Neale, P. J., & Lesser, M. P. 1992. Biological weighting function for the inhibition of phytoplankton photosynthesis by ultraviolet radiation. *Science* 258: 646-650.
- Diner, B.A., & deVity, C. (1985) In *Advance in Photosynthesis Research*, Vol. 1 (Sybesma, C., Ed) Martinus Nijhoff/Dr. W. Junk, The Hague. 407-411
- Dionisio, M. L., Tsuzuki, M. & Miyachi, S. 1989. Blue light induction of carbonic anhydrase activity in *Chlamydomonas reinhardtii*. *Plant Cell Physiol.* 30: 215-19.
- El-Sayed, S. Z., Stephens, F. C., Bidigare, R. R. & Ondrusek, M. E. 1990. Effect of ultraviolet radiation on Antarctic marine phytoplankton. In Kerry, K. R. & Hempel, G. (Eds.). *Antarctic Ecosystems. Ecological Change and Conservation*. Springer-Verlag, Berlin, pp. 379-85.
- Farman, J. C., Gardiner, B. G., & Shanklin, J. D. 1985. Large losses of total ozone in Antarctica reveal seasonal ClOx/NOx interaction. *Nature* 328: 207-210.
- Geacintov, N. E., & Breton, J. 1987. Energy transfer and fluorescence mechanisms in photosynthetic membranes. *CRC Crit. Rev. Plant Sci.* 5: 1-44.
- Govindjee. 1995. Sixty-three years since Kautsky: Chlorophyll a fluorescence. *Aust. J. Plant. Physiol.*, 22:131-160.
- Greenberg, B. M., Gaba, V., Canaani, O., Malkin, S., Mattoo, A. K. & Edelman, M. 1989. Separate photosensitizers mediate degradation of the 32-kDa photosystem II reaction center protein in the visible and UV spectral regions. *Proc. Nat. Acad. Sci.* 86: 6617-20.
- Guillard RRL (1975). Culturing of phytoplankton for feeding marine invertebrates. In Smith WL & Chanley MH (Eds) *Culture of marine invertebrate animals* Plenum Press, New York, pp.29-60.
- Helbing, E. W., Villafane, V., Ferrario, M., & Holm-Hansen, O. 1992. Impact of natural ultraviolet radiation on rates of photosynthesis and on specific marine phytoplankton species. *Mar. Ecol. Prog. Ser.* 80: 89-100.

- Iwanzik, W., Tevini, M., Dohnt, G., Voss, M., Weiss, W., Graber, P. & Renger, G. 1983. Action of UV-B on photosynthetic primary reactions in spinach chloroplasts. *Physiol. Plant* 58: 401-07.
- Jansen, M. A. K., Gaba, V., Greenberg, B., Mattoo, K. A. & Edelman, M. 1993. UV-B driven degradation of the D1 reaction-center protein of photosystem II proceeds via plastosemiquinone. In: Yamamoto, H. Y and Smith, C. M. (Eds.). *Photosynthetic Responses to the Environment*. American Soc. of Plant Physiologists, Rockville, Maryland, pp. 142-49.
- Jeffrey, S.W. & Humphrey, G.F. 1975. New spectrophotometric equations for determining chlorophylls a, b, c1 and c2 in higher plants, algae and naturel phytoplankton. *Biochem. Physiol. Pflanz.* 167:191-194.
- Jokiel, P. L. & York, R. H. Jr. 1984. Importance of ultraviolet in photoinhibition of microbial growth. *Limnol. Oceanogr.* 29: 192-99.
- Jones, L. W. & Kok, B. 1966. Photoinhibition of chloroplast reactions. I. Kinetics and action spectra. *Plant Physiol.* 41: 1037-43.
- Karentz, D. 1994. Ultraviolet tolerance mechanisms in Antarctic marine organisms. In Weiler, S. & Penhale, P. (eds). *Ultraviolet Radiation in Antarctica: Measurements and Biological Effects*. Ant. Res. Ser. 93:1-10.
- Karentz, D. Cleaver, J. E., & Mitchell, D. L. 1991. Cell survival characterisitcs and molecular responses of Antarctic phytoplankton to ultraviolet-B. *J. Phycol.* 27: 326-341.
- Kolber, Z.S. Prasil, O. & Falkowski, P.G. 1998. Measurements of variable fluorescence using fast repetition rate techniques: defining methodology and experimental protocols. *Biochim. Biophys. Acta.* 1367:88-106.
- Kroon, B. M. A., 1994. Variability of photosystem II quantum yield and related processes in *Chlorella pyrenoidosa* (Chlorophyta) acclimated to an oscillating light regime simulating a mixed photic zone. *J. Phycol.* 30: 841-852.
- Kulandaivelu, G. & Noorudeen, A. M. 1983. Comparative study of the action of ultraviolet-C and ultraviolet-B radiation on photosynthetic electron transport. *Physiol. Plant.* 58: 389-94.
- Lavorel, J. 1959. Induction of flourescence in quinone-poisoned *Chlorella* cells. *Plant Physiol.*, 34:204-209
- Lesser, M. P., Cullen, J. J. & Neale, P. J. 1994. Carbon uptake in a marine diatom during acute exposure to ultraviolet B radiation: Relative importance of damage and repair. *J. Phycol.* 30: 183-92.
- Lumsden, P.J. (ed) 1997. *Plants and UVB: responses to environmental change*. Cambridge University Press. Cambridge. 355 pp.
- Melis, A. & Duysens, L.N.M. 1979. Biphasic energy conversion kinetics and absorbance difference spectra of photosystem II of chloroplasts. Evidence for two differnent photosystem II reaction centers. *Photochem. Photobiol.* 29:373-382.
- Melis, A., Nemson, J. A. & Harrison, M. A. 1992. Damage to functional components and partial degradation of photosystem II reaction center proteins upon chloroplast exposure to ultraviolet-B radiation. *Biochim. Biophys. Acta.* 1100: 312-20.
- Melis, A. & Schreiber, U. 1979. The kinetic relationship between the c-550 absorbance change, the reduction of Q (A320) and the variable fluorescence yield change in chloroplasts at room temperature. *Biochim. Biophys. Acta* 547:47-57.
- Munday, J.C.M., Jr. & Govindjee 1969. Light-induced changes in the fluorescence yield of chlorophyll a in vivo. III. The dip and peak in fluorecence transient of *Chlorella pyrenoidosa*. *Biophy. J.*, 9:22-33.
- Neale, P. J., Cullen, J. J., Lesser, M. P. & Melis, A. 1993. Physiological bases for detecting and predicting photoinhibition of aquatic photosynthesis by PAR and UV radiation. In: Yamamoto, H. Y and Smith, C. M. (Eds.). *Photosynthetic Responses to the Environment*. American Soc. of Plant Physiologists, Rockville, Maryland, pp. 61-77.
- Neale, P.J., Davis, R.F. & Cullen, J.J. 1998. Interactive effects of ozone depletion and vertical mixing on photosynthesis of Antarctic phytoplankton. *Nature.* 392:585-589.
- Neale, P.J., & Kieber, D.J. 2000. Assessing biological and chemical effects of UV in the marine environment: spectral weighting functions. In Hester, R.E. & Harrison, R.M. (eds). *Causes and Environmental Implications of Increased UV-B Radiation*. Issues in Environmental Science and Technology, Num 14., The Royal Society of Chemistry, Cambridge pp. 61-83.
- Neale, P. J., Lesser, M. P., & Cullen, J. J. 1994. Effects of ultraviolet radiation on the photosynthesis of phytoplankton in the vicinity of McMurdo station, Antarctica. In Weiler, S. & Penhale, P. (eds). *Ultraviolet Radiation in Antarctica: Measurements and Biological Effects*. Ant. Res. Ser. 125-142.

- Ohad, I., Keren, N., Zer, H., Gong, H., Mor, T., Gal, A., Tal., & D. Y., (1994) Light -induced degradation of the photosystem II reaction centre D1 protein *in vivo*: an integrative approach. In: Baker NR, Bowyer, JR (eds) Photoinhibition of photosynthesis from molecular mechanisms to the field. BIOS scientific, Oxford, (161-177).
- Paillet G (1976) Movements of excitations in the photosynthetic domains of photosystem II. *J. theor. Biol.* 58: 237-252
- Prézelin, B. B., Boucher, N. P. & Schofield, O. 1994a. Evaluation of field studies of UVB radiation effects on Antarctic marine primary production. In: Biggs R. H., and Joyner, M. E. B. (Eds.). Stratospheric Ozone Depletion: UV-B Radiation in the Biosphere. NATO ASI Series 118: 181-94.
- Prézelin, B. B., Boucher, N. P., & Smith, R. C. 1994b. Marine primary production under the influence of the Antarctic ozone hole: Icecolors '90. In Weiler, S. & Penhale, P. (eds). Ultraviolet Radiation in Antarctica: Measurements and Biological Effects. Ant. Res. Ser. 159-186.
- Quate FE, Sutherland BM, Sutherland JC 1992. Action spectrum for DNA damage in alfalfa lowers predicted impact of ozone depletion. *Nature* 358:576-578.
- Renger, G., Völker, M., Eckert, H. J., Fromme, R., Hom-Veit, S. & Gräber, P. 1989. On the mechanism of photosystem II deterioration by UV-B radiation. *Photochem. Photobiol.* 49: 97-105.
- Richter, M., Rühle, W. & Wild, A. 1990. Studies on the mechanism of photosystem II photoinhibition I. A two-step degradation of D1-protein. *Photosynthesis Res.* 24: 229-35.
- Rundel, R. D. 1983. Action spectra and estimation of biologically effective UV radiation. *Physiol. Plant.* 58: 360-366.
- Sakshaug, E., Bricaud, A., Dandonneau, Y., Falkowski, P.G., Kiefer, D.A., Legendre, L., Morel, A. Parslow, J. & Takahashi, M. 1997. Parameters of photosynthesis: definitions, theory and interpretation of results. *J. Plank. Res.* 19(11):1637-1670.
- Savitsky, A. & Golay, M.J. 1964. Smoothing and differentiation of data by simplified least squares procedure. *Anal. Chem.* 36:1627-1638.
- Schneitger, B., Critchley, C., Santore, U. J., Graf, M., & Krause, G. H. 1994. Relationship between photoinhibition of photosynthesis, D1 protein turnover and chloroplast structure. Effects of protein synthesis inhibitors. *Plant Cell Environ.* 17: 55-64.
- Schofield, O., Prézelin, B. B., & Kroon, B. M. A. 1995. Impact of ultraviolet-B radiation on photosystem II activity and its relationship to the inhibition of carbon fixation rates for Antarctic ice algae communities. *J. Phycol.* 31: 703-715.
- Schreiber, U. Hormann, H., Neubauer, C. & Klughammer, C. 1995. Assessment of photosystem II photochemical quantum yield by chlorophyll fluorescence quenching analysis. *Aust. J. Plant Physiol.* 22(2): 209-220.
- Smith, R. C., Baker, K., Holm-Hansen, O., & Olson, R. S. 1980. Photoinhibition of photosynthesis in natural waters. *Photochem. Photobiol.* 31: 585-592.
- Smith, R. C., Prézelin, B. B., Baker, K. S., Bidigare, R. R., Boucher, N. P., Coley, T., Karentz, D., MacIntyre, S., Matlick, H. A., Menzies, D., Ondrusek, M., Wan Z., & Waters, K. J. (1992) Ozone depletion: Ultraviolet radiation and phytoplankton biology in Antarctic waters. *Science* 255: 952-959.
- Strid, A. Chow, W. S. & Anderson, J. M. 1990. Effects of supplementary ultraviolet-B radiation on photosynthesis in *Pisum sativum*. *Biochim. Biophys. Acta*, 1020: 260-68.
- Trissl H-W, Lavergne J (1994) Fluorescence induction from photosystem II: analytical equations for the yields of photochemistry and fluorescence derived from analysis of a model including exciton-radical pair equilibrium and restricted energy transfer between photosynthetic units. *Aust. J. Plant Physiol.* 22: 183-193
- Teramura AH, Ziska LH Szein AE. (1991) Changes in growth and photosynthetic capacity of rice with increased UV-B radiation. *Physiologia Plantarum* 83: 373-380.
- Vass, I., Sass, L., Spetea, C., Bakou, A., Ghanotakis, D., & Petrouleas, V., 1996. UV-B-induced inhibition of photosystem II electron transport studied by EPR and chlorophyll fluorescence. Impairments of donor and acceptor side components. *Biochemistry*. 35(27):8964-73.
- Vernet, M., Brody, E. A., Holm-Hansen, O., & Mitchell, B. G. 1994. The response of Antarctic phytoplankton to ultraviolet radiation: Absorption, photosynthesis, and taxonomic composition. In Weiler, S. & Penhale, P. (eds). Ultraviolet Radiation in Antarctica: Measurements and Biological Effects. Ant. Res. Ser. 143-158.

Ziska L.H., Teramura A.H., Sullivan J.H. (1983) Physiological Sensitivity of Plants Along an Elevational Gradient to UV-B Radiation. *Amer. J. Bot.* **79**(8): 863-871.

3.7 Tables

Table 3.1 Symbols and abbreviations. Units are given in brackets unless dimensionless

F _o	Fluorescence yield when all Q _A is oxidised
F _m	Fluorescence yield when all Q _A is reduced
F _o '	Fluorescence yield when Q _A is oxidised after actinic illumination
F _m '	Fluorescence yield when Q _A is reduced by saturating light after actinic illumination
F _t	Fluorescence yield in the presence of actinic illumination
q	proportion of open PSII reaction centers
J _{con}	connectivity among reactions centers in PSII domains
σ _{psII}	geometric absorption cross section of the PSII reaction center [relative units] Units for σ are usually A ² (quanta) however for the calculations here units are relative to the incoming light which was constant in all instances
σ _{psu}	geometric absorption cross section of a photosynthetic unit that participated in the evolution of one molecule of oxygen
A	amplitude of PSII that shows a fast fluorescence decay after a single turnover flash
B	amplitude of PSII that shows a slow fluorescence decay after a single turnover flash
k _a	Fast fluorescence decay rate constant [ms ⁻¹]
k _b	Slow fluorescence decay rate constant [s ⁻¹]
Φ _{lle^o (DCMU)}	Maximum quantum yield of PSII for stable charge separations as calculated from Kautsky induction curves with DCMU
Φ _{lle^o (kaut)}	Maximum quantum yield of PSII for stable charge separations as calculated from Kautsky induction curves without DCMU
Φ _{exc}	Efficiency of photon trapping by open reaction centers of PSII in the presence of actinic light
Φ _{ll}	Apparent quantum yield of PSII for stable charge separations
Φ _i	Fluorescence yield of the rise of the Kautsky curve from F _o to F _i
Φ _d	Fluorescence yield of the rise of the Kautsky curve from F _o to F _d
Φ _p	Fluorescence yield of the rise of the Kautsky curve from F _o to F _p , equivalent to Φ _{lle^o (kaut)}
P _{max}	Maximum rate of carbon fixation [μg C μg Chl a ⁻¹ hr ⁻¹]
α	The light limited slope of the photosynthesis- irradiance relationship [mg C mg Chl a ⁻¹ hr ⁻¹ (μmol m ⁻² s ⁻¹) ⁻¹]
I _k	P _{max} / α, the irradiance at which P _{max} would be reached if photosynthesis was a linear function of photon flux [μmol m ⁻² s ⁻¹]

Table 3.2 Growth characteristics of *T. pseudonana*. (20° C, 12:12 L:D, 80 $\mu\text{mol photons m}^{-2} \text{s}^{-1}$)
Production units are $\mu\text{g C } \mu\text{g Chl a}^{-1} \text{hr}^{-1}$.

Parameter	Value
$\mu \text{ d}^{-1}$	0.85 ± 0.03
pg chl a/ Cell	11.0 ± 1.5
P versus I (Chl a specific)	
P_{max}	1.83 ± 0.2
	$0.012 \pm$
α	0.001
I_k	150 ± 6

Table 3.3 Calculated fluorescence parameters \pm the standard deviation from 30 minute treatments with PAR and UVR ($n>4$). Bold numbers indicate a significant difference from PAR ($p<0.05$)

Wavelength	ϕ_i	ϕ_d	ϕ_p	
PAR	0.159 \pm 0.047	0.142 \pm 0.049	0.633 \pm 0.039	
360	0.174 \pm 0.045	0.146 \pm 0.046	0.637 \pm 0.023	
340	0.215\pm0.034	0.184\pm0.038	0.619 \pm 0.027	
320	0.202\pm0.055	0.173 \pm 0.06	0.610\pm0.046	
300	0.141 \pm 0.022	0.113\pm0.026	0.534\pm0.051	
280	0.141 \pm 0.022	0.113\pm0.031	0.548\pm0.042	
	k_a (ms ⁻¹)	k_b (s ⁻¹)	σ_{psII}	J_{con}
PAR	8.2 \pm 1.0	84.8 \pm 26.9	52.3 \pm 14.4	0.93 \pm 0.22
360	7.3 \pm 1.2	107.0 \pm 66.2	53.1 \pm 7.0	0.97 \pm 0.07
340	6.3\pm1.7	95.6 \pm 45.0	46.6 \pm 13.6	0.83\pm0.1
320	7.5 \pm 1.5	82.1 \pm 57.7	40.6 \pm 10.2	0.79\pm0.12
300	7.9 \pm 1.8	108.0 \pm 144.7	49.7 \pm 17.9	0.44\pm0.11
280	7.1 \pm 1.2	88.5 \pm 52.5	49.9 \pm 2.8	0.54\pm0.12
	a	b		
PAR	0.422 \pm 0.041	0.108 \pm 0.059		
360	0.407 \pm 0.039	0.102 \pm 0.014		
340	0.386 \pm 0.053	0.133 \pm 0.064		
320	0.410 \pm 0.045	0.134 \pm 0.058		
300	0.389 \pm 0.046	0.128 \pm 0.028		
280	0.387 \pm 0.021	0.116 \pm 0.031		

Table 3.4 Parameters for type II linear regressions from the data in figure 3.6b comparing the weightings of the fluorescence parameters to the damage to carbon fixation. Linear regressions were solved using a cubic equation and the standard deviations of the error in both the x and y directions. Values of the slope and Y-intercept are shown \pm the 95% confidence interval.

	Slope	Y-intercept	R²
Kautsky w/ DCMU	3.78 \pm 1.3	0.0006 \pm 0.005	0.44
Kautsky w/o DCMU	1.43 \pm 0.24	0.0002 \pm 0.004	0.78
ϕ_{max}	1.43 \pm 0.25	0.0002 \pm 0.004	0.77
ϕ_{a}	1.97 \pm 0.30	0.0002 \pm 0.004	0.81

3.8 Figures

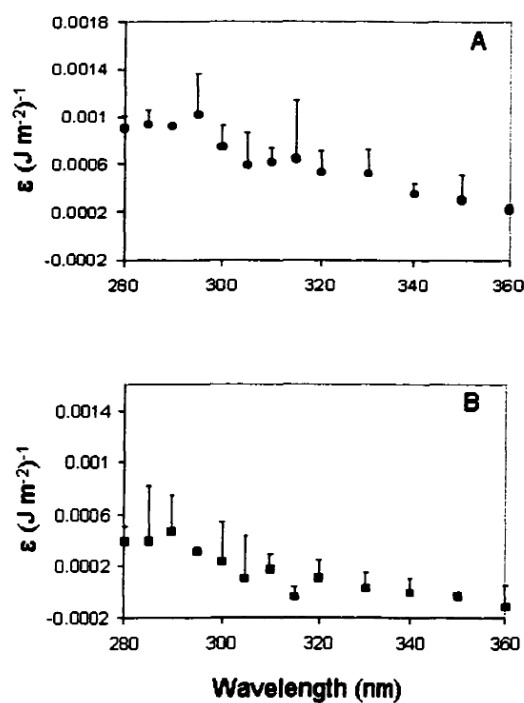


Figure 3.1 A. Action spectra of damage to the maximum quantum yield as calculated from induction curves without DCMU $\phi\text{IIeo(Kaut)}$ (circles) after a thirty minute incubation under monochromatic UVR only (error bars are the 95% confidence limits, $n > 4$). Calculations of ϵ are explained in the methods. B. As in A, but as calculated from the maximum quantum yield as calculated from induction curves with DCMU $\phi\text{IIeo(DCMU)}$ (squares).

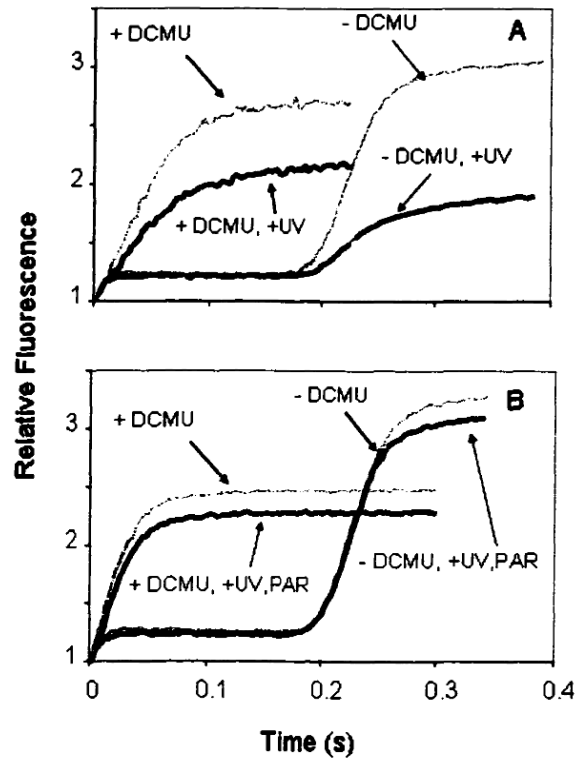


Figure 3.2. A. Induction curves with and without DCMU before (grey) and after (black) a 30 minute treatment with 300 nm UVR. Curves were normalized to F_0 because the majority of the decrease in F_v/F_m was due to changes in F_m . B. As in A, but after a 30 minute treatment with both 300nm UVR and $60 \mu\text{mol photons m}^{-2} \text{s}^{-1}$ PAR. The measurements and light intensities of the induction curves are explained in the methods.

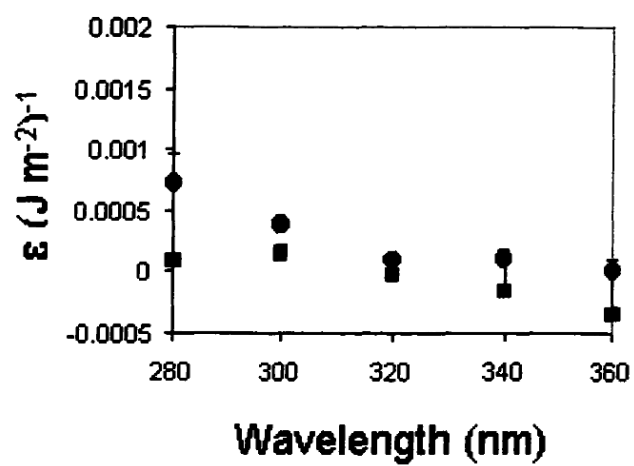


Figure 3.3 Action spectra of damage to ϕ IIeo(Kaut) (circles) and ϕ IIeo(DCMU) (squares) after a thirty minute incubation under monochromatic UVR and $60 \mu\text{mol photons m}^{-2} \text{s}^{-1}$ PAR (error bars are the 95% confidence limits, $n>4$).

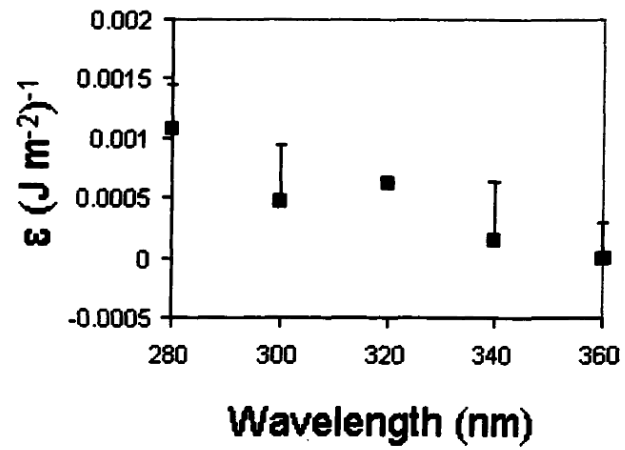


Figure 3.4 Action spectrum of damage to carbon fixation after a thirty minute incubation under monochromatic UVR and $60 \mu\text{mol photons m}^{-2} \text{s}^{-1}$ PAR (error bars are the 95% confidence limits, $n > 4$).

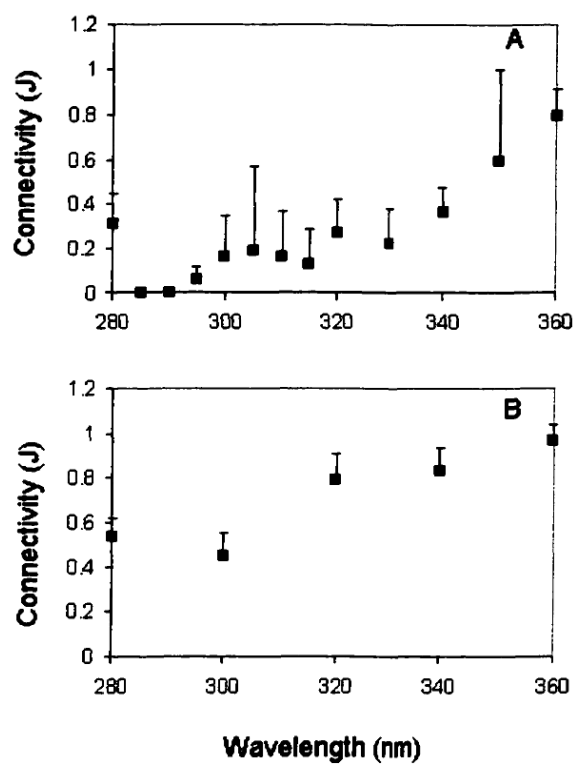


Figure 3.5 A. Measurement of the parameter J_{con} as calculated from induction curves with DCMU after a thirty-minute incubation under monochromatic UVR only (error bars are the 95% confidence limits). B. As in A, but after a 30 minute incubation under monochromatic UVR and $60 \mu\text{mol photons m}^{-2} \text{s}^{-1}$ PAR.

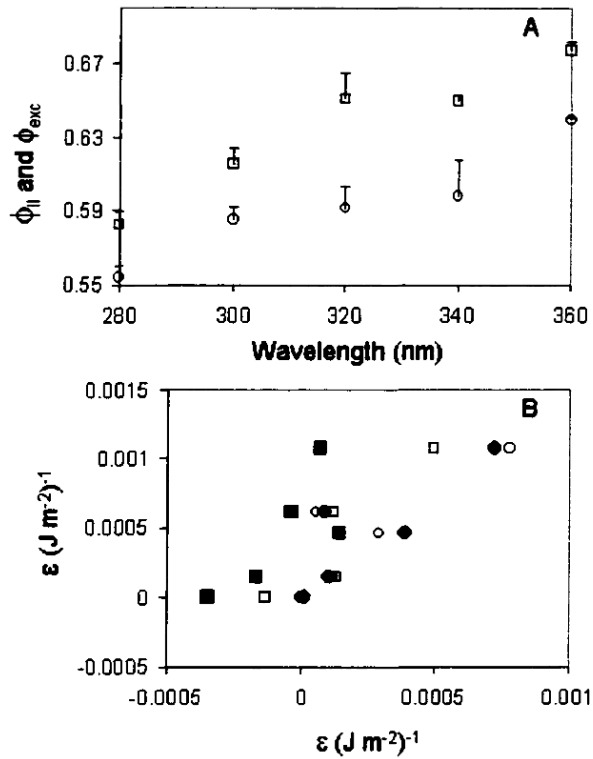


Figure 3.6 A. Circles indicate measurements for the efficiency of photon trapping by PSII after a 30 minute incubation under monochromatic UVR and $60 \mu\text{mol photons m}^{-2} \text{s}^{-1}$ PAR (ϕ_{exc}) (error bars are the 95% confidence limits, $n > 4$). Squares indicate measurements for the apparent quantum yield of PSII (ϕ_{II}) after a 30 minute incubation under monochromatic UVR and $60 \mu\text{mol photons m}^{-2} \text{s}^{-1}$ PAR (error bars as indicated above). Values of ϕ_{II} and ϕ_{exc} under PAR alone were 0.68 (0.005) and 0.63 (0.01) respectively. B. The relationship between the weights ϵ as calculated from fluorescence parameters, ϕ_{II}^0 (closed circle), ϕ_{II}^0 (dcmm) (closed square), ϕ_{II} (open square), and ϕ_{exc} (open circle) versus the weights ϵ as calculated from measurements of carbon fixation. The corresponding type II linear regressions of the slopes and R^2 values are presented in Table 4.4 for clarity.

4 *Nonionella stella*, a modern analog to the protist undergoing secondary endosymbiosis 250 Mya: plastid structure and function

4.1 Abstract

The unknown function of sequestered chloroplasts in the benthic foraminifer *Nonionella stella* is investigated. We characterize and identify the chloroplasts sequestered in the foraminifer inhabiting sediments collected off California from a water depth of about 600 m. Using electron microscopy and a variety of molecular techniques including western blotting of foraminiferal proteins, cloning and sequencing of the 16S rDNA it is shown that this foraminifer sequesters diatom plastids. More specifically two unique sequences of diatoms were found in all samples examined: a diatom 16S rDNA sequence resembling *Skeletonema costatum* was the most prevalent and a diatom sequence resembling *Odontella sinensis* was also abundant. Identical sequences matching these two organisms were found in samples collected on different cruises over three years despite minimal or no occurrences of these diatoms in the water column or the sediments. Examinations of electron micrographs, fluorescence and absorption spectra, chloroplast proteins and enzyme assays reveal intact, functional chloroplasts. The chloroplasts housed in the foraminifer are long lived. Samples up to one year old remained intact and were biophysically functional. Western blots of three major chloroplast proteins: ribulose bis-phosphate carboxylase oxygenase (RuBisCO), the D1 protein and the fucoxanthin chlorophyll *a* protein complex confirm the presence of both nuclear and chloroplast encoded proteins of the chloroplast and provide information about the condition of chloroplast proteins that most likely were synthesized many months prior to the analysis. The presence of intact D1 protein is especially surprising

given the rapid turnover of the protein *in vivo*. As well, the two enzymes examined, RuBisCO and phosphoenol pyruvate carboxylase (PEPc) remained active. Three hypotheses on the possible function of sequestered chloroplasts in the deep sea are presented. Our results suggest that the potential for photo or chemoautotrophy is low and instead the chloroplasts are used to meet the nitrogen requirements of the host. Immunolocalization of the nuclear encoded protein nitrate reductase is presented in support of this hypothesis. This is a protein universally found in plants but not in foraminifera. The organism and its metabolic adaptations are presented as a modern analog of protistan evolution and the evolution of nitrogen metabolism.

4.2 Introduction

The retention of algae and algal plastids or other organelles by marine invertebrates is a much studied phenomenon (Blackbourn et al. 1973; Chai and Lee 2000; Correia and Lee 2000; Felbeck et al. 1983; Johnson et al. 1995; Lee and Zucker 1969; Muller-Merz and Lee 1976; Rumpho et al. 2000). Yet the relationship between photosynthetic microbe and host is not well understood and is limited to protists or invertebrates (Smith 1991). The classic symbiotic relationship is mutually beneficial, as in the coral-zooxanthellae symbiosis where the algae provides reduced carbon to the host and nitrogen is recycled between the two organisms (Falkowski 1993; Rahav et al. 1989). Over thirty years ago ultrastructural analysis of the marine ciliate *Mesodinium rubrum* revealed an "incomplete symbiosis" involving functional chloroplasts and nonciliate mitochondria (Taylor et al. 1969; Taylor et al. 1971). In recent years studies of algal chloroplast- host associations have been termed symbioses given their long lived association and the ability of the host to acquire a new metabolic property- as in the case

of Sacoglossan sea slugs (Green et al. 2000; Rumpho et al. 2000; Sanders 1991). In fact, symbiotic relationships involving chloroplasts were thought to provide similar nutrient feedbacks as found in the coral reef ecosystem (Lee and Bock 1976). This implies that the algal-host relationship is established to preserve and recycle limited nutrients such as nitrogen. Chloroplasts can be a rich source of carbohydrate and reduced nitrogen due to the presence of the Calvin cycle and a nitrogen pathway that reduces nitrate to glutamate and transports it out of the chloroplast (Falkowski and Raven 1997). However, the half-life of a functional chloroplast varies depending on numerous factors, most importantly light intensity but also the production of reactive oxygen species. Many proteins in the light harvesting apparatus of the chloroplast are turned over on the order of hours (Falkowski and Raven 1997). In some symbiotic relationships between algal chloroplasts and hosts chloroplast proteins are synthesized (Green et al. 2000; Mujer et al. 1995; Mujer et al. 1996; Pierce et al. 1996). It has also been demonstrated that some chloroplast proteins are synthesized in the animal cytosol and actually translocated back into the chloroplast (Pierce, Biron et al. 1996).

Foraminifera are among the marine organisms that either retain algae or sequester algal chloroplasts (Bernhard and Bowser 1999; Chai and Lee 2000; Correia and Lee 2000; Lee and Bock 1976; Lee et al. 1974; Lee and Zucker 1969; Leutenegger 1984). Like other chloroplast-host relationships chloroplasts provide photosynthate to the cell (Lee and Bock 1976; Lee and Zucker 1969). The specificity of host-algal associations has been determined by ultrastructure analysis (Leutenegger 1984) and also by feeding experiments (Correia and Lee 2000). Although foraminifer-diatom associations dominate, rhodophytes, chlorophytes, chrysophytes and dinoflagellates have also been

identified (Chai and Lee 2000; Leutenegger 1984; Muller-Merz and Lee 1976). It is thought that the widely distributed relationship between foraminifera and diatoms is not simply coincidental but is based on signal-receptor system between the surface of some algae and the foraminiferal pseudopod (Chai and Lee 2000). Eighteen different species of diatoms have been identified in the foraminifer *Amphistegina lobifera* (Lee et al. 1991; Lee et al. 1992). Diatom and chloroplasts found in foraminifera are sometimes not endemic to the specific habitat of the host (Lee et al. 1989). However, regardless of the specificity of the association, the following observations are axiomatic. Despite being able to sequester organelles, foraminifera retain the ability to feed and digest food (Chai and Lee 2000). Chloroplast retention in foraminifera reaches high density (3.7×10^4 /individual (Correia and Lee 2000). Otherwise stated, relationships between foraminifer and phytoplankton are different than casual associations between host and its food.

Finally, one might assume that all host- algal associations occur in organisms that live in the photic zone. This assumption is erroneous, however, because chloroplasts have been found in large numbers in specimens of the benthic foraminifer *Nonionella stella* collected from water depths >500 m (Bernhard and Bowser 1999). *N. stella* is the dominant biovolume contributor to the benthos of the Santa Barbara Basin (Bernhard et al. 2000), which is severely depleted in dissolved oxygen as well as enriched in hydrogen sulfide (Reimers et al 1996; Kuwabara et al 1999). Previous microscopic observations indicate the vast majority of chloroplasts in *Nonionella stella* are intact, well pigmented, and distributed throughout the foraminiferal cytoplasm suggesting that they are not merely being consumed and digested as a food source (Bernhard and Bowser 1999).

The myriad studies of photic symbiotic relationships involving plastids provide the basis for three hypotheses to explain plastid symbiosis in the benthic foraminifer *N. stella*. Plastids photosynthesize at extremely low light levels and provide reduced CO₂ to the host. In the absence of light, the plastids utilize the chemical gradients of the Santa Barbara Basin and provide certain reduced compounds to the host. Finally, given that foraminifera are unable to synthesize inorganic sources of nitrogen, the plastids are sequestered to meet the nitrogen requirements of the cell.

The potential for a light driven set of reactions to be used in an aphotic environment is an exciting biological phenomenon. To this end, we have characterized the major molecular and biophysical properties of the sequestered chloroplasts of *N. stella* and present an analysis of the potential utility of the plastids to the host.

4.3 Materials and methods

4.3.1 Sample collection

Samples were collected from the Santa Barbara Basin (USA, 34 15' N, 120 02' W, 551-591m) during three cruises: April 1999, October 2000 & February 2001. Details on collection methods are given in Bernhard et al. (1997). Briefly, as soon as possible after a box core was recovered on deck (i.e., within 10 minutes), bulk surface sediments (~1-3 cm) were placed in 125 ml or 250 ml opaque HDPE bottles. Sediments were added to the bottles to a depth of about 2 cm; the bottle was filled with chilled bottom water so that as little air space as possible was present. Bottles with samples were maintained at 5°C during transport and until sample processing or measurements.

4.3.2 Electron microscopy

Sediments were taken into an environmental room maintained at ambient temperature (5°C) soon after box core recovery (within 5 minutes). Sediments containing *N. stella* were fixed in 3% glutaraldehyde buffered with 0.1 M Na-cacodylate (pH 7.2). Samples were kept at 5°C during transport. Sediments were sieved over a 63 µm screen using chilled 0.1 M cacodylate buffer and individual foraminifers were removed from the coarse fraction when observed with a dissecting microscope. Specimens were further processed for ultrastructural analyses using standard protocols described in Bernhard and Bowser (1999). Material was examined with a Phillips 301 transmission electron microscope.

4.3.3 Molecular identification of chloroplasts

Mud samples for DNA extraction were sieved through a 63 µm stainless steel sieve using filtered cold seawater and individual foraminifera were isolated from the sediments with the aid of a dissecting microscope and maintained in cold seawater until extraction. Samples were mildly sonicated and washed in phosphate buffered saline three times to free other small particles or bacteria. DNA extraction protocols follow those of Holzmann and Pawlowski (1996). Briefly, between 25-50 foraminifera were sonicated for 5 s. on low power in 50 µl buffer (50 mM Tris pH 8.4, 2 mM EDTA, 0.1% triton x-100 and 0.5% Na deoxycholate) and incubated for 1 hour at 55°C. Particulate matter was removed by centrifugation and DNA extract was dialyzed against ultra-pure H₂O on a 0.02µm filter for 1 hour. DNA was amplified with universal 16S rDNA primers (27f and 1492r primers, 30 cycles 30s 94°C, 30s 52°C 45s 72°C (Field et al. 1997). PCR products were gel purified (Qiagen) and ligated into the pCR ®II vector (Invitrogen, TA cloning

Kit) and transformed into TOP10F' cells. Unique clones were screened by restriction fragment length polymorphism using the tandem tetrameric enzymes MSP I and HAE III (Promega). The DNA was run on a 2.5% metaphor gel (FMC Bioproducts) at 4°C for 1.5 hours (75 Volts). Unique clones were sequenced on an ABI 310 (Perkin Elmer) following the manufacturer's protocol.

4.3.4 Chloroplast proteins

Foraminiferal specimens were picked and cleaned as described above. Samples were disrupted by centrifugation in 50 µl buffer A (8% SDS, 0.2 M Na₂CO₃, 4mM PMSF, 50mM DTT). Controls of the marine diatom *Thalassiosira pseudonana* were treated the same way. Prior to loading SDS gels samples were diluted in one volume buffer B (4% SDS, 15% glycerol and 0.05% Bromothymol blue). Gels were run on 12% polyacrilamide gels at 150 V for 1.5 hours. Gels were transferred to PVDF membranes following the protocols of Towbin et al. (1970) for 1 hour at 60 volts. Immunoblots were performed using antibodies against fucoxanthin- chlorophyll a protein complex from the haptophyte algae *Isochrysis galbana* (FCP), RuBisCO protein also from *I. galbana* and the D1 protein from a conserved synthesized, amino acid sequence (kindly provided by Autar Mattoo). Immunoblots were visualized using the West Pico chemiluminescent substrate (Pierce chemicals) according to the manufacturer's protocol.

4.3.5 Pigment characterization

Samples of individual foraminifera as well as 1.0ml of bulk sediment were extracted overnight in 100% acetone and diluted to 90% acetone prior to HPLC, fluorescence or absorption measurements. HPLC samples were run on a Shimadzu HPLC. Absorption measurements were run on an Aminco DW-2a spectrophotometer.

Fluorescence excitation and emission spectra were run on an Aminco-Bowman series 2 luminescence spectrometer. Emission maximum for fluorescence excitation spectra was 680 nm (4nm slit width). 77K spectra were performed in quartz tubes that were slowly cooled over liquid nitrogen, plunged in liquid nitrogen and equilibrated for ten minutes.

4.3.6 Photochemical yields

Measurements of variable fluorescence on foraminiferal samples or mud diluted in filtered seawater were performed using the protocols outlined in Kolber et al. (Kolber et al. 1998). Samples were incubated in either blue or far red light in order to measure changes in reaction center size and changes in the quantum yield of photochemistry due to photoacclimation. Electron transport rates (ETR, units= $e RC^{-1} s^{-1}$) shown in table 4.1 were calculated from the equation:

$$ETR = \sigma_{psII} \cdot I \cdot Q_p \quad \text{Eq. 4.1}$$

Where σ_{psII} is the cross sectional area of photosystem II (m^2/quanta), I is the irradiance with units of $\text{quanta } m^{-2} s^{-1}$ and Q_p is the photochemical quenching (electrons/reaction center). We estimate Q_p to be equivalent to the measured F_v/F_m given the fact that the samples in this environment are essentially dark adapted. Irradiance estimates are made from theoretical estimates of clear sky irradiance and K_{440} the attenuation of seawater at 440 nm as the upper limit of light transmittance and K_{440} with the equivalent of $1 \text{ mg } m^{-3} \text{ chl } a$ (Morel 1988). Light at depth d is calculated from Beer's law:

$$I_d = I_0 \exp[-kd] \quad \text{Eq. 4.2}$$

4.3.7 Enzyme assays

Measurements of RuBisCO and PEPc activity were performed on foraminifera after isolation and cleaning (see above). Samples were suspended in ice-cold permeabilization buffer (50mM Bicine pH 8.0, 1mM EDTA, 10 mM MgCl₂, 5mM DTT, 1.5 M Glycerol, 10 mM NaHCO₃⁻, 0.2 mg ml⁻¹ lysolecithin). Cells were disrupted twice in an ice-cold Yeda press. Cells homogenates were aliquoted and incubated for 30 minutes at 25°C in the dark and then either ribulose bis-phosphate or phospho(enol)pyruvate was added (2.3 and 5.0 mM final concentration, respectively). Upon addition of substrate 7400 Bq NaH¹⁴CO₃⁻ (final activity) was added to each sample. Samples (including blank with no substrate) were incubated at 25°C for 30 minutes. Reaction was stopped by adding 20 µl 6N HCL. After the samples were counted in a scintillation counter (Beckman LS 6000IC), they were normalized to chlorophyll *a* content. Chlorophyll *a* was calculated using the tri-chromatic equation of Jeffries and Humphrey (1975). Measurements were done in triplicate. PEP enzyme rates are considered to be the sum of PEP carboxylase and PEP carboxylkinase as no attempt was made to distinguish between the two.

4.3.8 Redox chemistry of the NADP⁺/NADPH couple

Measurements of NADPH/NADP⁺ ratios were made under mildly reducing conditions in an agar gel intended to mimic the Santa Barbara Basin sediments. NADP⁺ reduction was performed spectrophotometrically and fluorometrically on abiotic samples incubated for 24 hours. Measurements of NADPH spectra were made on an Aminco DW-2000 spectrophotometer in 1cm quartz cuvettes (300–400 nm). Fluorometric measurements were made on a Molecular Devices plate reader (Spectra max gemini XS, 280 excitation, 340 emission). Aerobic, anaerobic and reducing conditions were created

in sealed tubes or micro-titer plates by making agar layers of various redox couples, incubating NADP^+ and measuring the fraction of reduced NADPH. The experimental setup involved creating a redox gradient by layering test tubes first with sulfuric agar, made from autoclaved seawater, agar (15g/L) Na_2S (final concentration between 1-500 μM) and the redox indicator, resazurin (final concentration 1.6 μM). Agar mixture was aseptically added to test tubes after degassing with nitrogen. Tris-buffered seawater (pH 7-8) with NADP^+ (final concentration 1-10mM) and resazurin were added to the agar plug after solidification. Samples were bubbled with air (oxic) or nitrogen gas (anoxic) or 500 μM Na-Dithionite was added (reducing, $E_{m7}=610\text{mV}$). The ratio of seawater to agar plug varied from 2:1 to 16:1. In this system sulfur chemistry is defined by the redox couple:

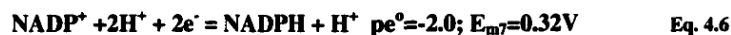


The acid-base chemistry of reduced sulfur is governed by:



Equation 4.5 in the biological system we are dealing with is obviously irrelevant.

The relationship between redox poise of a given chemical system, pH and the $\text{NADP}^+/\text{NADPH}$ couple can be derived from the following:



$$\text{pe} = 1/n[\log K - \log (\text{red})/(\text{ox})] \quad \text{Eq. 4.7}$$

$$\text{Eh} = (2.3RT/F)\text{pe} \quad \text{Eq. 4.8}$$

Where pe° is a non-dimensional scale of electron activity and Eh, the redox potential is measured in volts (V). Equation 4.7 is the Nernst equation which defines the electrical potential of any redox half reaction. From these equations we can derive the relationship between the redox poise of a system (Pe_{sys}), pH and the NADPH/NADP⁺ ratio (defined in the following equation as Q):

$$pe_{sys} = pe^{\circ} - 1/n \log[Q] + 1/n \log[H^+] \quad \text{Eq. 4.9}$$

If we also assume that the intracellular environment of the chloroplast varies and is not equal to pH 7 the relationship between the $pe^{\circ}_{w(pH=7)}$ of the NADP⁺/NADPH half reaction and pe° is:

$$pe^{\circ}_w = pe^{\circ} + 1/n \log[H^+] \quad \text{Eq. 4.10}$$

4.3.9 Immunolocalization of nitrate reductase

A nitrate reductase antibody from the marine diatom *Thalassiosira weissflogii* was tagged with a green fluorescent probe (Alexa 488, Molecular Probes) according to manufacturer's protocols. Frozen samples of *N. stella* were thawed, rinsed in PBS (phosphate buffered saline pH 7.8) and permeabilized with 1% DMSO in PBS overnight at 4 °C. Samples were then rinsed twice and incubated in a 1:200 dilution of antibody with PBS. Samples were incubated in microtiter plates overnight and rinsed three times in PBS. Samples were mounted on slides and examined under an epi-fluorescence microscope (Zeiss, axioscop 20). Cultures of *T. weissflogii* grown with NH₄⁺ were used as a negative control.

4.4 Results

4.4.1 Chloroplast identification

Ultrastructural analysis indicates that the gross features of the engulfed chloroplasts have morphologic attributes from diatoms. A three layer thylakoid lamella surrounds the inside of the chloroplast and there are interconnections between the lamella (figure 4.1). These are features of diatoms rather than dinoflagellate chloroplasts (Dodge 1973). As well, the centrally located pyrenoid with a single lamella passing through the center is also characteristic of a diatom.

Molecular identification of the chloroplasts was performed by PCR, RFLP, cloning and sequencing of the 16S rDNA gene. A typical RFLP gel from the 16S rDNA PCR product reveals two dominant patterns of clones that are diatom in origin (figure 4.2). Two 400bp sequences were consistently identified in all samples from three different cruises and partial sequences are shown compared to two marine diatom species (figure 4.3). *Nonionella stella* chloroplast 1 (NsChl1) is a close relative of the cosmopolitan diatom *Skeletonema costatum* (figure 4.3a). NsChl2 is a close relative of *Odontella sinensis* (figure 4.3b). Fifty clones from three independent samples of foraminifera were digested and approximately 80% of the clones exhibited the two dominant restriction digest patterns of figure 4.2. Of the 15 unique clones partially sequenced only 2 other chloroplast sequences were retrieved from BLAST searches. These were uncultured, unidentified marine 16S rDNA chloroplasts. Despite collecting samples from different years and in both the fall and spring the same diatom sequences and RFLP patterns were found in *N. stella*. The most significant difference between NsChl1 and NsChl2 is an 8 base pair difference starting at #189 on the *S. costatum* published sequence. This feature distinguishes the chloroplast sequences from each other and is seen in all samples. This

feature is a major sequence difference between *Skeletonema costatum* and *Odontella sinensis* (96.1%, homologous, figure 4.3). The major differences in 16S rDNA sequences between the three significant functional groups of algae: diatom, dinoflagellates and prymnesiophytes are shown in figure 4.3c. The dinoflagellate and prymnesiophytes are only 50% homologous to diatoms. This is shown to emphasize the major difference at the 16S sequence level between these major groups and the *N. stella* chloroplasts. The identification of the other partial sequences is beyond the scope of this work.

4.4.2 Chloroplast proteins

Western blot analyses of total protein extracts from *N. stella* confirm both the presence and intact nature of three key chloroplast proteins. The fucoxanthin-chlorophyll *a* pigment-protein complex for found in chromophytes and some dinoflagellates is encoded in at least 5 genes. The two major pigment-proteins are about 21.6 and 23.8 kDa (figure 4.4a). The diatom *Thalassiosira pseudonana* is presented as a comparison. The FCP antibody identically cross reacts with both the foraminiferal chloroplast and the diatom indicating that the fucoxanthin-chlorophyll *a* protein is the dominant light harvesting complex. A control antibody for the squash chlorophyll *a*-*b* protein complex was also challenged against the diatom and foraminifera proteins (figure 4.4a). The minor, single band cross-reaction is presumed to be the chlorophyll *a* component of the complex. The D1 component of the photosystem II structural D1/D2 dimer is present at 32 kDa (figure 4.4c). The large subunit of the ubiquitous carbon fixing enzyme, RuBisCO is present at 53 kDa (figure 4.4b). The D1 and RuBisCO proteins are encoded in the chloroplast while the FCP complex is encoded in the nucleus of the diatom. The blots presented from foraminifera samples that are between 9 and 12 months old.

4.4.3 Pigment characterization

HPLC pigment analyses as well as *in vitro* absorption of extracted pigments indicate that the dominant pigments are chlorophylls a and c and the carotenoids fucoxanthin, diadinoxanthin and beta-carotene (figure 4.5). The majority of the pigments contained in foraminiferal chloroplasts are pigment protein complexes as seen in HPLC chromatograms, Western blots, and 77K excitation/emission spectra. The chlorophyll degradation products, chlorophyllide *a* pheophytin are also present. In order to assess both the energy transfer capabilities of the chloroplasts and the relative ratios of free pigment, photosystem I (PSI) and photosystem II (PSII) 77K fluorescence excitation and emission spectra were measured. Excitation spectra measure the relative emission of chlorophyll a associated with PSII throughout the absorption range of pigments. Emission spectra measure the intensity of chlorophyll a fluorescence at the wavelength of maximum absorption. At biological temperatures the rate constant of fluorescence for PSI is effectively zero; therefore, cryogenic temperatures are used to decrease the rate constant of photochemistry (electron transfer reactions) and effectively increase the rate of both PS I and PSII fluorescence. At these temperatures it is possible to distinguish between the two reaction centers.

The fluorescence excitation spectrum of bulk Santa Barbara Basin mud is an abiotic spectrum, most likely a combination of degraded pigments and fluorescent organic matter. This is compared to the excitation spectrum of individual organisms (Figure 4.6a). The foraminiferal spectrum exhibits characteristic excitation energy transfer to chlorophyll *a* with high signal in the blue (400-450nm) due to the absorption peaks of chlorophyll and fucoxanthin. The broad maximum between 400-500 nm, due to increased light harvesting pigments, implies that the cell is low-light adapted. The

excitation spectrum of basin mud does not exhibit the characteristic energy transfer peaks of chlorophylls or fucoxanthin and is instead probably a mixed signal of degraded chlorophylls and other organic substances. The extraction of the pigments and *in vitro* absorption spectrum of *N. stella* reveal that the majority of pigments are intact and not degraded (figure 4.6b). *In vitro* absorption of chlorophylls and other pigments that are degraded typically have high blue to red ratios (>5) and have a significant blue peak shift to lower wavelengths. The *in vitro* absorption properties of *N. stella* are characteristic of intact, chlorophyll a-c containing phytoplankton with peaks at 432 nm, a broad shoulder at 460-500nm, 618nm and 664nm. The blue to red peak ratio is about 5, also characteristic of non-degraded *in vitro* absorption properties of diatoms.

The results of the 77K emission spectrum from about 20 foraminifera are shown in figure 4.7 along with a deconvolution analysis of the major Gaussian peaks contributing to the curve. The major Gaussian curves at 658, 673, 686, 704 and 735 correspond to chlorophyll c, light harvesting complex II, photosystem II and both 700 peaks can be attributed to photosystem I. Part of 686 peak could also be due to PSI without the LHCI (Brown 1988). The 77K emission curve provide further evidence that intact reaction centers capable of transferring light energy to the reaction center chlorophylls, P680 and P700 exist.

4.4.4 Photochemical yields and enzyme activity assays

Foraminifera removed from the mud and placed in cold seawater exhibited a fluorescence transient with a very low quantum yield of photochemistry (Figure 4.8, Table 4.1). Nonetheless, stable charge separation and a small reduction in Q_A were recorded. However, cells and mud exposed to varying levels of both blue and far-red

light did not exhibit changes in the quantum yield or sigma- phenomena characteristic of photo-acclimation. Light levels at 600 meters could vary between $1e^{-13}$ - $5.0e^{16}$ quanta $m^{-2} s^{-1}$ depending on the attenuation coefficient (table 4.1). The upper range is only a theoretical maximum and assumes no attenuation of light from any substance other than water. Electron transport rates were calculated from the measured absorption cross section, the quantum yield of photochemistry and the light flux. From equation 4.1 it is clear that light flux (or lack thereof) is the dominant variable responsible for the rate of electron flow; theoretical fluxes of light could vary by 19 orders of magnitude given Beer's law! Thus, electron transport rates in foraminiferal chloroplasts could potentially vary between no transfer of electrons and one electron every 50 seconds. It should be emphasized that without another source of light flux the theoretical upper limit of electron transport is less than the $t_{1/2}$ of a stable S_3 state making oxygen evolution highly improbable (Radmer and Kok 1973).

Nonionella stella stored at 4°C in the laboratory had measured RuBisCO and PepC activity that averaged 0.12 and 0.04 $\mu\text{mol C (mg chl a) hr}^{-1}$. These results are presented in table 4.1. RuBisCO activity is significantly lower than activities published elsewhere (Macintyre et al. 1996) where activities ranged from about 10-20 $\mu\text{mol C (mg chl a) hr}^{-1}$. However, sample preparations, cell breakage and obviously time, factor into the different measurements. Our rates are measured on samples that are approximately one year old. The half-life of the RuBisCO enzyme activity can be estimated to be at least 50 days.

4.4.5 Abiotic NADPH reduction

Our experimental system for testing abiotic NADPH reduction did not yield results significantly different from calculations based on redox potential ($p > 0.1$). The pH of the

system was fixed and the pe° of our system was equivalent to the H_2S/SO_4^{2-} couple $pe^{\circ}_w = -3.5$, therefore, according to equation 4.9 we could verify the pe° of the NADPH/NADP⁺ couple (-2.0 ± 0.2). These values are similar to -1.9 and -2.0 reported elsewhere (Morel and Hering 1993; Nicholls and Ferguson 1992). The range of Q given different redox couples and pH is plotted (figure 4.9). The error in the measurements are equal to about a decade change in Q (NADPH/NADP⁺) however we consider this minor at relevant biological pH's equaling between 3-30nM NADPH in 100 μ M NADP⁺ at pH 7. The change in Q given the published pe° s of -1.9 and -2.0 approximates a 10nM change under the same circumstances. The plot of pH and Q illustrates the important effect of pH (given a constant pe_{sys}) on both the pe° of the system and the pe° of NADPH. For example, given the dominant redox couple H_2S/SO_4^{2-} as pH increases the pe° of the system becomes more reducing thus increasing Q according to equation 4.9 (figure 4.9a). Changes in Q are also affected in systems where pH is held constant and the dominant redox couple changes (figure 4.9b). Both plots are graphed given the errors in our laboratory measurements.

4.4.6 Immunolocalization of nitrate reductase

Samples of *N. stella* cross reacted with the fluorescent nitrate reductase antibody and had a green fluorescence signal (figure 4.12b & 4.13a,b). These samples also correlated well with the auto-fluorescence from the *N. stella* plastids (figure 4.12a). Samples of *T. weissflogii* grown on NH_4^+ had no cross reaction with the antibody except for a small background signal from the diatom frustule. The strongest fluorescent signal from the antibody was associated with the chloroplasts (figure 4.13b). These data agree

well with immunolocalization of NR from *T. weissflogii* grown with NO_3^- which shows a high green fluorescent signal associated with the diatom plastid (figure 4.11).

4.5 Discussion

Chloroplast husbandry or sequestration by marine protists and invertebrates is not an uncommon phenomenon in photic regimes (Blackbourn et al. 1973; Green et al. 2000; Johnson et al. 1995; Mujer et al. 1995; Mujer et al. 1996; Rumpho et al. 2000). However, identification and characterization of chloroplasts sequestered by organisms living in aphotic regimes do not exist although their presence has been noted (Bernhard and Bowser 1999). Nothing is known about their possible function. We have taken the first step to understanding the possible roles of sequestered chloroplasts in aphotic zones by characterizing the major physical, molecular and biophysical signatures of the chloroplasts of *Nonionella stella*.

4.5.1 Ultrastructure and sequence identity

Structurally and molecularly the chloroplasts in *N. stella* are intact. However the mechanisms of chloroplast selection and capture are unknown. Foramanifera feed phagocytotically. Therefore, it would seem highly unlikely that so many chloroplasts would be found throughout the chambers undigested without some selective mechanism. This is supported by the even distribution of autofluorescence seen in cells of *N. stella* (Bernhard and Bowser 1999). Further support comes from our sequence data which suggest that some selective digestion or ingestion occurs in these organisms. Whether or not it is related to the capture of specific species of phytoplankton is unknown. The lack of any other chloroplast sequences in our library of 16S data from *N. stella* suggests that the feeding and subsequent partial digestion of phytoplankton is limited to the two close

relatives of *S. pseudocostatum* and *O. sinensis* designated NsChl1 and NsChl2. Chai and Lee (2000) have detected a glycoprotein on the surface of diatoms that foraminifera sequester. Diatoms that did not have the surface protein were not sequestered. Regardless of the specific intracellular or extracellular mechanism responsible for *N. stella* plastid capture, the data from three different cruises are consistent with specificity of plastid endosymbiosis in *N. stella*. Furthermore, there is no relationship between the natural abundances of phytoplankton in a given ecosystem and their presence in foraminifera (Chai and Lee 2000; Lee et al. 1989). The two dominant sequences found in *N. stella* are not the major phytoplankton in the overlying water of the Santa Barbara Basin or in the sediment (Reimers et al. 1990).

4.5.2 Bio-optical properties of sequestered plastids

All of our spectroscopic data suggest that the plastids are capable of energy transfer given a photon source. This does not imply that the plastids are used for photoautotrophy. The differences between excitation spectra of in vivo plastids and Santa Barbara basin mud (which presumably contain plastids and whole phytoplankton) offer proof that the intracellular environment of the foraminifera is a refuge from chloroplast degradation. Foraminifera in general have been noted to be particularly good micro-habitats for the establishment and maintenance of algal symbioses (Lee and Anderson 1991). While the absence of light and hypoxia in the Santa Barbara basin probably help reduce the rate at which the plastid degrades it is not an environment where chloroplasts or phytoplankton maintain energy transfer capabilities without further protection. The cryogenic emission spectra of the foraminifera reveal 5 significant peaks when deconvolved into their Gaussian curves. The curves indicate the presence of PSI,

PSII, FCP and free pigment. Brown reports that the relative yield of PSII fluorescence is about 10 times that of PSI (Brown 1988). The amplitudes of our fit yield a PSII:PSI ratio of 16. A higher ratio would be expected given the low light environment- regardless of whether or not photochemistry occurs. Not surprisingly there was a signal also associated with free pigment and/or lower vibrational energies of Chl *a* and degradation products. The importance of the measurement is to demonstrate that the fucoxanthin-chlorophyll protein complexes that were seen in Western Blots were in fact associated with reaction centers and were capable of transferring light energy to the reaction center chlorophylls of PSI and PSII.

4.5.3 Enzyme activity and longevity of proteins

A significant problem exists for the host of a plastid irregardless of plastid function. That is, how do you maintain plastid proteins when the majority is derived from nuclear genes? We did Western blot analysis of numerous nuclear and chloroplast encoded proteins. The fucoxanthin-chlorophyll protein complex is encoded in the nucleus. As many as 6 genes may be responsible for this structural and functional complex. All of our samples regardless of age contained the intact proteins as diagnosed by Western blot. The same is true for all other proteins we challenged with antibodies. This implies that the proteins are imported into the chloroplast from remnant diatom nuclei or from actual foraminifera nuclei containing FCP genes or, most likely, the proteins like the chloroplast are extremely stable. Similarly, enzyme assays on two proteins RuBisCO and pepC yielded activities that were suggestive of extremely slow turnover of chloroplast proteins. The RuBisCO enzyme is comprised of two subunits that in diatoms are both encoded in the chloroplast. Therefore, if the host organism was utilizing the chloroplast for carbon

reduction *de novo* synthesis of the protein would have to occur or the pool of enzymes captured would have to remain functional. Chloroplast gene expression in sequestered chloroplasts has been reported (Green et al. 2000).

The D1 protein is the 32 kDa product of the *psbA* gene. The D1/D2 dimer is the major structural complex of photosystem II and is encoded in the chloroplast. The D1 component is rapidly degraded and re-synthesized under photic conditions. Turnover is strongly correlated to light flux (Tyystjarvi and Aro 1996). It has also been shown in pea thylakoid preparations that D1 protein turnover is very slow under anaerobic or reducing conditions (Nedbal et al. 1990). We have data to show that similar processes occur in diatoms (unpublished data). Therefore, while it is possible that D1 protein turnover proceeds and is *de novo* synthesized, the parsimonious explanation is one of environmental protection. Regardless of the origin of the chloroplast over time it is exposed to exponentially decreasing light and decreasing pe°_w . Thus, turnover pressure is reduced and the protein remains stable. Adding to the stability of the environment is the pe°_w of the system's affect on the chloroplast. Unless the pe°_w of the chloroplast were to remain oxidizing in the mildly reducing environment of the mud, the plastoquinone pool ($pe^{\circ}_w \approx -0.5$) would be almost completely reduced. This would have a similar effect on electron transport as the herbicide DCMU which blocks electron transport from Q_A to Q_B . DCMU treated chloroplasts have significantly decreased D1 turnover rates (Kirilovsky 1994; Setlik et al. 1983). In light of these data and our own, it is likely that the sequestered chloroplasts are stable for at least a year and even if *de novo* protein synthesis does not occur the chloroplasts could be a favorable metabolic addition to the

host. The upper limit of sequestered chloroplast survival in these environments is unknown.

4.5.4 Chloroplast function: the light hypothesis

Our measurements of the quantum yield of photochemistry and the calculations of light flux preclude the possibility of photosynthesis and oxygen evolution in the Santa Barbara Basin from the sun. The maximum theoretical electron transport rates in these chloroplasts is far slower than the rate constants for back reaction of photosynthesis. For example, oxygen evolution occurs after the accumulation of four positive charges in the Mn cluster of the oxygen evolution complex. After this accumulation, termed the S_4 state, two molecules of water are oxidized producing one molecule of O_2 . The penultimate S-state before oxygen evolution, the S_3 state, has a half-time of decay around 13 seconds (Radmer and Kok 1973). Thus, it is highly unlikely that an electron transfer rate of 0.02 s^{-1} would enable the system to ever proceed beyond S_3 . It should be noted that many other back reactions occur on much faster time scales (μs -ms).

More than likely the biological signals we measured from the chloroplasts are a product of environmental stability resulting from no light, constant cold temperatures, and some synergism between host and chloroplast. The low oxygen levels and no light allow the chloroplasts, especially light sensitive pigments and proteins to remain preserved and functional. However, other aspects of photosynthetic regulation, especially photoacclimation are lost. We would expect cells to change the fluorescent characteristics, the quantum yield of photochemistry and the size of the PSII reaction center when exposed to blue and red light regimes. However, this did not occur. Despite

having functional pigment protein complexes and both photosystems the chloroplasts do not begin photosynthesizing upon exposure to light.

The oxidation of sulfide is a chemiluminescent reaction and is potentially responsible for the reports of light production in deep-sea hydrothermal vent environments (Pelli and Chamberlain 1989; Tapley et al. 1999; Van Dover et al. 1988). However, chemiluminescence is positively correlated with sulfide concentration and requires oxygen. In the Santa Barbara Basin sulfide concentrations can reach 250 μM at sediment depths of 7cm; however there is no oxygen, and foraminifera have only been found to depths of 3cm where sulfide concentrations are just increasing from zero (Bernhard and Reimers 1991). Therefore sulfide oxidation is not responsible for a significant light flux (capable of generating oxygen via photosynthesis) in the Santa Barbara Basin.

4.5.5 Chloroplast function: the sulfur hypothesis

Sulfur chemistry has other potentially important biological roles in the Santa Barbara Basin ecosystem. The spontaneous oxidation of sulfide in the presence of oxygen is highly favorable ($K = 10^{32}$) and yields damaging oxygen and sulfide radicals (Tapley et al. 1999). Sulfide is extremely toxic. It disrupts mitochondrial respiration and the NADH/O_2 redox reaction by poisoning the cytochrome c complex (Hochachka and Somero 1984). Given the success of the *N. stella* in this environment it is possible that it has adapted to sulfide toxicity by using the chloro-respiratory pathway during periods of sulfide toxicity in its own mitochondria. Metabolically this means that the chloroplast is the site of ATP production. Chlororespiration is an aphotic process that utilizes stored reductant (NADPH) to reduce the PQ pool and create the electrochemical gradient

necessary to generate ATP (Bennoun 1982). We think this is unlikely for the following reason: sulfide toxicity occurs in the absence of oxygen which means unless there is an unknown oxidase in the chloroplast there is not a sufficiently strong oxidizer to complete the oxidation of PQ. Furthermore, our measurements of abiotic NADPH reduction given the Santa Barbara Basin and cellular redox environment suggest that this type of process would NOT be renewable. In the simultaneous presence of both sulfide and oxygen the foraminifera would be exposed to oxidative radicals and sulfide toxicity would be not the most important biochemical concern. The generation of H_2O_2 via sulfide oxidation could explain the large number of peroxisomes present in *N. stella* (Bernhard and Bowser 1999). The organism seems to be able to deal with multiple but temporally and spatially separate problems: sulfide toxicity, anoxia, sulfur and oxygen radical generation.

4.5.6 Chloroplast function: the nitrogen hypothesis

We have noted the presence and activity of the carboxylating enzyme RuBisCO in the sequestered chloroplasts of *N. stella*. The strategy of sequestering chloroplasts in photic environments and living off of the reduced carbon from photosynthesis is well documented however, in an oligotrophic environment this would certainly lead to nitrogen starvation. The coral-zooxanthellae symbiosis is a model system for effective nitrogen cycling especially since the assimilation of ammonia by glutamate dehydrogenase (GDH) may not be favored in numerous marine invertebrates (Moyes et al. 1985; Muscatine et al. 1979). Assuming periods of high rates of denitrification in the upper sediments of the basin, foraminifera might not be able to meet their nitrogen requirements. Diatoms assimilate inorganic nitrogen via the glutamine synthetase and glutamate 2-oxo-glutarate amidotransferase (GOGAT) pathway after the reduction of

NO_3^- and NO_2^- (Zehr and Falkowski 1988). Therefore, given an unfavorable host GDH pathway or high fluxes of nitrite or nitrate from overlying water, presumably glutamate could be provided to the host by the chloroplast nitrogen assimilation pathway. In fact, blocking GOGAT activity in zooxanthellae results in NH_4^+ release from corals suggesting that the role of GDH is more closely tied to respiration than to ammonium assimilation (Rahav et al. 1989). The presence of the nuclear encoded enzyme nitrate reductase in these foraminifera supports this hypothesis. The protein represents the first step in being able to use inorganic sources of nitrogen to make glutamate, glutamine and other amino acid precursors.

Multiple secondary symbioses have led to the origin of the “golden algae”, a diverse group comprised of heterokont and haptophyte algae, from their protistan heterotrophic ancestors. A modern analog to the endosymbiotic origin of the golden algae, 250 Ma, ago, is the protist *N. stella*. However, the primary metabolic advantage in this instance is not photoautotrophy. In heterotrophic algae that contain plastids a major metabolic advantage is the ability to grow on oxidized forms of nitrogen. An engineered heterotroph from the marine diatom *Phaeodactylum tricornutum* is a potential model system of our described adaptation of the chloroplast. The *Phaeodactylum tricornutum* mutant (Glut1-17) has the same growth rate on glucose in the light or dark implying a reduced role of the chloroplast (Zaslavskaja et al. 2001). Much like *N. stella* the quantum yields of photochemistry and electron transport rates in *P. tricornutum* are very low. In the dark the chloroplast ceases to function autotrophically, yet it is maintained. This can be considered an engineered symbiosis analogous to the foraminifera. Instead of capturing chloroplasts the organism obviously, has the genetic machinery to synthesize

them despite not using them in their primary role. The mutant's only source of nitrogen is NO_3^- which is imported into the chloroplast after reduction to nitrite. The chloroplast is the site of nitrite reduction and the formation of glutamine. Thus, in these mutants and all heterotrophic, plastid containing algae growing on NO_3^- one of the major roles of the chloroplast is ammonia assimilation. This suggests that in oxidized environments or in environments depleted in organic nitrogen, the chloroplast becomes increasingly important to meet the metabolic requirements of the cell- in or out of the dark.

4.6 References

- Bennoun, P. 1982. Evidence for a respiratory chain in the chloroplast. *Proc Natl Acad Sci USA* **79**: 4352-4356.
- Bernhard, J. M., and S. S. Bowser. 1999. Benthic foraminifera of dysoxic sediments: Chloroplast sequestration and functional morphology. *Earth Science Reviews* **46**: 149-165.
- Bernhard, J. M., K. R. Buck, M. A. Farmer, and S. S. Bowser. 2000. The Santa Barbara Basin is a symbiosis oasis. *Nature* **403**: 77-80.
- Bernhard, J. M., and C. E. Reimers. 1991. Benthic foraminiferal population fluctuations related to anoxia: Santa Barbara Basin. *Biogeochemistry* **15**: 127-149.
- Blackbourn, D. J., F. J. R. Taylor, and J. Blackbourn. 1973. Foreign Organelle Retention by Ciliates. *J. Protozol.* **20**: 286-288.
- Brown, J. S. 1988. Photosynthetic pigment organization in diatoms (Bacillariophyceae). *Journal of Phycology* **24**: 96-102.
- Chai, J., and J. J. Lee. 2000. Recognition, establishment and maintenance of diatom endosymbiosis in foraminifera. *micropaleontology* **46**: 182-195.
- Correia, M. J., and J. J. Lee. 2000. Chloroplast retention by *Elphidium excavatum* (Terquem). Is it a selective process? *Symbiosis* **29**: 343-355.
- Dodge, J. D. 1973. *The fine structure of the algal cells*. Academic Press.
- Falkowski, P. G., and J. A. Raven. 1997. *Aquatic photosynthesis*. Blackwell.
- Falkowski, P. G. D. Z. M. L. M. L. 1993. Population control in symbiotic corals. Ammonium ions and organic materials maintain the density of zooxanthellae. *BioScience* **43**: 606-611.
- Felbeck, H., G. N. Somero, and J. J. Childress. 1983. Biochemical interactions between molluscs and their symbionts, p. 331-358. *In* P. W. Hochachka [ed.], *The Mollusca*. Academic Press.
- Field, K. and others 1997. Diversity and depth-specific distribution of SAR11 cluster rRNA genes from marine planktonic bacteria. *Appl. Environ. Microbiol.* **63**: 63-70.
- Green, B. J., W.-Y. Li, J. R. Manhart, and e. al. 2000. Mollusc-algal chloroplast endosymbiosis. Photosynthesis, thylakoid protein maintenance, and chloroplast gene expression continue for many months in the absence of the algal nucleus. *Plant Physiology* **124**: 331-342.
- Hochachka, P. W., and G. N. Somero. 1984. *Biochemical Adaptation*. Princeton University Press.
- Johnson, P. W., P. L. Donaghay, E. B. Small, and J. M. Sieburth. 1995. Ultrastructure and ecology of *Perispira ovum* (Ciliophora: Litostomatea): An aerobic, planktonic ciliate that sequesters the chloroplasts, mitochondria, and parmylon of *Euglena proxima* in a micro-oxic habitat. *J. Euk. Microbiol.* **42**: 323-335.
- Kirilovsky, D. R. W. E. A. L. 1994. Influence of DCMU and ferricyanide on photodamage in photosystem 2. *Biochemistry* **33**: 3087-3095.

- Kolber, Z. S., O. Prasil, and P. Falkowski. 1998. Measurements of variable chlorophyll fluorescence using fast repetition rate techniques: defining methodology and experimental protocols. *Biochim. Biophys. Acta* **1367**: 88-106.
- Lee, J. J., and O. R. Anderson. 1991. Symbiosis in foraminifera, p. 157-220. *In* J. J. Lee and O. R. Anderson [eds.], *Biology of the foraminifera*. Academic Press.
- Lee, J. J., and W. D. Bock. 1976. The importance of feeding in two species of soritid foraminifera with algal symbionts. *Bull. Mar. Sci.* **26**: 530-537.
- Lee, J. J., L. J. Crockett, J. Hagen, and R. J. Stone. 1974. The taxonomic identity and physiological ecology of *Chlamydomonas hedleyi* sp. Nov., algal flagellate symbiont from the foraminifer *Archaias angulatus*. *Br. phycol. J.* **9**: 407-422.
- Lee, J. J., W. W. Faber, and R. E. Lee. 1991. Granular reiculopodial digestion- a possible preadaptation to benthic foraminiferal symbiosis? *Symbiosis* **10**: 47-51.
- Lee, J. J., W. W. Faber, B. Nathanson, R. Rottger, and M. Nishihira. 1992. Endosymbiotic diatoms from larger foraminifera collected in the Pacific habitats. *Symbiosis* **14**: 265-281.
- Lee, J. J. and others 1989. Identification and distribution of endosymbiotic diatoms in larger foraminifer. *Micropaleontology* **35**: 353-366.
- Lee, J. J., and W. Zucker. 1969. Algal Flagellate symbiosis in the foraminifer *Archaias*. *J. Protozool.* **16**: 71-81.
- Leutenegger, S. 1984. Symbiosis in benthic foraminifera: Specificity and host adaptations. *J. Foram. Res.* **14**: 16-35.
- Macintyre, H. L., R. J. Geider, and R. M. McKay. 1996. Photosynthesis and Regulation of Rubisco Activity in Net Phytoplankton From Delaware Bay. *Journal of Phycology* **32**: 718-731.
- Morel, A. 1988. Optical modeling of the upper ocean in relation to its biogenous matter content (case I waters). *Journal of Geophysical research* **93**: 10749-10768.
- Morel, F. M. M., and J. G. Hering. 1993. Principles and applications of aquatic chemistry. John Wiley and Sons.
- Moyes, C. D., T. W. Moon, and J. S. Ballantyne. 1985. Glutamate catabolism in mitochondria from *Mya arenaria* mantle: Effects of pH on the role of glutamate dehydrogenase. *J. Exp. Biol.* **236**: 293-301.
- Mujer, C. V., D. L. Andrews, J. R. Manhart, S. K. Pierce, and M. E. Rumpho. 1995. Expression of Chloroplast Psba and 16S Ribosomal-Rna Genes During Endosymbiosis of Algal Plastids From *Vaucheria* With the Mollusk Host *Elysia*. *Plant Physiology* **108**: 34-34.
- . 1996. Chloroplast genes are expressed during intracellular symbiotic association of *Vaucheria litorea* plastids with the sea slug *Elysia chlorotica*. *Proc. Natl. Acad. Sci. USA* **93**: 12333-12338.
- Muller-Merz, E., and J. J. Lee. 1976. Symbiosis in the larger foraminiferan *Sorites marginalis* (with notes on *Archais* spp.). *J. protozool.* **23**: 390-396.
- Muscantine, L., H. Masuda, and R. Burnap. 1979. Ammonium uptake and release by symbiotic and aposymbiotic reef corals. *Bull. Mar. Sci.* **29**: 725-734.
- Nedbal, L., J. Masojidek, J. Komenda, O. Prasil, and I. Setlik. 1990. Three types of PSII photoinactivation. 2. Slow processes. *Photosynth Res* **24**: 89-97.
- Nicholls, D. G., and S. J. Ferguson. 1992. Bioenergetics. Academic Press.
- Pelli, D. G., and S. C. Chamberlain. 1989. The visibility of 350C black body radiation by the shrimp. *Nature* **337**: 460-461.
- Pierce, S. K., R. W. Biron, and M. E. Rumpho. 1996. Endosymbiotic chloroplasts in molluscan cells contain proteins synthesized after plastid capture. *The Journal of Experimental Biology* **199**: 2323-2330.
- Radmer, R., and B. Kok. 1973. A Kinetic Analysis of the Oxidizing and Reducing Sides of the O₂-Evolving System of Photosynthesis. *Biochim. Biophys. Acta* **314**: 28-41.
- Rahav, O., Z. Dubinsky, Y. Achituv, and P. G. Falkowski. 1989. Ammonium metabolism in the zooxanthellate coral, *Stylophora pistillata*. *Proc Roy Soc (London)* **B236**: 325-327.
- Rumpho, M. E., E. J. Summer, and J. R. Manhart. 2000. Solar-powered sea slugs. *Mollusc/Algal chloroplast symbiosis*. *Plant Physiology* **123**: 29-38.
- Sanders, R. W. 1991. Mixotrophic Protists in Marine and Freshwater Ecosystems. *Journal of Protozoology* **38**: 76-81.
- Setlik, I., E. Setlikova, and L. Nedbal. 1983. The effect of DCMU on the photodegradation of the herbicide-binding protein in photosystem 2 of algae and cyanobacteria. poster and lecture, International Workshop on Mode of action of Herbicides in Photosynthesis, Wageningen. the Netherlands.

- Smith, D. C. 1991. Why Do So Few Animals Form Endosymbiotic Associations with Photosynthetic Microbes. *Philosophical Transactions of the Royal Society of London Series B - Biological Sciences* **333**: 225-230.
- Tapley, D. W., G. R. Buettner, and M. J. Shick. 1999. Free radicals and chemiluminescence as products of the spontaneous oxidation of sulfide in seawater and their biological implications. *Biological Bulletin* **196**: 52-56.
- Taylor, F. J. R., D. J. Blackburn, and J. Blackburn. 1969. Ultrastructure of the chloroplasts and associated structures within the marine ciliate *Mesodinium rubrum* (Lohmann). *Nature* **224**: 819-821.
- . 1971. The red-water ciliate *Mesodinium rubrum* and its "incomplete symbionts": a review including new ultrastructural observations. *Journal Fisheries research board of Canada* **28**: 391-407.
- Tyystjarvi, E., and E. M. Aro. 1996. The Rate-Constant of Photoinhibition, Measured in Lincomycin-Treated Leaves, Is Directly Proportional to Light-Intensity. *Proceedings of the National Academy of Sciences of the United States of America* **93**: 2213-2218.
- Van Dover, C. L., J. Delaney, M. Smith, and J. R. Cann. 1988. Light emission at deep-sea hydrothermal vents. *EOS, Transactions of the American Geophysical Union* **69**: 1498.
- Zaslavskaja, L. A., J. C. Lippmeier, C. Shih, D. Ehrhardt, A. R. Grossman, and K. E. Apt. 2001. Trophic conversion of an obligate photoautotrophic organism through metabolic engineering. *Science* **292**: 2073-2075.
- Zehr, J. P., and P. G. Falkowski. 1988. Pathway of ammonium assimilation in the marine diatom determined with the radiotracer ^{13}N . *Journal of Phycology* **24**: 588-591.

4.7 Tables

Table 4.1 Measured and calculated parameters of electron transport rates and enzyme activities in *N. stella*.

	Lower limit		Upper limit
I_d (quanta $m^{-2} s^{-1}$)	1.60E-13		5.00E+16
I_o (quanta $m^{-2} s^{-1}$)		1.2046E+21	
d (m)		600	
K440w (m^{-1})		0.0168	
K440 for 1mg Chl a m^{-3} (m^{-1})		0.13	
f_v/f_m		.22 (± 0.07)	
sigma PSII (m^2 quanta $^{-1}$)		7.8e-19(± 1.8)	
Q_p (e RC^{-1})		.22 (± 0.07)	
ETR (e $RC^{-1} s^{-1}$)	1.25E-31		3.94E-02
Rubp (μg C mg CHL hr^{-1})		0.12 (± 0.04)	
PEP (μg C mg CHL hr^{-1})		0.04(± 0.03)	

4.8 Figures



Figure 4.1 Electron micrographs of three *N. stella* plastids. Note the similarity of the plastids: the outer lamella and the single pyrenoid with the transverse lamella.

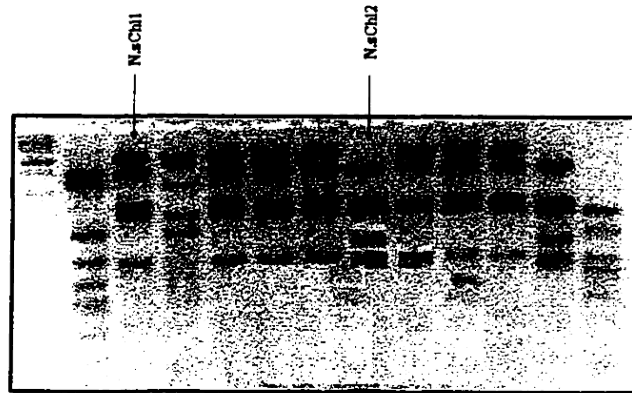


Figure 4.2 Restriction fragment length polymorphism of 16S clonal library from *N. stella*. The two dominant patterns denoted N.sChl1 and N.sChl2 are highlighted by arrows. Sequences for these chloroplasts are shown in 4.3

	1	11	21	31	41	51	61	71
<i>osinensis16s</i>	TTGATCTTGGCTCAGGATGAACCTGGCGGTATGCTTAACACATGCAAGTCGTACGAGAGTTTAACTCAAGTGGCGGA							
68	-----CCCTTTTATA-----CGCCC-CGTATGCTT--TTCATGCAAGTCGTACGAGAGTTTAACTCAAGTGGCGGA							
Consensus	cc	t a	cgc	cgtatgctt	catgcaag	cgtacg	gagtttttaactcaagtggcgg	
	81	91	101	111	121	131	141	151
<i>osinensis16s</i>	CGGCTGAGTAACACGTGAGAAATCTGCTTTAGGAGGGGGACAACTGGAACGGTTGCTAATACCCCATATCTTTTCG							
68	CGGCTGAGTAACACGTGAGAAATCTGCTTTAGGAGGGGGATCAACTGGAACGGTTGCTAATACCCCATATCTTTTCG							
Consensus	cgggtgagtaacacgtgagaaatctgcctttaggaggggga	eacactggaaacggttgctaataccatctatgcttttcg						
	161	171	181	191	201	211	221	231
<i>osinensis16s</i>	AAGTAAATAGATTATCTGCTAAGAGGAGCTGCGGCTGATTAGCTTGTGTGTAAGTAATGGCTTACCAAGGC-GAC							
68	AAGTAAATAGATTATCTGCTAAGAGGAGCTGCGGCTGATTAGCTTGTGTGTAAGTAATGGCTTACCAAGGC-TNAC							
Consensus	agt aat gattatc gctta agagagctgcggttgattagcttgttgta agtaa ggc taaccaagtc ac							
	241	251	261	271	281	291	301	311
<i>osinensis16s</i>	GATCAATATCTGCTTTGAGAGGAGTACAGACACTGGAACTGAGACAGGTCAGACTCTACGGGAGGAGCAG-TG							
68	TTTCTATTATCTGCTTTGAGAGGAGTACAGACACTGGAACTGAGACAGGTCAGACTCTACGGGAGGAGCAGCTG							
Consensus	tc	tacttggtttgagagagcga	cagacacactggaactgagacacggtccagactctacgggagggcagtcg					
	321	331	341	351	361	371	381	391
<i>osinensis16s</i>	GGGAATTTTCGCAATGGCGAAAGC-TGACGGAGCAATACCGGTGAGGGAAGACGGCTATGGGTTGTAACCTCTTT							
68	GGGAATTTTCGCAATGGCGAAAGCCTGACGGAGCAATACCGGTGAGGGAAGACGGCTATGGGTTGTAACCTCTTT							
Consensus	gggaatttttcgcaatggcgaaagc	tgacggagcaataccggtgagggagagacggcctatgggttgtaaacctcttt						
	401	411	421	431	441	451	461	471
<i>osinensis16s</i>	TCTCAGGGAGAAATCAATGACGTGTACCTGAGGAATAAGCATCGGTAACCTGTCAGCAGCCGGGTAAGACGGAG							
68	TCTCAGGGAGAAATCAATGACGTGT-CCTGAGGAATAAGCATCGGTAACCTGTCAGCAGCCGGGTAAGACGGAG							
Consensus	tctcagggagaaatcaatgacgtgt	cctgaggaataagcatcggttaactcctgagcagccgggtaagacggag						
	481	491	501	511	521	531	541	551
<i>osinensis16s</i>	GATCAGAGTGTATCTCGGAATCACTGGCGTAAAGCGTCTGTAGGTGTTTAAATGTAACCTTTAAATTTGAGGCT-							
68	GATCAGAGTGT-ATCTCGGAATC-CTGGCGTAA-CCGCTCTGTAGGTGTTT-AAATG--TAACTGTTAA-TCTTGAGGCTA							
Consensus	gatcagagtgat atcgggaatc ctggcgtaa gcgtctgtaggt gtt aata	aactgttaa tcttgaggtc						
	561	571	581	591	601	611	621	631
<i>osinensis16s</i>	-----CAAC----							
68	CTTAAATCCAATCCAATTTA							
Consensus		caac						

181
193
Alexandrium fundyense T A C A T G G C A A C A -
Emiliania huxleyi C G C A C G G C T C T A C
Skeletonema costatum T A T A T T T A T C C G -
Odontella sinensis T A T - - - - - C T G -

Figure 4.4 Top panel: Sequence comparisons for one of the dominant chloroplast in *N. stella*, N.sChl2 and the diatom *O. sinensis*. Bottom panel: Sequence comparisons between representative of diatoms, dinoflagellates and prymnesiophytes- the major functional groups of phytoplankton in the ocean. The sequence differences between *S. costatum* and *O. sinensis* were consistently seen between N.sChl1 and N.sChl2.

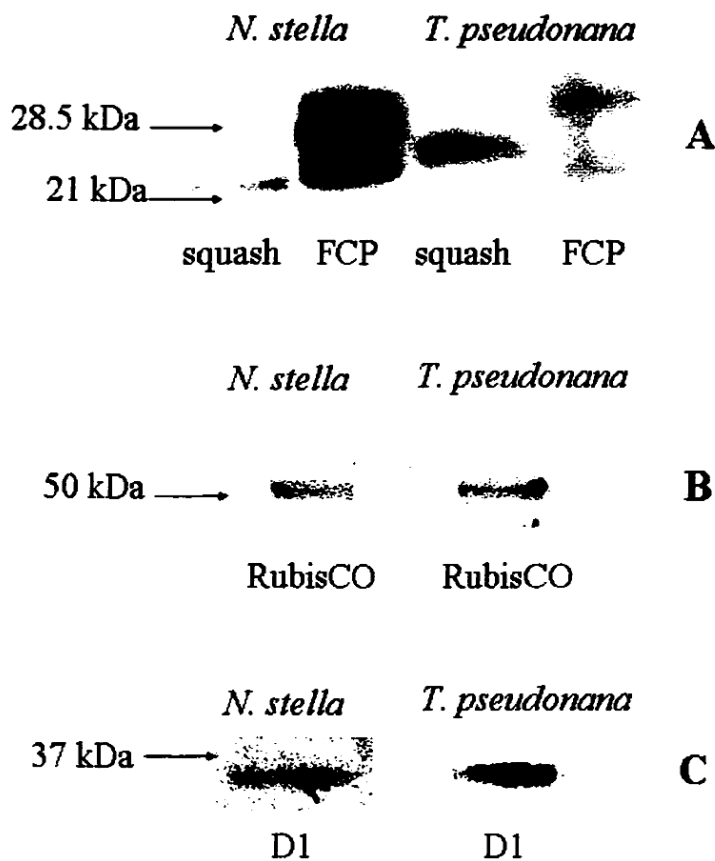


Figure 4.5 Digitized images from Western blots of protein extract from *N. stella* and the marine diatom *Thalassiosira pseudonana*. A. Proteins challenged with the antibody for the major light harvesting complex of Chromophyte algae, FCP and the major light harvesting complex for the chlorophyll a-b containing plant, squash. B. Proteins challenged with the antibody for the carboxylating enzyme RuBisCO. Shown is the cross reaction with the 53 kDa large subunit. C. Proteins challenged with the antibody for the 32.5 kDa, D1 component of the major structural dimer of photosystem II.

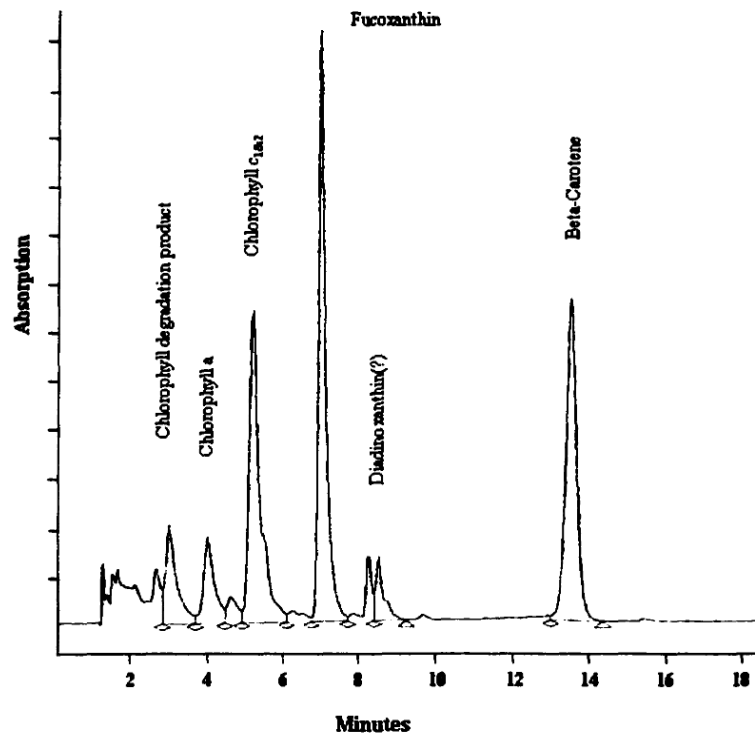


Figure 4.6 HPLC chromatogram for pigment extracts of *N. stella*. Peaks are labeled from the wavelength signatures of the corresponding absorption and fluorescence spectra.

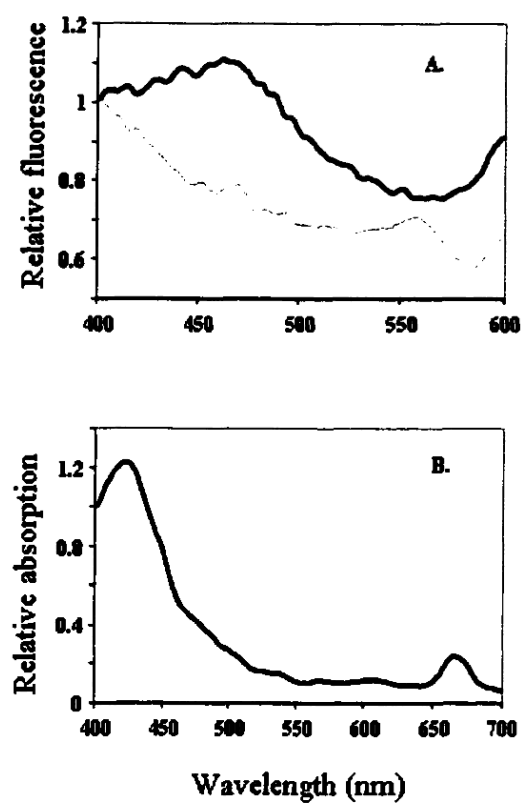


Figure 4.7 A. Fluorescence excitation spectra scaled to 1 at 400nm (440 ex, 680 em) for *N. stella* (bold line) and Santa Barbara Basin mud (faint line). B. *In vitro* absorption spectrum for a 90% acetone extract of *N. stella*.

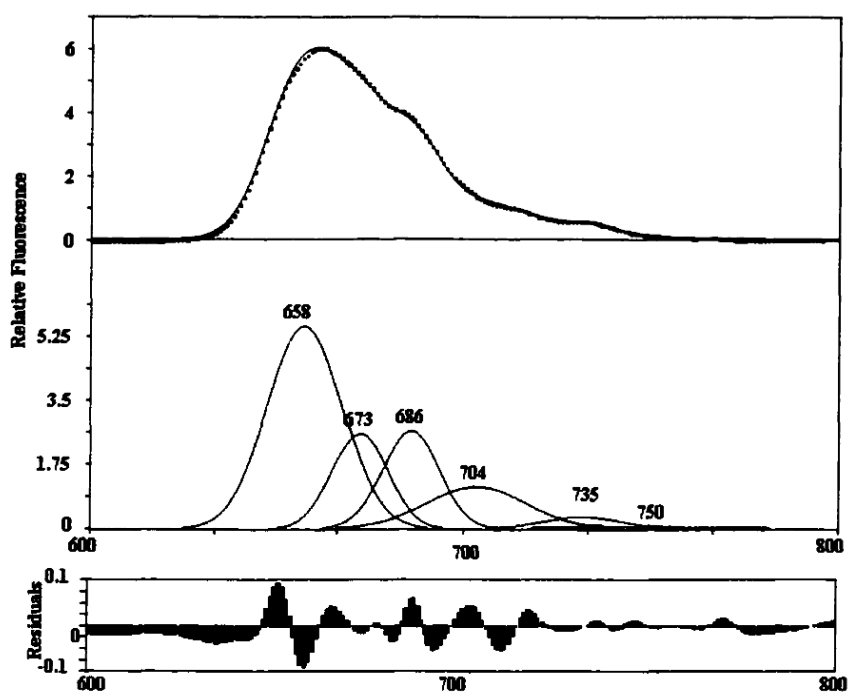


Figure 4.8 A. 77k emission spectrum (squares) of *N. stella* (440 ex) and the corresponding fit of the Gaussian peaks (smooth line). B. Gaussian curves of the 6 major components of the emission spectrum and the residuals of the fit. The major components of the spectrum are explained in the text.

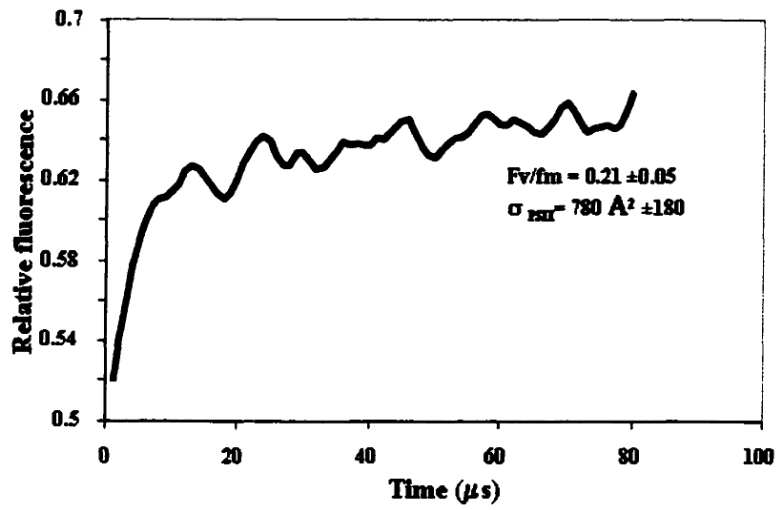


Figure 4.9 Fast repetition rate fluorometric measurement of *N. stella*. The curve is an average of 10 measurements and shows the change in fluorescence after a series of sub-saturating blue LED flashes as described in the text.

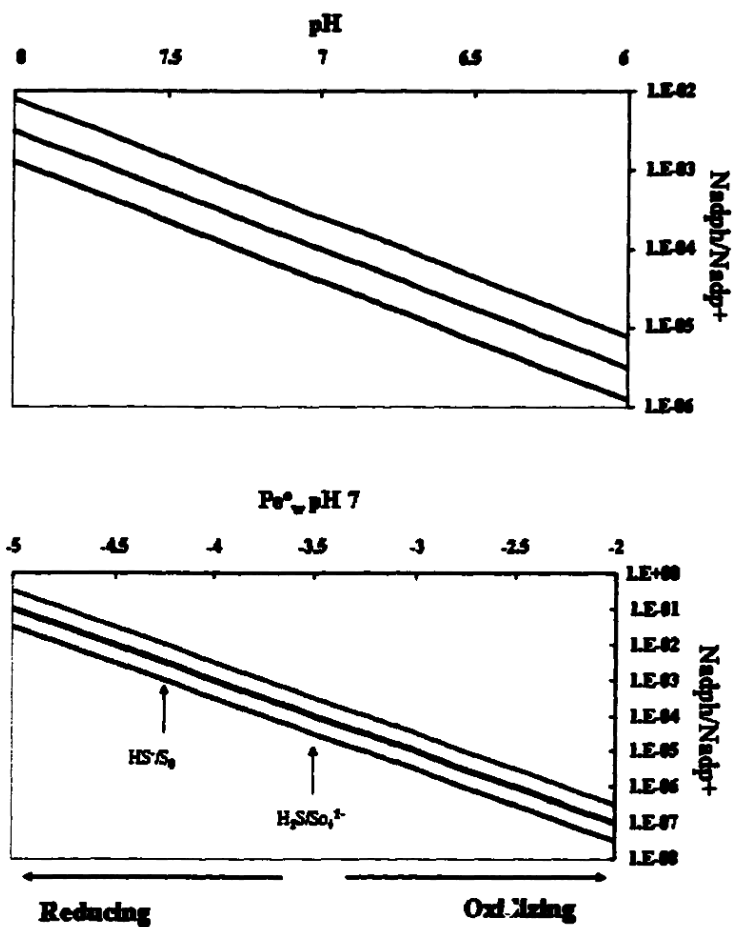


Figure 4.10 A. Relationship between pH and Q (NADPH/NADP⁺) different reducing conditions. Previously published pe's for the NADPH/NADP⁺ couple correspond to the black line. Upper and lower error limits are presented. B. The relationship between the redox poise of a system and Q calculated from the equations in the text.

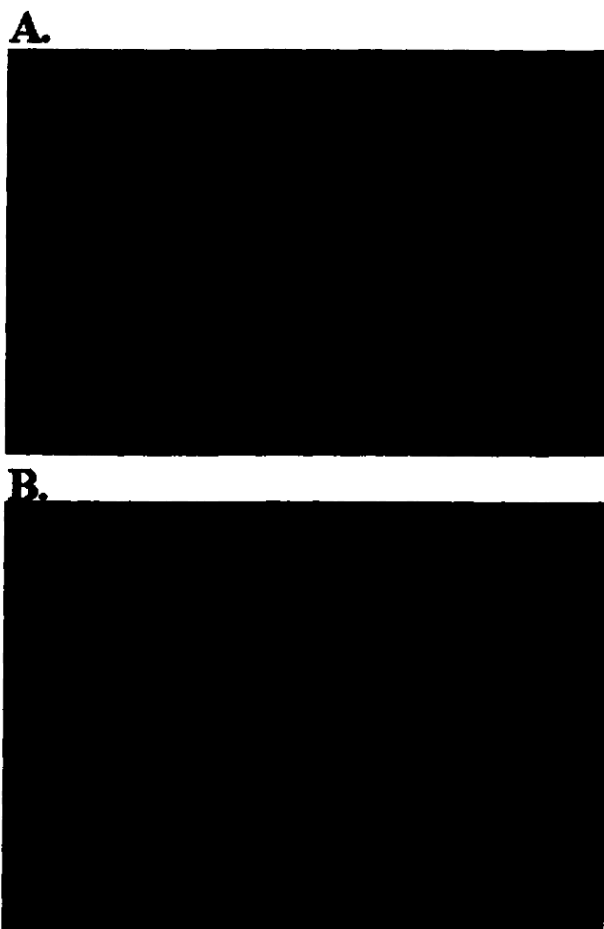


Figure 4.11 A. Epifluorescence micrograph of *Thalassiosira weissflogii* grown with NO_3^- showing the location of the chloroplasts. B. As in A, except showing the labeling of the Alexa 488 tagged nitrate reductase antibody.

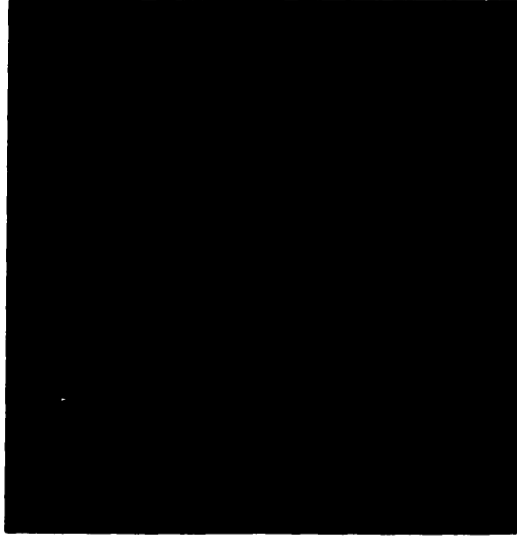
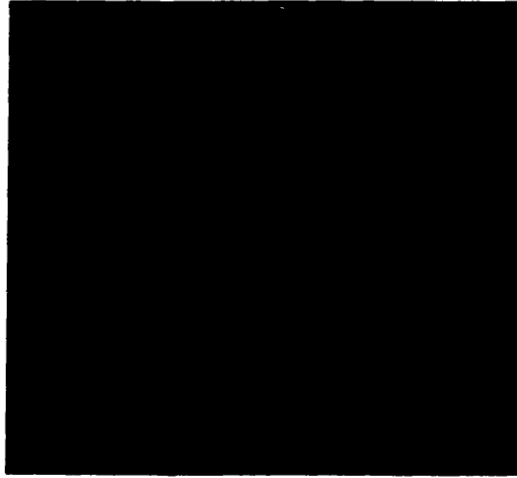
A.**B.**

Figure 4.12 A. Epifluorescence micrograph (100x) of *Nonionella stella* showing the location of the chloroplasts. B. As in A, except showing the labeling of the Alexa 488 tagged nitrate reductase antibody.

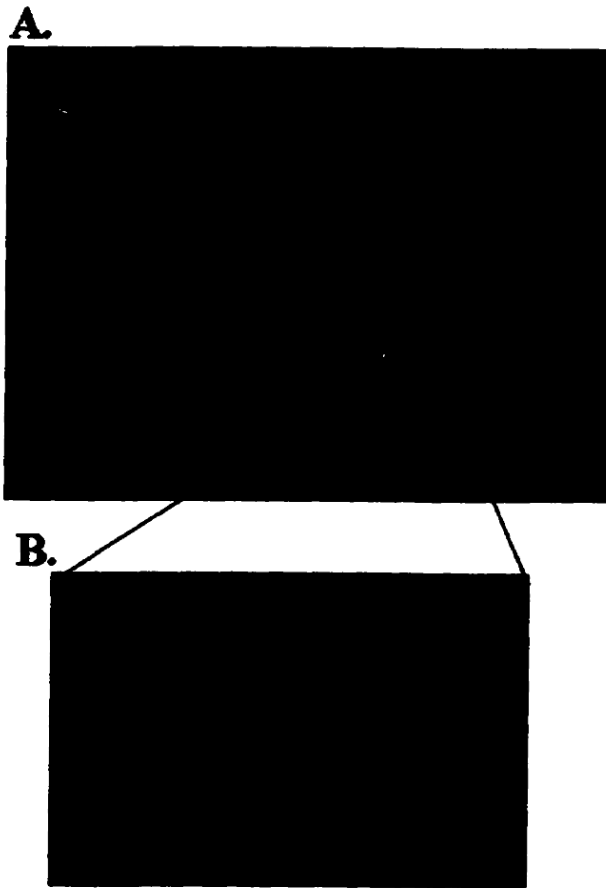


Figure 4.13 A. Epifluorescence micrograph (400x) of one chamber of *Nonionella stella* showing the location of the Alexa 488 tagged nitrate reductase enzyme. B. As in A except 1000x showing individually labeled microbodies which are presumably plastids.

5 Curriculum Vita

Joseph John Grzymiski

Education:

- 1990-1994 B.A. Biology and Philosophy, Bowdoin College, Brunswick, Maine.
 1994-1995 Fulbright Scholarship, Trondheim Biological Station, Trondheim, Norway
 Prof. Egil Sakshaug
 1996-2001. Ph.D. Program, Oceanography, Institute of Marine and Coastal Sciences, Rutgers University, New Brunswick, NJ.

Thesis Committee: Prof. Oscar Schofield (IMCS, Rutgers University), Prof. Paul Falkowski (IMCS, Rutgers University), Prof. John Reinfelder (IMCS, Rutgers University), Prof. John Raven, F.R.S. (University of Dundee)

Publications:

- Grzymiski, J. Moline, M.A., and Cullen, J.T. (2000). Modeling the atmosphere/ocean CO₂ cycle in relation to surface Iron concentrations. In: Modeling Dynamic Systems: Dynamic Modeling for Marine Conservation and Ecological Understanding. Lindholm, J. and Ruth, M. (eds) Springer Verlag (In press).
- Grzymiski, J., Orrico, C., Schofield, O. 2000. Monochromatic ultraviolet light induced damage to photosystem II efficiency and carbon fixation in the marine diatom *Thalassiosira pseudonana* (3H). Photosynthesis Research (In press)
- Grzymiski, J., Johnsen, G., and Sakshaug, E. 1997. The significance of intracellular self shading on the biooptical properties of brown, red, and green macroalgae. J. Phycol. 33, 408-17
- Moline, O., Schofield, O., Grzymiski, J. 2000. Impact of dynamic light and nutrient environments on phytoplankton communities in the coastal ocean. In: Modeling Dynamic Systems: Dynamic Modeling for Marine Conservation and Ecological Understanding. Lindholm, J. and Ruth, M. (eds) Springer Verlag (In press).
- Moline, M. A., Claustre, H., Frazer, T., Grzymiski, J., Schofield, O., and Vernet, M. 2000. Changes in phytoplankton assemblages and potential implications for the Antarctic food web. In: (Davidson, B. ed.) Antarctic Ecosystems: Models for Wider Ecological Understanding. Cambridge University Press, (In press).
- Schofield, O., Grzymiski, J., Moline, M.A., and Jovine, R.V.M. 1997 Impact of temperature on photoinhibition of photosynthesis in the red-tide dinoflagellate *Alexandrium fundyense* (Ca28). J. Plank. Res. 20(7): 1241-1258.
- Schofield, O., Grzymiski, J., Bissett, P., Kirkpatrick, G., Millie, D.F., Moline, M.A., Roesler, C. 1999. Optical monitoring and forecasting systems for harmful algal blooms: Possibility or pipedream? Journal of Phycology. 35(6):1476-96.
- Stocks, K., Grzymiski J., Hentschel, B., Scala, D., Teo, S. 2000. "Scientific Inquiry in Oceanography" - development of a new undergraduate course in marine science. J. Scanlon (ed). Teaching/Learning: Proceeding of the 1998 and 1999 Teaching/Learning Conferences at Rutgers University. Teaching Assistant Project, Graduate School - New Brunswick, New Jersey. May. pp 71-74.